STUDIES OF THE MECHANISM OF INSULIN RESISTANCE IN HYPERTENSIVE RATS

A thesis submitted to

The Institute of Biomedical and Life Sciences

For the degree of

DOCTOR OF PHILOSOPHY

by **Fiona Cairns**

Department of Biochemistry and Molecular Biology

Institute of Biomedical and Life Sciences

University of Glasgow

November 2002

Declaration

I declare that the work presented in this thesis has been carried out by myself, unless otherwise stated. It is entirely of my own composition and has not, in whole or in part, been submitted for any other degree.

Fiona Cairns

November 2002

Abstract

Insulin resistance in skeletal muscle is of major pathogenic importance in several common human disorders including diabetes, hypertension and obesity, but the underlying mechanisms are unknown. In order to define mechanisms of insulin resistance, studies have been undertaken in skeletal muscle of the SHRSP, an animal model of hypertension, which exhibits insulin resistance in skeletal muscle and adipose tissue, when compared to the normotensive WKY control animal.

Anti-peptide antibodies, directed against the phosphorylated or unphosphorylated residue Ser-1177 of human eNOS, were prepared and characterised, to allow the study of eNOS regulation in SHRSP skeletal muscle by phosphorylation at this residue. However, some doubt exists over the specificity of these antibodies and future studies have not been undertaken at this stage.

Flotillin is a protein known to be involved in a PI3-kinase independent pathway, which is required for GLUT 4 translocation and increased glucose uptake in response to insulin. Flotillin expression is increased in skeletal muscle from SHRSP and for this reason a yeast two-hybrid screen was undertaken using flotillin-1 as bait, the aim being to identify flotillin interacting proteins which have possible roles in insulin-stimulated glucose uptake. A number of interesting putative flotillin interacting proteins were identified in this screen, however one must be cautious as no duplicate clones were identified. Also, due to time constraints no biochemical studies have been undertaken to determine if the proteins identified do indeed bind flotillin.

Studies of the 'classical' PI3-kinase-dependent insulin-signalling pathway were also undertaken. It was demonstrated that key proteins involved in the insulin-signalling pathway (GLUT 4, IRS-1, IRS-2 and the PI3-kinase p85 subunit) are expressed at similar levels and have similar subcellular distribution (on crude fractionation of skeletal muscle) in skeletal muscle of the SHRSP and the control WKY. Furthermore, levels and activity of PKB (a protein kinase downstream of PI3-kinase) were similar in WKY and SHRSP, suggesting that the insulin-signalling pathway leading to activation of PKB in SHRSP skeletal muscle is intact.

Regulation of glycogen metabolism in SHRSP skeletal muscle was also investigated. Levels of muscle glycogen, glycogen synthesis, glycogen phosphorylase activity and GSK-3α and GSK-3β activity were all shown to be similar in skeletal muscle from SHRSP and WKY. However, expression of GSK-3α protein was decreased in SHRSP skeletal muscle, yet the activity of the protein was similar in the two strains.

Skeletal muscle from SHRSP and WKY was subjected to fibre type analysis, in order to determine if any differences in fibre type distribution could be observed which may account for the insulin resistance observed in the SHRSP. However, WKY and SHRSP skeletal muscle have similar number and distribution of the various fibre types, suggesting that fibre abnormalities are not the cause of the observed insulin resistance.

In this study, two defects have been presented that have been identified to occur in SHRSP skeletal muscle, compared to WKY. These are increased expression of flotillin and decreased expression of GSK-3α. Whether these changes in protein expression are a cause or effect of the observed insulin resistance, or whether they are unrelated to this defect is unknown. Further studies are required to define more clearly the mechanism involved in the insulin resistance observed in the SHRSP.

Acknowledgements

Firstly, I would like to thank my supervisor, Prof. Gwyn Gould, for the privilege of working in his laboratory, it's been great fun and I've learned loads. I would also like to thank the British Heart Foundation for funding the studentship.

I wish to thank the Dominczak laboratory for providing specimens to work with and Dr. Ian Montgomery for undertaking the histochemistry and EM work.

I wish to thank all the members of lab C36/C6/241 (past and present), for the constant help and encouragement over the past three years, and for keeping me sane during numerous lunch times and biscuit munching tea breaks. Special thanks must go to Declan James, who initiated the muscle project on the SHRSP, and who expertly taught me the dissection technique. I also wish to thank Drs. Ian Salt and Luke Chamberlain, for their continued support, from technical advice to help with mathematical puzzles and for their helpful comments on reading this thesis.

I would like to thank my parents, without their support over the years undertaking my PhD would never have been possible. I thank 'the girls' for reminding me it's good to take a break and relax now and then, and for always being there when I need a good moan. Finally, I wish to thank Richard for not killing me once in the past three years. I know you've probably come close to it on numerous occasions and while I'd like to say I'll be easier to live when this is all over, I'd probably be lying! Thanks for always being there.

Table of Contents **Page No.**

List of Figures

List of Tables

Abbreviations

3-AT	3-amino-1,2,4-triazole
AICAR	5-aminoimidazole-4-carboxamide-riboside
AMP	adenosine monophosphate
AMPK	AMP-activated protein kinase
AMPKK	AMPK kinase
ATP	adenosine 5'-triphosphate
BCR	break point cluster
BH	BCR homology domain
BH_4	tetrahydrobiopterin
BSA	bovine serum albumin
CAP	c-Cbl associated protein
DAG	diacylglycerol
DDO	double dropout
DMSO	dimethyl sulphoxide
dNTPs	deoxynucleotide triphosphates
DTT	dithiothreitol
EDL	extensor digitorum longus
ECL	Enhanced chemiluminescence
EDTA	sodium diaminoethanetetra-acetic acid
EGF	endothelial growth factor
EGTA	ethylene glycol-bis (β-aminoethylether)-N,N,N',N'-tetra acetic acid
eEF	eukaryotic elongation factor
eIF	eukaryotic initiation factor
4E-BP1	eIF 4E binding protein 1
eNOS	endothelial nitric oxide synthase
ERK	extracellular regulated kinase
FAD	flavin adenine nucleotide
FDB	flexor digitorum brevis
FG	fast twitch glycolytic
FMN	flavin mono-nucleotide
FOG	fast twitch oxidative glycolytic

G6P	glucose 6-phosphate
GLUT	glucose transporter
GSVs	GLUT 4 storage vesicles
GSK-3	glycogen synthase kinase-3
GDP	guanine diphosphate
GTP	guanine 5'-triphosphate
HAECs	Human Aortic Endothelial Cells
HMIT1	H^+/myo-inositol co-transporter
HRP	horseradish peroxidase
IGF	insulin-like growth factor
iNOS	inducible nitric oxide synthase
IP	immunoprecipitation
$IR^{-/-}$	insulin receptor knockout mouse
IRS	insulin receptor substrate
KLH	keyhole limpet haemocyanin
L-NAME	N^G-nitro-L-arginine methyl ester
L-NMMA	N^G-monomethyl-L-arginine monoacetate
MAPK	mitogen activated protein kinase
MBS	3-maleimidobenzoic acid N-hyroxysuccinimide ester
MIRKO	muscle insulin receptor knockout
MEK	MAPK kinase
mTOR	mammalian target of rapamycin
NADP	β-Nicotinamide adenine dinucleotide phosphate
NADPH	nicotinamide adenine dinucleotide phosphate
NO	nitric oxide
NOS	nitric oxide synthase
nNOS	neuronal nitric oxide synthase
NSF	N-ethyl-maleimide-sensitive fusion protein
$p90^{RSK}$	p90 ribosomal S6 kinase
PBS	phosphate buffered saline
PCOS	polycystic ovarian syndrome
PCR	polymerase chain reaction
PDGF	platelet derived growth factor
PDK1	phosphoinositide dependent protein kinase-1

PEG	polyethylene glycol
PH	pleckstrin homology
PI3-kinase	phosphoinositide 3-kinases
PKA	cAMP-dependent protein kinase
PKB	protein kinase B
PKC	protein kinase C
PMS	phenazine methosulphate
PMSF	phenylmethylsulfonyl fluoride
PP1	protein phosphatase 1
PS	phosphatidyl serine
PtdIns	phosphatidylinositol
QDO	quadruple dropout
SBTI	soyabean trypsin inhibitor
SDS	sodium dodecyl sulphate
SDS-PAGE	SDS-polyacrylamide gel electrophoresis
SH2	src homology 2
SHR	spontaneously hypertensive rat
SHRSP	stroke-prone spontaneously hypertensive rat
α-SNAP	soluble NSF attachment protein
SNAP	synaptosomal associated protein
SNARE	soluble NSF attachment protein receptor
t-SNARE	target SNARE
v-SNARE	vesicle SNARE
SO	slow twitch oxidative
TDO	triple dropout
TEMED	N, N, N', N',-tetramethylethylenediamine
TfR	transferrin receptor
UDP	uridine diphosphate
VAMP	vesicle associated membrane protein
VEGF	vascular endothelial growth factor
WKY	Wistar-Kyoto rat

List of Amino Acids

Amino Acid	Three Letter Symbol	One Letter Symbol
Alanine	Ala	A
Asparagine	Asn	N
Aspartic Acid	Asp	D
Arginine	Arg	R
Cysteine	Cys	C
Glutamic Acid	Glu	E
Glutamine	Gln	Q
Glycine	Gly	G
Histidine	His	H
Isoleucine	Ile	I
Leucine	Leu	L
Lysine	Lys	K
Methionine	Met	M
Phenylalanine	Phe	F
Proline	Pro	P
Serine	Ser	S
Threonine	Thr	T
Tryptophan	Trp	W
Tyrosine	Tyr	Y
Valine	Val	V

List of Publications

James DJ, **Cairns F**, Salt IP, Murphy GJ, Dominiczak AF, Connell JMC, and Gould GW:
Skeletal muscle of SHRSP exhibits reduced insulin stimulated glucose transport and elevated levels of caveolin and flotillin.
Diabetes 50: 2148-2156, 2001

Mackenzie C, Wakefield J, **Cairns F**, Dominiczak AF, and Gould GW:
Regulation of glucose transport in aortic smooth muscle cells by cAMP and cGMP.
Biochemical Journal 353; 513-519, 2001

Abstracts

Cairns F, James DJ, Salt IP, Murphy GJ, Dominiczak AF, Connell JMC and Gould GW:
Reduced Insulin-Stimulated Glucose Transport in Skeletal Muscle of the Stroke-Prone Spontaneously Hypertensive Rat.
Diabetic Medicine 18, P19, 2001

F Cairns, DJ James, I Montgomery, AF Dominiczak, JMC Connell, GW Gould and IP Salt:
Analysis of proximal insulin signalling components and biological effects in skeletal muscle from stroke-prone spontaneously hypertensive rats.
Keystone Symposia, Diabetes Mellitus: Molecular Mechanisms, Genetics and New Therapies, Keystone, Colorado, 2002

CHAPTER 1

INTRODUCTION

1.1 Glucose

Glucose has a fundamental role in cellular homeostasis and metabolism, with many cellular processes including cell proliferation and chemotaxis requiring an increase in glucose transport into the cell to fulfil an increased energy requirement. When taken up into a cell, D-glucose (see figure 1.1) is phosphorylated by hexokinase to form glucose 6-phosphate (G6P), which has a number of fates. For example G6P can be used to form glycogen, the storage form of glucose, which is utilised when increased energy demands are placed on the cell/tissue. G6P can also be converted to pyruvate via the glycolytic pathway, with the subsequent release of ATP.

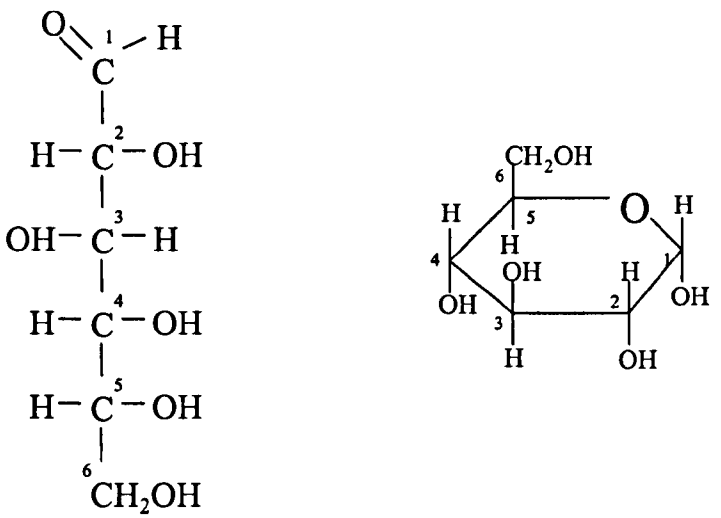

Figure 1.1 Linear and ring forms of D-glucose

Glucose can exist as a linear or ring form, however the predominant form in solution is the ring form.

Blood glucose concentration is controlled by a variety of hormones. For example when blood glucose concentration is low, the α-cells of the pancreas secrete glucagon which acts on the liver to promote glycogen breakdown, and release of glucose into the bloodstream. Conversely, insulin is released by the pancreatic β-cells when blood glucose concentration increases, following ingestion of a meal. Insulin has various actions, the main function being to increase glucose uptake and

utilisation in peripheral tissues such as fat and muscle (see section 1.2), which results in lowering of the blood glucose concentration.

1.1.1 The facilitative glucose transporter family

Glucose cannot freely diffuse across the plasma membrane of a cell, but is transported across the membrane by the energy-independent process of facilitated diffusion. A family of facilitative glucose transporters exists which transport glucose into and out of cells. The erythrocyte glucose transporter, GLUT 1, was the first glucose transporter to be isolated (Mueckler et al., 1985) with subsequent identification of a number of other transporters (GLUTs 2-7) (reviewed in Gould and Holman, 1993). Recently a number of other transporters have been identified, due to sequence similarities with the known GLUTs (reviewed in Joost and Thorens, 2001). There are now at least 13 known GLUT molecules, which represent a family of transporters that can be sub-divided into three classes (see table 1.1).

CLASS	ISOFORM	EXPRESSION	SUGER TRANSPORTED
I	GLUT 1	erythrocytes, brain	glucose
	GLUT 2	liver, pancreas	glucose
	GLUT 3	brain	glucose
	GLUT 4	skeletal muscle, adipose	glucose
II	GLUT 5	intestine, testis, kidney	fructose transporter
	GLUT 7	unknown	unknown
	GLUT 9	liver, kidney	unknown
	GLUT 11	heart, skeletal muscle	glucose/fructose
III	GLUT 6	spleen, leukocytes, brain	glucose
	GLUT 8	testis, blastocyst, brain	glucose
	GLUT 10	liver, pancreas	unknown
	GLUT 12	heart, prostate	unknown
	HMIT	brain	myo-inotistol transporter

Table 1.1 The extended GLUT family (adapted from Joost and Thorens, 2001)
The 13 known GLUTs are divided into three sub-classes on the basis of sequence similarity and preliminary functional characterisation. The nomenclature used is that recommended by Joost and Thorens, 2001.

The class I transporters consist of the previously identified glucose transporters GLUTs 1-4. Class II comprises the fructose transporter, GULT 5, and three related proteins, GLUT 7, GLUT 9 and GLUT 11, and class III consists of GLUTs 6, 8, 10, 12 and HMIT1 (H^+/myo-inositol co-transporter). As the class II and III proteins have only been identified in recent years, much less is known about these proteins than the class I transporters, thus further discussion will focus on GLUTs 1-4.

As previously stated, GLUT 1 was the first glucose transporter to be isolated. GLUT 1 is expressed at high levels in erythrocyte membranes, and is enriched in brain, placenta and retina. GLUT 1 expression is also observed in muscle and fat, however GLUT 1 expression is very low in liver (Gould and Holman, 1993). It has been reported that GLUT 1 may oligomerise to form tetramers, resulting in cooperativity to further enhance glucose transport (Hebert and Carruthers, 1992). GLUT 2 is expressed at high levels in liver, and is also expressed in pancreatic β-cells, kidney and the small intestine (Gould and Holman, 1993). The primary functions of GLUT 2 are to permit the release of glucose from the liver during fasting states and glucose sensing in the pancreas. GLUT 3 is predominantly expressed in brain, but with lower levels found in placenta, liver, heart and kidney (Gould and Holman, 1993). GLUT 3 expression overlaps somewhat with the tissue expression pattern of GLUT 1, and it is possible these proteins act in concert to meet the energy requirements of these tissues. GLUT 4 is also known as the insulin responsive glucose transporter as it is found in the insulin sensitive tissues, muscle and adipose tissue. In the basal state GLUT 4 is sequestered in intracellular vesicles and insulin promotes an increase in glucose transport by promoting the translocation of GLUT 4 to the plasma membrane (see section 1.1.3 and Pessin et al., 1999).

1.1.2 Structure of the facilitative glucose transporters

Although no GLUT crystal structure is available, a model, based on the sequence of GLUT 1 has been proposed (Mueckler et al., 1985) and all of the GLUTs identified appear to fit this model (Joost and Thorens, 2001). The GLUTs are composed of 12 membrane spanning α-helices, with both the N- and C- termini being located intracellularly (see figure 1.2). A large intracellular loop between helices 6 and 7 divides the transporter into two N- and C- terminal halves. The remainder of the

intracellular loops are short (8-12 residues) and place severe constraints on the structure of the molecule. It has been proposed that the transporter may form a bilobal structure, each lobe consisting of the 6 helices from either the N- or C-terminal domains (Bell et al., 1993). However, recent studies using molecular modelling of GLUT 1 have suggested a somewhat different structure for these transporters (Zuniga et al., 2001). The authors suggest helices 1-5, 8 and 10-12 form a 9 membered barrel-like structure, with helix 7 projecting into the channel. They also report the presence of two channels in the molecule. One channel traverses the whole molecule, which they suggest may be the glucose channel. The second channel is open only at the endofacial site, and they suggest this may be a pathway for substrates other than sugars.

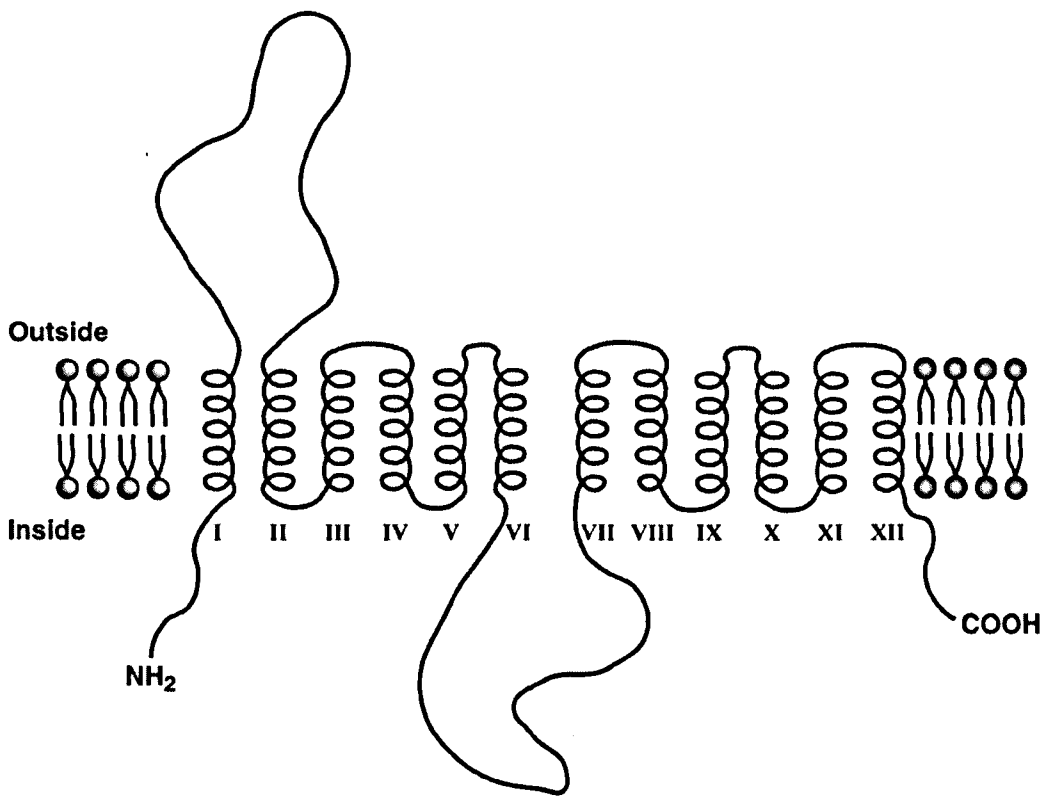

Figure 1.2 Schematic of the proposed structure of the glucose transporters
The molecule is composed of 12 membrane spanning a-helices, and has such an orientation that the N- and C-termini are located intracellularly. A large loop exists between helices 6 and 7 that may separate the molecule into two lobes.

1.1.3 GLUT 4 is stored in intracellular vesicles

Work in the 1980's reported that insulin caused the redistribution of a glucose transporting activity from inside the cell to the plasma membrane in adipocytes (Suzuki and Kono, 1980). The later isolation and characterisation of the insulin responsive glucose transporter GLUT 4 (James et al., 1988, James et al., 1989) helped confirm the hypothesis that insulin recruited glucose transporter proteins to the cell surface. To date, GLUT 4 is still believed to be the major transporter responsible for the insulin-induced increase in glucose uptake into muscle and fat.

It is generally accepted that in the basal state as much as 95% of cellular GLUT 4 resides intracellularly. Under basal conditions GLUT 4 is suggested to continually recycle between this intracellular location and the plasma membrane. The action of insulin has been reported to promote a large increase in the rate of GLUT 4 exocytosis from this intracellular compartment and a somewhat smaller decrease the rate of GLUT 4 internalisation by endocytosis of the transporter (Satoh et al., 1993). Hence, the result is an increased number of transporters at the plasma membrane.

Much research has focused on the nature of the intracellular GLUT 4-storage compartment and how it is recruited to the plasma membrane in response to insulin. GLUT 4 has been reported to be located in various intracellular structures including the trans-Golgi network, (TGN), the endosomal system, clathrin-coated vesicles and small vesicle and tubulo-vesicular structures (Pessin et al., 1999). However, Livingstone et al. (1996) suggested that only around 40% of GLUT 4 is co-localised with the transferrin receptor in the recycling endosomes. It was suggested that the remaining intracellular GLUT 4 may be present in vesicles that are distinct from the recycling endosomes, and which are specifically translocated to the plasma membrane in response to insulin (see figure 1.3). GLUT 4 vesicles also contain the insulin responsive aminopeptidase (IRAP), which is transported in a manner similar to GLUT 4 (Ross et al., 1996) and has been a useful marker in studying GLUT 4 vesicle trafficking. These vesicles also contain a number of proteins that are most likely involved in the insulin regulated trafficking of these GLUT 4 storage vesicles.

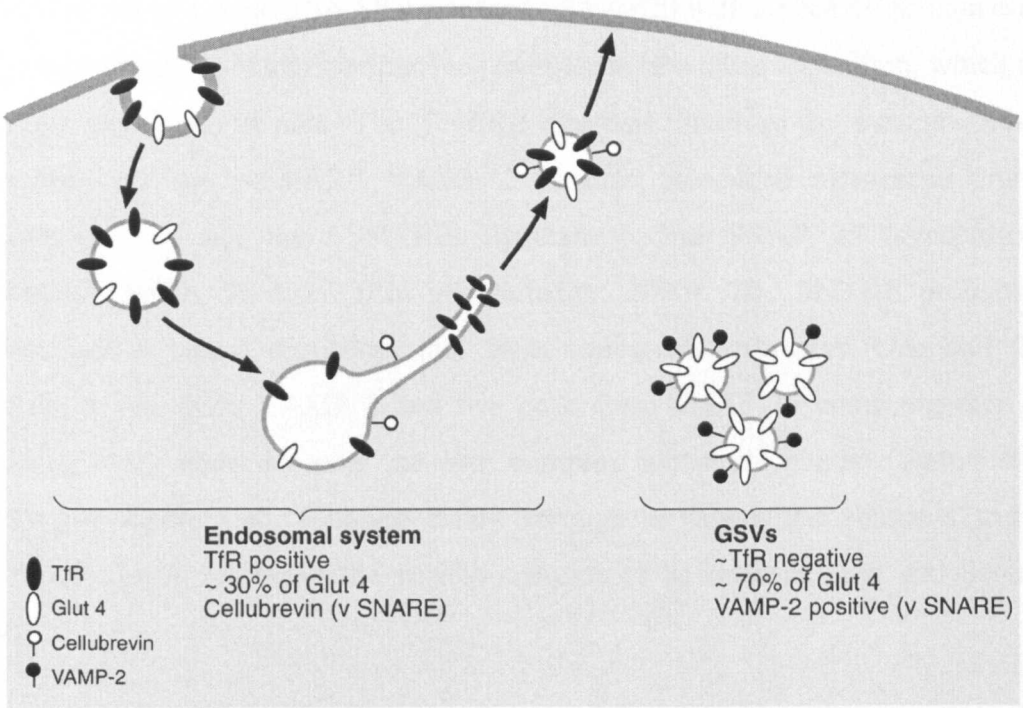

Figure 1.3 GLUT 4 has a distinct sub-cellular localisation

GLUT 4 is found in the endosomal compartment, co-localised with the transferrin receptor (TfR). However GLUT 4 is also present in distinct GLUT 4 storage vesicles (GSVs) that lack the transferrin receptor.

1.1.4 GLUT 4 vesicle trafficking

Much of the knowledge of GLUT 4 vesicle trafficking has come from analogy with the well-characterised system of synaptic vesicle exocytosis. This process involves the mobilisation of synaptic vesicles from within the pre-synaptic cell. These vesicles then tether or dock with the plasma membrane, and following fusion of the vesicle membrane with its target plasma membrane (a process which is triggered by a rise in intracellular Ca^{2+}), the vesicle contents are released. Recycling of the synaptic vesicle components then occurs by endocytosis (Lin and Scheller, 2000).

In eukaryotic cells, all intracellular membrane fusion events appear to be regulated by a conserved set of proteins called SNAREs (soluble NSF attachment protein

receptor, where NSF is N-ethyl-maleimide-sensitive fusion protein). It is thought that the interaction of a vesicle SNARE protein (v-SNARE) with a SNARE protein on the target membrane (t-SNARE) brings the membranes into close apposition, which may promote membrane fusion. The SNARE proteins involved in synaptic vesicle exocytosis are the v-SNARE VAMP 2 (vesicle associated membrane protein-2)/synaptobrevin and the t-SNAREs syntaxin 1 and SNAP 25 (synaptosomal associated protein, 25 kDa) (Lin and Scheller, 2000). The SNARE proteins all contain heptad repeat sequences that form coiled-coil structures. One coil from syntaxin 1, one from VAMP 2 and two coils from SNAP 25 come together in a zippering mechanism, forming the core complex four-helix bundle (Sutton et al., 1998) (see figure 1.4). Calcium influx through voltage-gated channels triggers membrane fusion, allowing the vesicle contents to be released (Lin and Scheller, 2000).

In addition to SNARE proteins, various other proteins have been implicated in regulating vesicle fusion, for example, the small GTP binding Rab proteins have been suggested to function in nucleation of the complex (Chen and Scheller, 2001). Furthermore, the ATPase NSF and the adapter protein α-SNAP (soluble NSF attachment protein) are required in disassembly of the SNARE complex (Chen and Scheller, 2001) and likely function after membrane fusion to allow recycling of SNAREs to their appropriate compartments. Another important protein is Munc18a/nSec1, which interacts with monomeric syntaxin 1, forming a complex that is mutually exclusive with SNARE complex formation. The role of Munc18a/nSec1 in membrane fusion has been controversial and this protein may have both positive and negative effects on SNARE complex formation, by controlling the availability of syntaxins (Misura et al., 2000).

Translocation of GLUT 4 to the plasma membrane is presumed to occur by regulated exocytosis of GLUT 4 vesicles in a manner similar to that described for synaptic vesicle exocytosis. GLUT 4 vesicles are enriched in the v-SNARE VAMP 2, which appears to be required for insulin stimulated GLUT 4 translocation (Pessin et al., 1999). Syntaxin 4 and SNAP 23 are enriched in plasma membranes of muscle and fat cells and various studies have implicated these proteins as the t-SNAREs involved in this process (Pessin et al., 1999). Another important protein involved in GLUT 4-

vesicle fusion is Munc18c (a homologue of Munc18a/nSec1) which interacts with syntaxin 4. Synip has also been implicated in GLUT 4 vesicle fusion and is another syntaxin 4 binding protein which may represent a target for insulin regulation of SNARE complex assembly (Pessin et al., 1999).

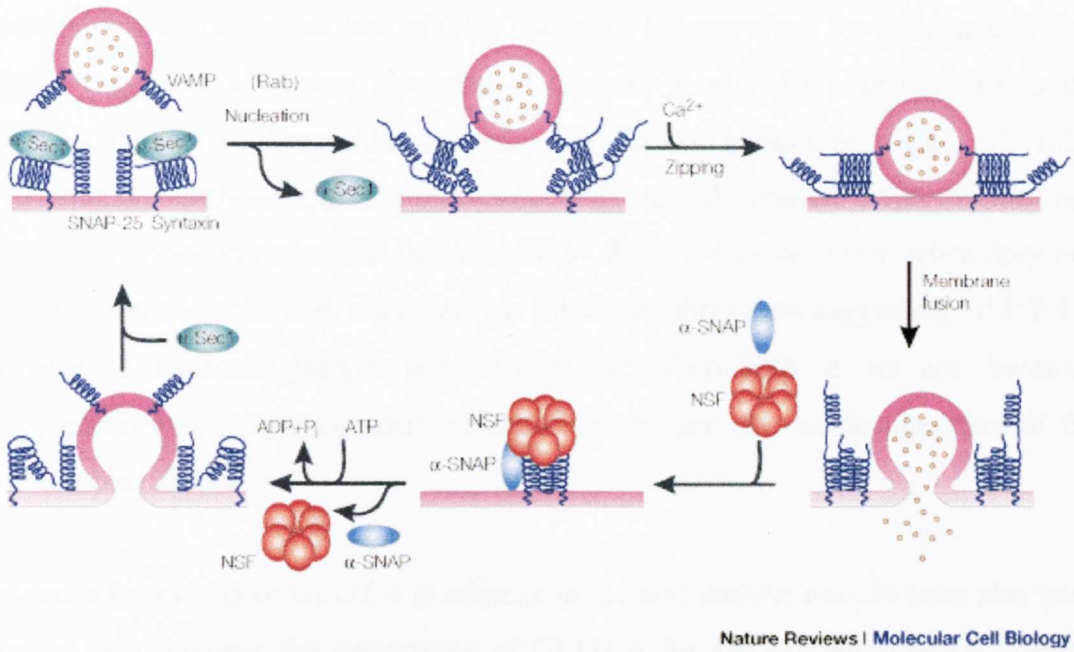

Figure 1.4 **Vesicle fusion is driven by SNARE proteins** (taken from Chen and Scheller, 2001), see text for details.

Although much is known about the transport of GLUT 4 to the plasma membrane, many questions still remain unanswered. For example, what is the exact nature of the intracellular storage compartment? As calcium influx does not appear to be the signal that causes fusion of the GLUT 4 vesicle with the plasma membrane, what is the signal? Does the role of the SNARE proteins in bringing the membrane into close apposition drive membrane fusion or is another signal required? As much effort is focused on studying these processes these questions will likely be answered in due course.

1.1.5 Studies of GLUT 4 knockout mice

To determine the role of GLUT 4 in glucose homeostasis various knockout mouse models have been created in which GLUT 4 expression is disrupted. Surprisingly the

whole body GLUT 4 knockout did not develop diabetes (Katz et al., 1995). GLUT 4-null mice were smaller than control animals and exhibited decreased adipocyte mass, cardiac hypertrophy and died within 5-7 months, likely due to the cardiac abnormalities. These mice also developed hyperinsulinaemia in the fed state and increased expression of GLUT 2 was observed in liver and GLUT 1 in heart tissue (Katz et al., 1995), suggesting the GLUT 4-null mice develop compensatory mechanisms to counter the loss of GLUT 4. Mice heterozygous for the expression of GLUT 4 (GLUT $4^{+/-}$) were also studied (Stenbit et al., 1997). In contrast to the GLUT 4 null mice, these mice did develop a diabetic phenotype. GLUT $4^{+/-}$ mice exhibited hyperglycaemia, hyperinsulinaemia, and developed hypertension and insulin resistance in peripheral tissues such as skeletal muscle. Thus, when only one GLUT 4 allele is disrupted, mice develop a diabetic phenotype suggesting GLUT 4 is required to maintain glucose homeostasis, but when both alleles are disrupted compensatory mechanisms ensue which somehow prevent the development of the diabetic phenotype.

Selective knockouts of GLUT 4 in adipose tissue and skeletal muscle have also been studied to investigate the importance of GLUT 4 for glucose homeostasis in these tissues. Mice with a GLUT 4 knockout in adipose tissue showed normal growth, and had normal adipose tissue mass, despite having greatly reduced insulin-stimulated glucose uptake in adipose tissue (Abel et al., 2001). These mice developed insulin resistance in liver, with the inability of insulin to suppress hepatic glucose output, and in muscle, in that *in vivo* glucose uptake was greatly reduced in response to insulin. In contrast, insulin stimulated glucose uptake in skeletal muscle was normal when studied *ex vivo*, and the authors suggest the possible release of specific molecules from fat cells may cause these effects in skeletal muscle. Whole body glucose uptake was also decreased by up to 50% due to reductions in glycolysis and glycogen synthesis. Hence the adipose specific GLUT 4 knockout mice became glucose intolerant and hyperinsulinaemic. Therefore there is a requirement for GLUT 4 in adipose tissue to maintain normal glucose homeostasis. Specific knockout of GLUT 4 in skeletal muscle resulted in development of a phenotype similar to that observed in the adipose specific GLUT 4 knockout suggesting adipose tissue and skeletal muscle are similarly involved in regulation of glucose homeostasis. In muscle specific GLUT 4 knockout mice, neither insulin nor contraction could elicit

an increase in glucose transport (Zisman et al., 2000). However, glucose uptake into liver was increased by around 450%, with a similar increase in glycogen content, but no alterations in glucose uptake in adipose tissue were observed, suggesting the liver partially compensates for the lack of glucose uptake by muscle. These mice also developed hyperglycaemia and hyperinsulinaemia with a subset developing severe diabetes.

1.2 Insulin signalling

The major role of insulin is in regulation of blood glucose concentration, which in humans is strictly controlled and maintained. Blood glucose concentration is typically around 4 mM in the fasting state and increases to around 7-8 mM in the fed state. As blood glucose concentration increases, following ingestion of a meal, insulin is released by the pancreatic β-cells, and acts in a number of ways to lower blood glucose level. Insulin acts on muscle and fat causing increased glucose uptake and acts on liver to suppress hepatic glucose output. Insulin stimulates the storage of substrates in muscle, adipose tissue and liver by stimulating lipogenesis, glycogen synthesis and protein synthesis and inhibiting lipolysis, glycogenolysis and protein breakdown. Insulin also prevents gluconeogenesis in the liver.

As much as 75% of insulin-dependent glucose disposal may occur in skeletal muscle, with only a small percentage occurring in adipose tissue. Therefore, insulin resistance (as is observed in diabetes and the metabolic syndrome) in the peripheral tissues can lead to elevations in blood glucose concentration.

Diabetes mellitus is a disease in which insulin is not secreted in sufficient amounts or does not efficiently stimulate its target cells, resulting in elevated blood glucose levels. There are two forms of diabetes. Type 1 (insulin dependent) diabetes is an autoimmune disorder in which the β-cells of the pancreas are destroyed, resulting in loss of insulin secretion. Type 2 (non-insulin dependent) diabetes is characterised by insulin resistance and/or abnormal insulin secretion and is associated with a sedentary lifestyle and obesity. Therefore in order to combat these diseases a precise knowledge of how insulin functions at the cellular level is required.

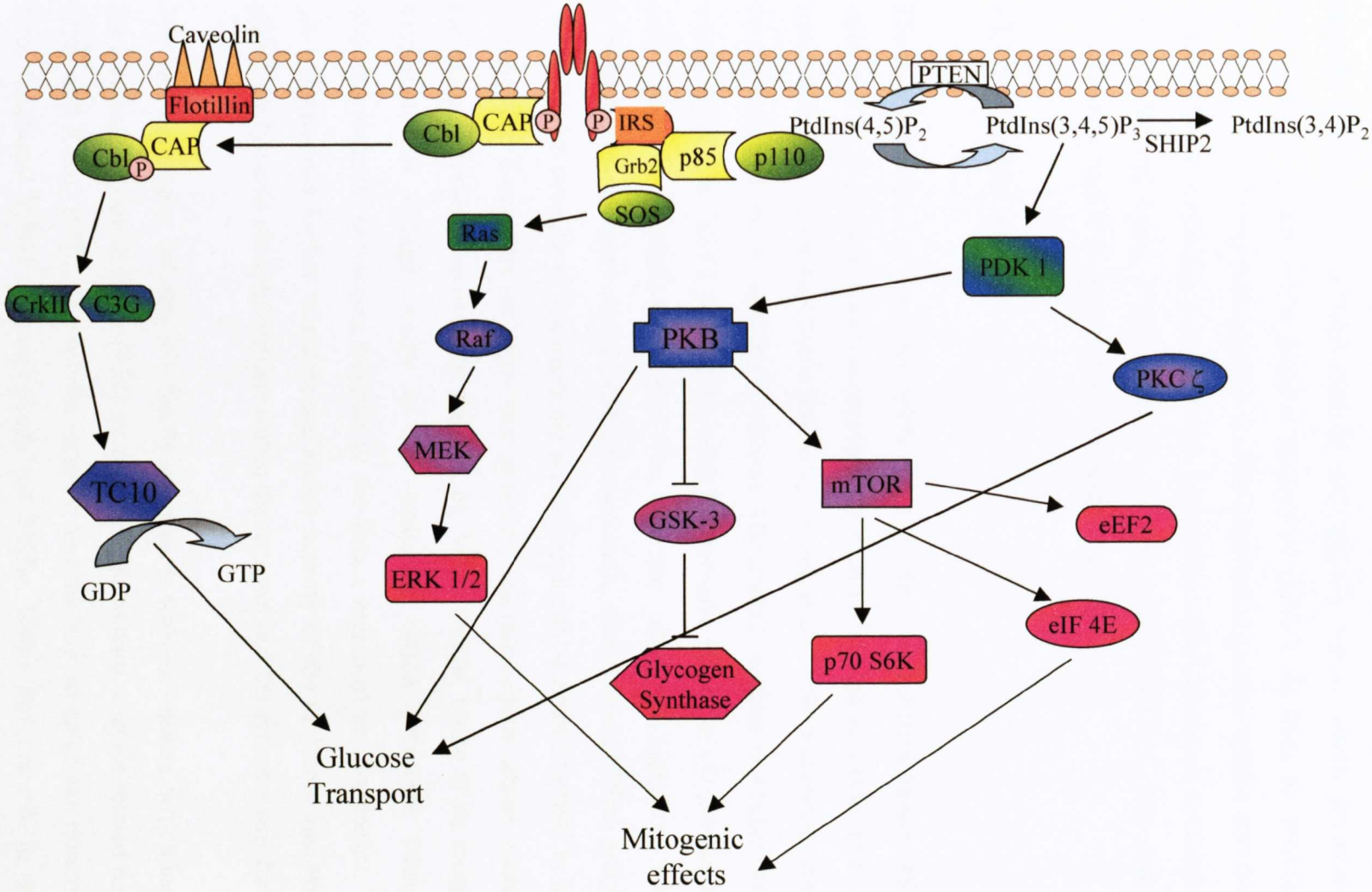

Figure 1.5 Schematic representation of the insulin signalling pathways

Insulin's actions on the various tissues described involves a huge number of molecules which participate in a highly specialised and complex signalling cascade (see figure 1.5). For example, as previously described, insulin activates a signalling cascade described in skeletal muscle and adipose tissue, which promotes the movement of a specialised glucose transporter (GLUT 4) from an intracellular location to the plasma membrane to facilitate increased glucose uptake into the cell. Insulin also activates the processes that lead to increased glycogen synthesis, and inhibits the processes, which culminate in glycogen breakdown. The signalling cascades involved in these processes are described below.

1.2.1 The insulin receptor

The insulin receptor is expressed fairly ubiquitously in mammalian tissues, with the most insulin responsive tissues expressing the receptor at highest levels. The insulin receptor is initially produced as a pro-receptor, and proteolytic processing results in the formation of one α– and one β-subunit. The mature receptor is a heterotetramer consisting of 2 α– and 2 β–subunits, with 2 α-subunits linked to a β-subunit and to each other by disulphide bonds. The receptor also has complex N-linked carbohydrate side chains capped with terminal sialic acid residues (White and Kahn, 1994). The α-subunits of the molecule are extracellular, and are involved in insulin binding. The β-subunits are membrane spanning, the intracellular region containing the receptor tyrosine kinase (see figure 1.6). When insulin binds to its receptor a conformational change occurs in the molecule, which promotes trans-auto-phosphorylations on tyrosine residues in the kinase region of the β-subunits. These phosphorylations further stimulate the kinase activity of the molecule and promote additional tyrosine phosphorylation within the receptor and the receptor substrates.

The insulin receptor belongs to a family of receptor tyrosine kinases, which includes the insulin-like growth factor (IGF) receptor and the insulin receptor-related receptor (Patti and Kahn, 1998). The insulin receptor and the IGF receptor can dimerise, to form functional hybrid receptors (Soos and Siddle, 1989). For example in skeletal muscle the insulin receptor is in excess, therefore the IGF receptor exists largely as hybrids with the insulin receptor, while a large number of classical insulin receptors

are also present (Bailyes et al., 1997). Hybrid receptors bind both insulin and IGF-1, but they have been shown to have lower affinity for insulin than does an insulin receptor homodimer (Soos et al., 1993). However, the functional significance of these hybrids is not known.

While the insulin and IGF receptors activate similar pathways in a number of cell types, these receptors presumably also have distinct roles. In order to delineate distinct roles for the insulin receptor, various insulin receptor knockout mice have been studied. The insulin receptor knockout mouse ($IR^{-/-}$) was developed independently by two groups (Accili et al., 1996 and Joshi et al., 1996). $IR^{-/-}$ mice (which expressed no functional insulin receptors) were born with expected frequency and were indistinguishable from their control littermates suggesting that insulin receptors are not required for embryonic development. From birth the mutant mice showed growth retardation, skeletal muscle hypotrophy and liver steatosis (Joshi et al., 1996). They developed severe hyperglycaemia, hyperinsulinaemia and ketoacidosis (Accili et al., 1996, Joshi et al., 1996) which resulted in death a few days after birth.

To determine the role of the insulin receptor more specifically at the tissue level, a number of tissue specific knockout mice have been produced. Mice with a skeletal muscle knockout of the insulin receptor (MIRKO mice) were developed in which insulin receptor expression was reduced by around 95% in skeletal muscle (Bruning et al., 1998). These mice had increased serum triglycerides and free fatty acids (characteristics of the metabolic syndrome) and increased adipocyte mass, however blood glucose, serum insulin and glucose tolerance appeared to be normal (Bruning et al., 1998). Hence, the authors suggested skeletal muscle insulin resistance may contribute to the altered fat metabolism observed in type 2 diabetes and other tissues may also have roles in insulin regulated glucose disposal. Furthermore, insulin-stimulated glucose uptake in adipocytes was shown to be increased in the MIRKO mouse (Kim et al., 2000), suggesting a partial compensatory mechanism for the loss of insulin receptors in muscle which likely leads to increased adiposity and development of the pre-diabetic syndrome.

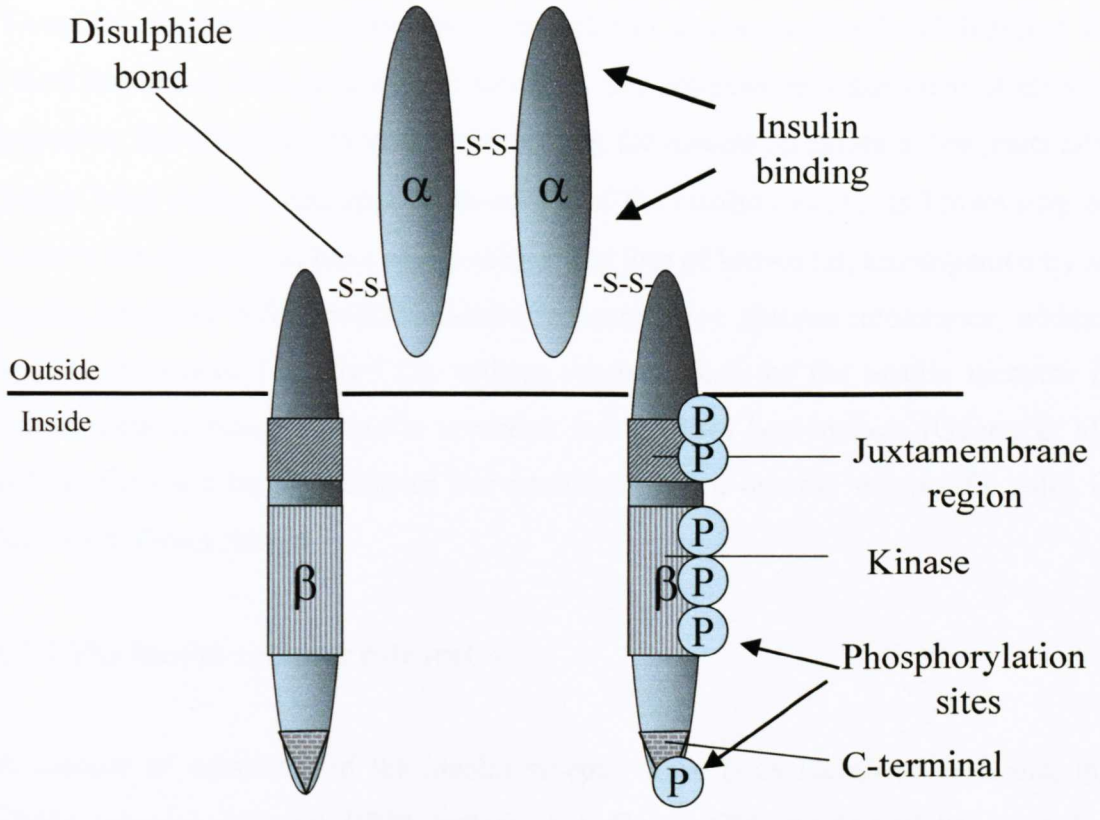

Figure 1.6 Schematic of the insulin receptor

The insulin receptor is a heterotetramer of α and β subunits, linked by disulphide bonds. The α-subunits are extracellular and contain the insulin-binding region. The β-subunits are membrane spanning and contain the kinase and juxtamembrane regions, which are subject to phosphorylation on activation of the molecule.

Tissue specific knockout of the insulin receptor in hepatocytes resulted in a failure of insulin to suppress hepatic glucose output resulting in mild fasting hyperglycaemia and resistance to the blood glucose lowering effects of insulin (Michael et al., 2000). Mice were also hyperinsulinaemic due to increased insulin secretion from the pancreas and decreased insulin clearance by the liver. As these mice aged, liver function decreased resulting in the development of fasting hypoglycaemia (Michael et al., 2000). The authors suggest that liver insulin receptor function is required to maintain glucose homeostasis, but defects in other tissues are required for development of diabetes.

Tissue specific knockout of the insulin receptor in pancreatic β-cells (Kulkarni et al., 1999) resulted in defects in insulin secretion and progressive impairment of glucose tolerance, indicating a role in glucose sensing for insulin receptors in the pancreatic β-cell. Mice with a tissue specific knockout of the insulin receptor in brown adipose tissue were observed to have an age-dependent loss of brown fat, accompanied by an insulin secretion defect, which resulted in progressive glucose intolerance, without insulin resistance. Therefore the authors suggest roles for the insulin receptor in brown adipose tissue in insulin secretion and glucose homeostasis (Guerra et al., 2001). Thus the insulin receptor has been assigned a number of specific roles in various different tissues.

1.2.2 The insulin receptor substrates

A number of substrates of the insulin receptor have been identified including the insulin receptor substrate (IRS) proteins 1-4, Gab-1, Cbl and Shc (Patti and Kahn, 1998) which act to link the insulin receptor to a number of signalling pathways (see figure 1.5). The juxtamembrane region of the insulin receptor (see figure 1.6) is thought to be of importance in substrate (IRS protein) binding. At least one tyrosine residue in this region (Tyr 960), lying within an NPXY motif (where X is any amino acid), is known to be auto-phosphorylated on ligand binding. Mutation of this residue was reported to interfere with downstream signal transduction (White et al., 1988), presumably due to disruption of substrate (e.g. IRS-1) binding.

IRS-1 is a large (180 kDa) cytosolic protein, which contains 21 potential tyrosine phosphorylation sites and also contains over 30 potential serine/threonine phosphorylation sites (White and Kahn, 1994). At least 8 of these tyrosine residues are phosphorylated by the activated insulin receptor (Sun et al., 1993). The phosphorylated tyrosine residues on IRS-1 then act as 'docking sites' for proteins containing SH2 (src homology 2) domains. Many of the SH2 domain-containing proteins are adapter molecules (for example, the p85 subunit of PI3-kinase, and Grb 2) which act to recruit other downstream signalling molecules to the complex.

The IRS proteins are highly homologous and various studies have been performed to delineate the roles of the individual proteins. Knockout mice have been created

which lack IRS-1 (Tamemoto et al., 1994, Araki et al., 1994). IRS-$1^{-/-}$ mice were smaller than their control littermates at birth and this growth retardation continued into post-natal development. Deletion of IRS-1 caused peripheral insulin resistance and glucose intolerance and the mice also exhibited hyperinsulinaemia. In the absence of IRS-1, IRS-2 became tyrosine phosphorylated and bound PI3-kinase in response to insulin (Araki et al., 1994). In mice lacking IRS-2 the diabetic phenotype was much more severe (Withers et al., 1998). IRS-$2^{-/-}$ mice were only around 10% smaller than their wild type littermates (a difference which persisted throughout their development). However, IRS-$2^{-/-}$ mice exhibited insulin resistance in skeletal muscle and liver, fasting hyperglycaemia and glucose intolerance. IRS-$2^{-/-}$ mice had significantly reduced β-cell mass and due also to the presence of insulin resistance, development of severe diabetes ensued (Withers et al., 1998). In contrast to the increased PI3-kinase activity associated with IRS-2 in the IRS-1 null mice, a 50% reduction in insulin stimulated PI3-kinase associated IRS-1 was observed in the IRS-2 null mice (Withers et al., 1998). Therefore, whilst the roles of IRS-1 and IRS-2 overlap somewhat they also appear to be distinct. For example there is a greater requirement for IRS-1 than IRS-2 for embryonic and post-natal growth. IRS-2 on the other hand is required to prevent development of diabetes by regulation of β-cell mass and in shaping insulin responsiveness of the peripheral tissues. In contrast to the phenotypes of the IRS-1 and IRS-2 null mutants, mice lacking functional IRS-3 showed no abnormalities in growth, blood glucose or insulin levels (Liu et al., 1999). IRS-4 null mice showed only mild defects in growth, reproduction and glucose homeostasis (Fantin et al., 2000). This suggests there may be some redundancy in the roles of IRS-3 and IRS-4, and recently it has been suggested that IRS-3 and IRS-4 may have roles in negative regulation of IRS-1 and IRS-2 (Tsuruzoe et al., 2001).

1.2.3 Phosphoinositide 3-kinases

A number of growth factors (including insulin and IGF-1) activate phosphoinositide 3-kinases (PI3-kinases), leading to a rise in 3-phosphorylated inositol lipids in the cell (Vanhaesebroeck et al., 1997). These lipids are thought to act as intracellular signalling molecules, which activate downstream signalling cascades.

PI3-kinase was originally identified as a PtdIns (phosphatidylinositol) kinase activity associated with viral oncoproteins and was reported to have a role in cell transformation (Cantley et al., 1991). PI3-kinases catalyse the phosphorylation of the D-3 position of the inositol ring resulting in the formation of PtdIns(3)P from PtdIns, PtdIns(3,4)-P_2 from PtdIns(4)P and PtdIns(3,4,5)P_3 from PtdIns(4,5)P_2 (Whitman et al., 1988, Auger et al., 1989, Carpenter et al., 1990) (see figure 1.7).

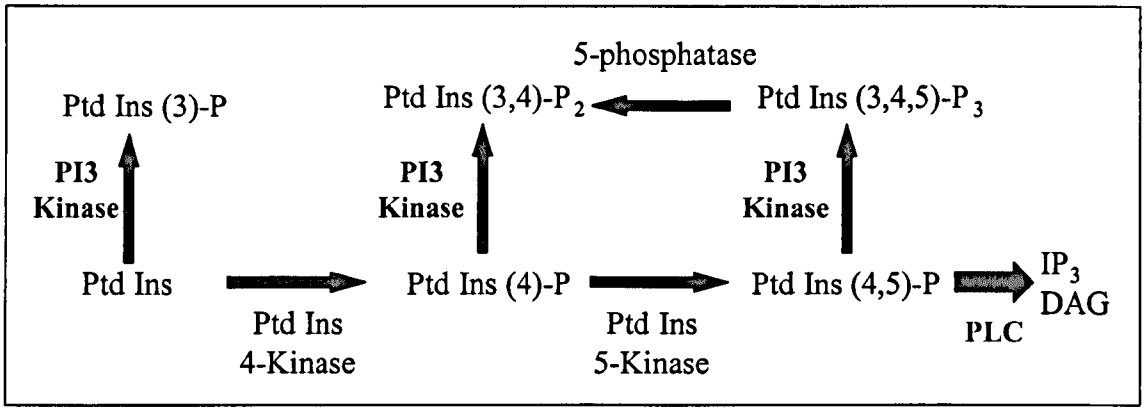

Figure 1.7 Pathways of phosphatidylinositol metabolism

PI3-kinases exist as heterodimers consisting of one regulatory and one catalytic subunit. The p85(reulatory)/p110(catalytic) dimer was the first PI3-kinase to be purified and characterised (Carpenter et al., 1990) and subsequently a number of isoforms of both the catalytic and regulatory subunits have been identified, the mammalian isoforms of which are detailed in table 1.2. The PI3-kinase catalytic subunits have been subdivided into 3 main classes on the basis of their lipid substrate specificity, structure and regulation (reviewed in Vanhaesebroeck et al., 1997). Class I PI3-kinases phosphorylate PtdIns, PtdIns(4)P, and PtdIns(4,5)-P_2 with PtdIns(4,5)-P_2 likely being the preferred substrate, and are further subdivided according to the adapter subunits with which they interact. Class IA PI3-kinases interact with adapter proteins that contain SH2 domains and mediate interactions with phosphorylated tyrosine residues. Class IB PI3-kinases are stimulated by G-protein $\beta\gamma$ subunits and do not interact with SH2 domain containing adapter proteins. Class II PI3-kinases phosphorylate PtdIns, PtdIns(4)P, but not PtdIns(4,5)-P_2 *in vitro* and class III PI3-kinases use only PtdIns as a substrate.

It is likely that class IA PI3-kinases (e.g. a p85α-p110α heterodimer) are the major PI3-kinases activated in response to insulin and IGF-1. The regulatory p85 subunits binds phosphorylated tyrosine residues on IRS proteins which have been recruited to the activated receptor. Adapter protein binding is facilitated by two SH2 domains, which recognise phosphorylated tyrosine within the sequence YxxM (where x is any amino acid), and it is reported that engagement of both SH2 domains is required for recruitment and activation of PI3-kinase (Ottinger et al., 1998). The p85 regulatory subunit also contains an SH3 domain, a proline rich region and a break point cluster (BCR) homology domain (BH) the roles of which are ill defined. The shorter forms of the regulatory molecules (e.g. p55 and p50) also contain two SH2 domains and have the ability to recruit catalytic subunits to proteins containing phosphorylated tyrosine residues. However they lack the SH3 and BH domains, but the functional significance of this is unknown (Shepherd et al., 1998). The class IA catalytic subunits contain the kinase domain and a p85-binding domain. It is likely that the adapter mediated translocation of the PI3-kinase catalytic subunit functions to bring the catalytic region into close proximity with its substrates, which reside in the plasma membrane.

CLASS	CATALYTIC	REGULATORY
IA	p110α p110β p110δ	p85α p85β p55α p55γ p50α
IB	p110γ	p101
II	p170	-
III	-	p150

Table 1.2 **Mammalian PI3-kinase isoforms** (adapted from Vanhaesebroeck et al., 1997)

PtdIns(3,4,5)P_3 is suggested to be the major product formed by class IA PI3-kinases in response to growth factors (Stephens et al., 1991) with PtdIns(4,5)P_2 being produced as a breakdown product. This lipid product is thought to play a role in downstream signalling, for example, increases in PtdIns(3,4,5)P_3 have been shown to occur before activation of downstream signalling events (van der Kaay et al., 1997). Furthermore, the PI3-kinase inhibitors wortmannin and LY294002 were reported to block PtdIns(3,4,5)P_3 production and subsequent activation of downstream processes (Yeh et al., 1995).

It has been suggested that the lipid signal is turned off by a tumour suppresser protein called PTEN (Leslie and Downes, 2002). PTEN is reported to dephosphorylate several phosphoinositides in the D-3 position, but PtdIns(3,4,5)P_3 is suggested to be the most physiologically relevant (Leslie and Downes, 2002). In PTEN null cells, elevated levels of PtdIns(3,4,5)P_3 have been detected concomitant with increased PKB activity (Stambolic et al., 1998). Lipid phosphatases have also been identified which remove phosphates from the D-5 position of inositol lipids, e.g. SHIP and SHIP2. SHIP2 is widely expressed, and is thought to metabolise PtdIns(3,4,5)P_3 to produce PtdIns(3,4)P_2. SHIP2 has been suggested to have a role in insulin sensitivity as SHIP2 null mice have increased insulin sensitivity and glucose tolerance (Clement et al., 2001).

It is generally accepted that activation of PI3-kinase is required to promote GLUT 4 translocation and increased glucose transport in response to insulin. Activation of PI3-kinase can be blocked by the use of inhibitors such as wortmannin and LY294002 and these compounds have been shown to inhibit GLUT 4 translocation and glucose transport (Okada et al., 1994, Cheatham et al., 1994). In addition to this, the presence of a constitutively active PI3-kinase p110 subunit caused translocation of GLUT 4 (Tanti et al., 1996). However, it has been suggested that pathways independent of PI3-kinase may also be necessary to activate GLUT 4 translocation and increase glucose transport (see section 1.2.7.3). For example, PDGF stimulates PI3-kinase activity to a similar extent as insulin, however PDGF does not significantly increase glucose transport (Wiese et al., 1995).

1.2.4 Protein Kinase B

Phosphoinositide signals are received by molecules which contain phosphoinositide binding domains, for example PH (pleckstrin homology) domains and FYVE domains (reviewed in Itoh and Takenawa, 2002). PH domains are around 100 residues in size, and proteins containing a PH domain have been shown to bind a variety of phospholipids, while FYVE domains bind solely to PtdIns(3)P. One molecule which is known to be regulated by insulin (via activation of PI3-kinase and production of PtdIns(3,4,5)P_3) is PKB (protein kinase B).

PKB is the cellular homologue of the product of the oncogene *v-akt*, of the acutely transforming retrovirus AKT8, found in a rodent T-cell lymphoma (Bellacosa et al., 1991). The PKB family contains 3 isoforms, PKBα (also called Akt1), PKBβ (Akt2) and PKBγ (Akt3), which display greater than 80% sequence identity. PKBα and PKBβ are expressed ubiquitously in cells, with PKBγ being expressed at highest levels in brain and testis. Each isoform consists of an N-terminal PH domain and a kinase domain (see figure 1.8).

Activation of PKBα requires phosphorylation of two residues (Alessi et al., 1996), Thr-308, which lies in the T-loop of the kinase domain and Ser-473, which lies in the C-terminal region of the molecule. PKBβ is also activated by dual phosphorylation on residues equivalent to those in PKBα (Thr-309 and Ser-474), while PKBγ lacks the C-terminal extension, and activation occurs only by phosphorylation of the residue equivalent to Thr-308 in PKBα (Thr-305 in PKBγ) (Alessi and Cohen, 1998) (see figure 1.8).

PDK1 (phosphoinositide dependent protein kinase-1) has been identified as the kinase that phosphorylates PKBα on Thr-308 (Alessi et al., 1997). Stokoe et al. (1997), reported that PtdIns(3,4,5)P_3 has a dual role in regulation of PKB function. Inositide binding to the PH domain of PKB was reported to recruit PKB to the membrane, and also cause a conformational change, allowing access of PDK1 to the Thr-308 residue, and phosphorylation to occur, thus stimulating PKB activity. PDK1 is likely also targeted to the plasma membrane by phosphoinositides, via an

interaction with its PH domain. The kinase that phosphorylates Ser-473 is yet to be identified, but has been tentatively named PDK2 (Alessi et al., 1997).

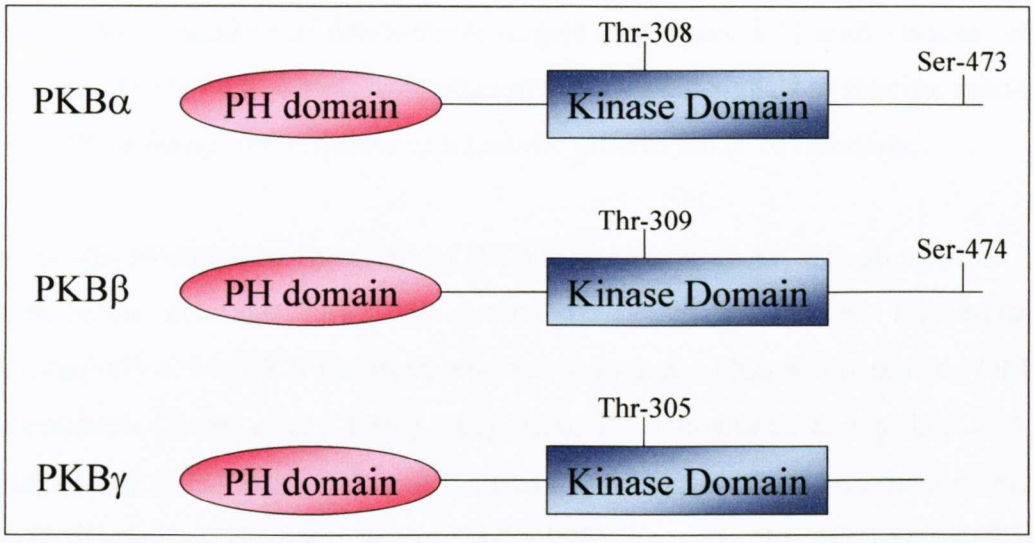

Figure 1.8 **Domain structure of PKB isoforms** (adapted from Alessi et al., 1997)

Despite the fact the PKB proteins exhibit distinct similarities in protein structure and cellular expression patterns, studies in which knockout mice have been generated which lack either the PKBα or PKBβ protein suggest very distinct roles for these proteins. Mice lacking PKBβ (Cho et al., 2001a) were reported to develop some features of Type 2 diabetes. PKBβ null mice displayed mild hyperglycaemia and hyperinsulinaemia and became mildly glucose intolerant. They also displayed mild insulin resistance in adipocytes and some skeletal muscles, elevated hepatic glucose output and increased β-cell mass, consistent with compensation for insulin resistance (Cho et al., 2001a). Thus the authors propose PKBβ is essential for the maintenance of normal glucose homeostasis, but the effects observed were all fairly mild, suggesting other proteins function in pathways similar to or in parallel with PKBβ in regulation of glucose homeostasis. However, mice lacking PKBα did not develop a diabetic phenotype. PKBα null mice had normal blood glucose and normal serum insulin levels (Cho et al., 2001a, Chen et al., 2001). Conversely, mice lacking functional PKBα exhibited defects in both foetal and post-natal growth (Cho et al.,

2001b, Chen et al., 2001) with a number of mice dying within three days of birth and the surviving animals were around 20% smaller than control littermates (Cho et al., 2001b).

As PKB has a number of downstream targets (see figure 1.5) with various cellular functions, it may be that each isoform exists to transmit signals to specific substrates, thus 'personalising' the response to a specific growth factor or hormone.

One of the downstream functions of PKB is suggested to be activation of GLUT 4 translocation although how this occurs is rather ambiguous. Expression of constitutively active PKB has been reported to increase glucose uptake and GLUT 4 translocation (Kohn et al., 1996), suggesting PKB functions to regulate GLUT 4 translocation. It has also been reported that insulin causes the recruitment of PKB to GLUT 4 storage vesicles (Calera et al., 1998), however the exact mechanism by which PKB activates GLUT 4 translocation and glucose uptake is unknown.

1.2.5 PKCs and insulin action

Members of the mammalian protein kinase C (PKC) superfamily have been implicated in a range of cellular processes. They transduce a variety of signals mediated by phospholipid hydrolysis, with the key 'on' switch for most PKCs being diacylglycerol (DAG). A number of PKC isoforms have been implicated in insulin action. For example, some PKCs are suggested to be downstream targets for signals generated by the insulin receptor, whilst others have been suggested to function as negative feedback inhibitors of the insulin receptor and IRS proteins.

The PKCs are a family of serine/threonine kinases comprised of at least 11 members (see table 1.3) in mammals (and many non-mammalian isoforms have also been identified). The isoforms have been further subdivided (conventional, novel and atypical PKCs) on the basis of their enzymatic properties (Mellor and Parker, 1998) (see table 1.3).

The conventional PKC subfamily consists of the α, β_I, β_{II} (the PKC β gene is alternatively spliced, and produces 2 gene products which differ only at the extreme

C-terminus) and γ isotypes. They are activated by phosphatidyl serine (PS) in a Ca^{2+}-dependent manner, and also bind DAG, increasing the specificity for PS and shifting the affinity of Ca^{2+} into the physiological range. Conventional PKCs are activated by the phorbol ester PMA, which eliminates the requirement for DAG and decreases the concentration of Ca^{2+} needed for activation. The novel PKC subfamily is comprised of the ε, η, δ and θ isotypes which are Ca^{2+}-insensitive, but are activated by DAG or phorbol esters in the presence of PS. The atypical subfamily consists of the ι, λ and ζ isoforms. These are also Ca^{2+}-insensitive, and do not respond to phorbol esters or DAG (Mellor and Parker, 1998).

Under basal conditions PKCs exist in a folded state in which a pseudosubstrate sequence in the N-terminal regulatory domain interacts with the substrate-binding site in the catalytic domain of the protein, thus inhibiting the protein (Farese, 2002). On activation of the protein a conformational change occurs and this auto-inhibition is relieved, possibly allowing activation of the protein by phosphorylation by other kinases and by autophosphorylation (Farese, 2002).

SUBFAMILY	ISOFORMS	REGULATION
Conventional	α, β_I, β_{II}, and γ	Activated by PS and DAG Ca^{2+}-dependent
Novel	ε, η, δ and θ	Activated by PS and DAG Ca^{2+}-insensitive
Atypical	ι, λ and ζ	Ca^{2+}-insensitive Not responsive to phorbol esters or DAG Possibly activated by polyphosphoinositides

Table 1.3 The PKC family

Insulin stimulation of a variety of cell types and tissues results in a number of PKC isoforms being translocated to the plasma membrane and/or activated. However, it is suggested that the activation of the atypical PKCs, (PKC ζ, and PKC λ/ι) is

important for increased glucose uptake (Bandyopadhyay et al., 1997a, Bandyopadhyay et al., 1997b, Standaert et al., 1997). Standaert et al. (1997) reported that insulin stimulation of PKC ζ was PI3-kinase dependent and resulted in PKC ζ autophosphorylation, an action which could also be mimicked by phosphoinositides ($PtdIns(3,4)P_2$, $PtdIns(3,4,5)P_3$ and $PtdIns(4,5)P_2$). Furthermore, PKC ζ phosphorylation in the activation loop was reported to be mediated by PDK1 (Le Good et al., 1998, Chou et al., 1998), suggesting PKC ζ is regulated in a manner similar to PKB.

Whilst the conventional and novel PKCs are also thought to be activated by insulin, it is suggested that they function primarily in feedback inhibition of the insulin receptor and IRS proteins (Letiges et al., 2002). It has also been reported that, while PKC ζ functions downstream of PI3-kinase, it may also function in a feedback loop to IRS-1. In NIH-3T3 cells, PKC ζ was shown to phosphorylate IRS-1, this phosphorylation was accompanied by impaired IRS-1-associated PI3-kinase activity (Ravichandran et al., 2001). Thus, while PKCs are implicated in propagating the insulin signal, they may also function in a feedback inhibition loop, to down-regulate the insulin signal.

1.2.6 Regulation of glycogen metabolism by insulin

1.2.6.1 Insulin inactivates GSK-3

GSK (glycogen synthase kinase)-3 was identified in 1980, as a kinase that phosphorylates and inactivates glycogen synthase (Embi et al., 1980). Insulin was subsequently reported to inhibit glycogen synthase by a mechanism that involved phosphorylation of GSK-3 (Cross et al, 1994), and the kinase mediating phosphorylation and inactivation of GSK-3 was identified as PKB (Cross et al., 1995).

Two isoforms of GSK-3 exist, GSK-3α and GSK-3β, which are ubiquitously expressed in mammals. The proteins exhibit 97% sequence similarity in the kinase domain, but vary significantly out-with this region, with GSK-3α having a glycine

rich N-terminal extension (Frame and Cohen, 2001). The residues phosphorylated by PKB in GSK-3, mediating inhibition of the protein, were identified as Ser 21 in GSK-3α and Ser 9 in GSK-3β (Cross et al., 1995).

GSK-3 has numerous substrates, including glycogen synthase, eIF2B (see section 1.1.8.3) and ATP citrate-lyase. GSK-3 appears to use a unique mechanism for substrate recognition. It requires that many of its substrates are first phosphorylated by another kinase before it can undertake phosphorylation of the substrate - it requires a 'priming' phosphate to be present (Cohen and Frame, 2001). This priming phosphate lies four residues C-terminal to the site of GSK-3 phosphorylation, and in the case of glycogen synthase is phosphorylated by casein kinase 2 (Frame and Cohen, 2001). It is this substrate specificity which is utilised by insulin and other growth factors in regulation of GSK-3 activity. When the N-terminal serine residue of GSK-3 is phosphorylated by PKB, this N-terminus can then act as a pseudosubstrate. The pseudosubstrate region is reported to interact with the residues involved in binding the priming phosphate, thus inhibiting the activity of GSK-3 by preventing substrate binding and blocking access to the catalytic site (Frame et al., 2001).

1.2.6.2 Glycogen synthesis

Glycogen synthesis is performed by three enzymes: glycogenin which forms short primer glycogen chains, glycogen synthase which extends the glycogen chains and a branching enzyme, which makes branches on an elongated glycogen chain (Bollen et al., 1998). Glycogen synthase performs the bulk of the glycogen synthesis, transferring glucose units onto the growing glycogen chain, using UDP (uridine diphosphate)-glucose as the glucosyl donor. Glycogen synthase is subject to regulation by allosteric effectors for example, glucose 6-phosphate is a potent allosteric activator of glycogen synthase, and by phosphorylation (phosphorylation causing a decrease in activity of the protein). The muscle isoform has at least nine phosphorylation sites that may be phosphorylated by multiple protein kinases, at least seven of which are located in the C-terminus of the molecule (Lawrence, Jr. and Roach, 1997). GSK-3 is reported to phosphorylate glycogen synthase at three serine residues, termed sites 3a, 3b and 3c (Rylatt et al., 1980), causing its inactivation, an

effect which is inhibited by insulin (Parker et al., 1983). It is suggested that insulin may also function to increase the activity of glycogen-targeted phosphatases that function to dephosphorylate glycogen synthase (Newgard et al., 2000).

1.2.6.3 Glycogen breakdown

Glycogen is degraded by the action of phosphorylase and debranching enzyme (Bollen et al., 1998). Phosphorylase liberates glucose 1-phosphate from the glycogen chain (in the presence of inorganic phosphate), the glucose 1-phosphate being converted to glucose 6-phosphate by phosphoglucomutase, for entry into glycolysis. Glycogen phosphorylase is subject to regulation by allosteric effectors, for example, glucose and glucose 6-phosphate are allosteric inhibitors of phosphorylase, and by phosphorylation (Browner and Fletterick, 1992). Phosphorylase exists in two forms: phosphorylase *a*, which is active and phosphorylase *b*, which is usually inactive (in muscle phosphorylase *b* is active only in the presence of high levels of AMP). Phosphorylase *b* is phosphorylated by phosphorylase kinase which, converts it to phosphorylase *a,* the active form of the enzyme. Dephosphorylation by PP1 returns the enzyme to the inactive conformation (Browner and Fletterick, 1992). It is possible that insulin inhibits glycogen phosphorylase activity by activating PP1.

1.2.7 The role of caveolae in insulin signalling

1.2.7.1 Caveolae, structure and function

Cavoelae are flask-like invaginations in the plasma membrane, which are around 50-100 nm in diameter. Caveolae may also fuse forming larger structures with sizes significantly larger than 100 nm (Smart et al., 1999). Caveolae are a subtype of lipid microdomain referred to as 'lipid rafts' and are abundant in various cell types, including adipocytes (Mastick et al., 1995), endothelial cells (Lisanti et al., 1994), and muscle cells (Chang et al., 1994). Lipid rafts are resistant to solubilisation in cold non-ionic detergents and hence are often referred to as detergent resistant membranes or DRMs (Simons and Toomre, 2000). The detergent insolubility of lipid rafts has greatly facilitated their biochemical characterisation.

Caveolae are enriched in cholesterol and sphingolipids (sphingomyelin and glycosphingolipids). The cholesterol and sphingolipids form a liquid ordered phase, that has a higher melting temperature (Tm) than phospholipid rich domains, and are resistant to detergent solubilisation (Brown and London, 1997). Depending on the cell type, caveolae reportedly contain up to 30% of plasma membrane cholesterol and as much as 95% of cellular sphingomyelin, indicating that these lipids are highly enriched within caveolar microdomains of the plasma membrane. Caveolae are also enriched in a number of signalling lipids including PtdIns(4,5)P_2, ceramide and diacylglycerol. It is thought that the precise lipid composition of caveolae is likely to be different in distinct cell types, and that altering lipid composition may be a way of regulating caveolar function (Smart et al., 1999).

Caveolin is the major structural protein of caveolae and it belongs to a caveolin family of 21-25 kDa proteins. Molecular cloning has identified 3 caveolin genes (caveolin-1, -2 and -3) from which 4 caveolin proteins are transcribed: caveolin-1α and -1β are derived from alternative initiation during translation. Caveolin-1 and -2 are predominantly expressed in adipocytes, endothelial cells and fibroblasts, and caveolin-3 is muscle specific (Okamoto et al., 1998). Caveolin proteins interact to form homo- and hetero-oligomers that bind directly to cholesterol. Caveolin-1 has a central hydrophobic domain (residues 102-134) which is thought to associate with the membrane, with both the N- (residues 1-101) and C- (residues 135-178) termini being completely cytosolic (Okamoto et al., 1998). A region (residues 82-101) within caveolin-1 has been named the scaffolding domain, as it is required for interaction with various caveolar signalling molecules. This scaffolding domain has been shown to interact directly with eNOS (endothelial nitric oxide synthase) (Ju et al., 1997), wild-type Src (c-Src) (Li et al., 1996), α-subunit of G-proteins (Li et al., 1995), and a number studies suggest that this interaction with caveolin-1 scaffold domain causes inactivation of these proteins. Other caveolin interacting proteins include Ha-Ras, many Src-family tyrosine kinases, the EGF receptor and related receptor tyrosine kinases, PKC isoforms and the insulin receptor (Anderson, 1998). Therefore, the role of caveolae may be to concentrate various signal transducers within a distinct region of the plasma membrane, and functionally regulate their activation state.

To further define the function of caveolae/caveolin, mice deficient in caveolin-1 have been produced (Razani et al., 2001, Drab et al., 2001). Caveolin-1 null mice are viable, but lack caveolae. Expression of caveolin-2 protein is reduced, and the remaining caveolin-2 is retained in an intracellular compartment (Razani et al., 2001), suggesting the presence of caveolin-1 is required for caveolin-2 oligomerisation and plasma membrane localisation. Caveolin-1 is expressed at high levels in lung tissue and these caveolin-1 knockout mice displayed various lung abnormalities including endothelial cell hyperproliferation and thickening of the alveolar septa, which resulted in a reduction in physical ability (Razani et al., 2001, Drab et al., 2001). eNOS has been suggested to be inhibited by caveolin-1 and in caveolin-$1^{-/-}$ mice nitric oxide release was increased, due to an increase in eNOS activity (Razani et al., 2001) and abnormalities in calcium signalling were observed in the cardiovascular system (Drab et al., 2001). Caveolin-1 null mice have a tendency to be smaller than their wild type littermates and were shown to be resistant to diet induced obesity (Razani et al., 2002a). They were shown to have smaller fat pads, although levels of serum insulin, glucose and cholesterol were all normal. However, caveolin-1 deficient mice have elevated triglycerides and free fatty acids, although lipoprotein lipase activity was normal. Hence the authors propose a role for caveolin-1 in lipid homeostasis.

To dissect any functional differences between caveolin-1 and caveolin-2, caveolin-2 null mice were created. In these mice caveolae still form with little change in expression of caveolin-1 protein observed (Razani et al., 2002b) unlike in the caveolin-1 knockout where caveolin-2 expression was greatly reduced. Caveolin-2 mice exhibit similar lung abnormalities to those reported for the caveolin-1 knockout and the authors suggest the lung abnormalities observed in the caveolin-1 knockout are likely due to the concomitant decrease in caveolin-2 expression and suggest a specific role for caveolin-2 in pulmonary function.

Mice deficient in caveolin-3 have also been created (Galbiati et al., 2001). Caveolin-3 is muscle specific and associates with dystrophin and dystrophin-associated glycoproteins and in humans mutations in caveolin-3 have been reported to result in development of a form of limb girdle muscular dystrophy (Volonte et al., 1999). Caveolin-3 null mice were shown to lack sarcolemmal caveolae and the loss of

caveolae from muscle cells resulted in loss of the dystrophin-glycoprotein complex from lipid raft domains and alterations in T-tubule organisation. Thus, caveolin-3 is required to maintain the integrity of the skeletal muscle architecture.

1.2.7.2 Insulin receptors are localised in, and signal from, caveolae

Insulin receptors are localised in caveolae by interaction with caveolin, but unlike a large number of proteins that are sequestered and inactivated in caveolae, it has been suggested that the insulin receptor is positively modulated by caveolar association. In 1999, Gustavsson and colleagues showed using immunogold electron microscopy and immunofluorescence microscopy, that insulin receptors are highly enriched in caveolae, and co-localise with caveolin in the plasma membrane of adipocytes. They reported that insulin receptors are functional in caveolae and indeed suggested that signalling through the insulin receptor was dependent upon caveolar association. This work supported previous studies showing that the insulin receptor co-fractionates with caveolae (Yamamoto et al., 1998) and that caveolin is an activator of the insulin receptor (Yamamoto et al., 1998). It has recently been reported that the insulin receptor catalyses the phosphorylation of caveolin-1 on tyrosine 14 (Kimura et al., 2002) although the functional significance of this is not yet understood.

1.2.7.3 The CAP-Cbl pathway of insulin signalling

For a number of years investigators believed that activation of PI3-kinase was the major or only pathway required to promote insulin-stimulated GLUT 4 translocation to the plasma membrane. For example, blocking PtdIns(3,4,5)P_3 generation by PI3-kinase prevented this insulin-stimulated GLUT 4 translocation (Cheatham et al., 1994, Sharma et al., 1998). However, a number of studies suggested that activation of PI3-kinase dependent and independent mechanisms may be required for increased glucose transport to occur. For example, inhibition of insulin stimulated IRS-PI3-kinase complex formation does not necessarily inhibit glucose uptake (Sharma et al., 1997), and in adipocytes, stimulation of integrin receptors mimics insulin action by recruiting PI3-kinase to IRS proteins, and activates the downstream effector PKB, without effecting GLUT 4 movement (Guilherme and Czech, 1998).

Thus, it was hypothesised that PI3-kinase independent pathways exist and Baumann and colleagues (2000) recently identified components of such a pathway (see figure 1.5). The pathway suggested involves the recruitment of an adapter protein, APS, to the activated insulin receptor. APS in turn recruits a protein called Cbl (Liu et al., 2002) and Cbl associated protein (CAP). Cbl is phosphorylated on recruitment to the insulin receptor. On phosphorylation of Cbl, the CAP-Cbl complex translocates to a lipid raft domain (Baumann et al., 2000), the translocation being mediated through the interaction of the sorbin-homology domain of CAP with flotillin, a protein enriched in lipid rafts, (Kimura et al., 2001). This localisation is likely to be needed for activation of glucose transport as a CAP deletion mutant that does not interact with flotillin (CAPΔSoHo) prevents insulin stimulated glucose transport (Kimura et al., 2001). Cbl is reported to recruit the CrkII-C3G complex to the lipid raft domain (Chiang et al., 2001), CrkII is an adapter protein, and C3G a guanine nucleotide exchange factor. C3G activates the small GTP-binding protein TC10, a process which is independent of PI3-kinase activation (Chiang et al., 2001). The authors report activation of TC10 to be essential for insulin-stimulated glucose uptake and GLUT4 translocation. They also suggest this pathway functions in parallel with the PI3-kinase pathway to stimulate GLUT 4 translocation in response to insulin. Further studies on TC10 (Chiang et al., 2002) suggest a role in the regulation of cortical actin structure, which may have a role in movement of GLUT 4 vesicles. A recent report details the identification of a TC10 interacting protein (CIP4/2), which is also required for insulin-stimulated GLUT 4 translocation (Chang et al., 2002). The functional significance of this interaction is not known, however CIP4/2 is suggested to act as an adapter protein, recruiting additional molecules to the plasma membrane in response to insulin, which may influence the trafficking of GLUT 4 vesicles (Chang et al., 2002).

1.2.8 Mitogenic actions of insulin

The insulin-regulated proteins described thus far are mainly involved in the actions of insulin to increase glucose uptake into the cell. However, insulin also acts to increase cell proliferation and protein synthesis.

1.2.8.1 Signalling via the MAP kinase pathway

p42/44 mitogen activated protein (MAP) kinases (ERK2/ERK1) are ubiquitously expressed in mammalian cells and activation results from a number of external stimuli. Activation of the MAP kinase pathway occurs via the adapter protein Grb2, which is recruited to the activated insulin receptor via an interaction with IRS-1 (Skolnik et al., 1993). Alternatively Grb2 can be recruited through an interaction with Shc, a 60 kDa adapter molecule which is a substrate for the insulin receptor kinase (Goalstone and Draznin, 1998). Grb2 recruits the guanine nucleotide exchange factor SOS to the activated receptor, via an interaction of the SH3 domain of Grb2 with a proline rich region in SOS. Recruitment of Grb-2/SOS to the plasma membrane brings the complex into close proximity to the small G-protein Ras, a substrate of SOS. SOS promotes the exchange of GDP for GTP on Ras, thus promoting the active conformation of the molecule. Ras binds the serine/threonine kinase Raf 1 (Vojtek et al., 1993) and is thought to modulate the activity of the kinase. Raf 1 phosphorylates and activates MEK (MAP kinase kinase) (Kyriakis et al., 1992). MEK is a dual specificity kinase with serine/threonine and tyrosine kinase activity, which acts to phosphorylate and activate ERK 1 and ERK 2 (p42/44 MAP kinases), as depicted in figure 1.5. MAP kinase phosphorylation and activation results in phosphorylation of their substrate proteins including the Ser/Thr kinase, p90 ribosomal S6 kinase ($p90^{RSK}$) (Sturgill and Wu, 1991) and the transcription factors c-Myc and c-Jun (Pulverer et al., 1991).

1.2.8.2 Signalling through mTOR

mTOR (mammalian target of rapamycin) is a large protein (290 kDa) which has been assigned to a family of protein kinases called the phosphatidylinositol kinase-related kinases (PIKKs). mTOR has been shown to have homology with lipid kinases, although no lipid kinase activity has been identified in the protein (Brown et al., 1995), however the protein is known to be a Ser/Thr kinase. Homologous proteins have also been identified in yeast (TOR1 and TOR2) and Drosophila (dTOR) (Raught et al., 2001).

mTOR is reported to be regulated by insulin, in that insulin treatment increased the activity of mTOR (Scott et al., 1998). Additionally, mTOR was reported to be downstream of PKB in the insulin-signalling pathway, and it was demonstrated that PKB directly phosphorylated mTOR (Nave et al., 1999).

mTOR regulates a number of proteins that function in control of translation. mTOR is reported to activate p70 S6 kinase (Brown et al., 1995). S6 is thought to function in regulation of translation of 5'TOP (terminal oligopyrimidine) tract mRNAs, which encode ribosomal proteins and elongation factors (Jefferies et al., 1997). mTOR also functions to phosphorylate eukaryotic initiation factor (eIF) 4E binding protein 1 (4E-BP1) and 2. eIF 4E has a key role in initiation of translation. When 4E-BP1 is hypophosphorylated it binds eIF 4E, thus preventing an interaction with the 5'cap (Sonenberg and Gingras, 1998). Phosphorylation of 4E-BP1 by mTOR, in response to insulin, releases binding of eIF 4E, allowing it to act in initiation of translation (Proud et al., 2001). mTOR is also suggested to regulate the eukaryotic elongation factor 2 (eEF2). Phosphorylation of eEF2 at Thr-56 inhibits its activity. In response to insulin this residue is dephosphorylated, due to the decreased activity of an eEF2 kinase (Redpath et al., 1996), possibly due to phosphorylation by mTOR.

1.2.8.3 Regulation of protein synthesis by GSK-3

Insulin also promotes initiation of translation through regulation of GSK-3. GSK-3 phosphorylates and inhibits the eukaryotic initiation factor 2B (eIF 2B). In the presence of insulin, GSK-3 is inhibited, due to phosphorylation by PKB, thus eIF 2B becomes dephosphorylated and activated, allowing initiation of translation to occur (Welsh et al., 1998).

1.3 Activation of glucose transport in skeletal muscle

The majority of the insulin signalling pathways described above have been identified in skeletal muscle. However, in skeletal muscle glucose transport is also activated by muscle contraction, and insulin and contraction are reported to activate glucose transport by distinct mechanisms. Thus it is appropriate to discuss these processes in somewhat more detail.

1.3.1 Skeletal muscle is composed of distinct fibre types

Skeletal muscle cells/fibres are long, multi-nucleated cells that may span the entire length of the muscle and skeletal muscles are composed of different fibre types, which have different contractile and metabolic properties. For example, skeletal muscle fibres are traditionally characterised as slow or fast twitch. Slow twitch (type I) fibres are rich in mitochondria and participate in oxidative phosphorylation whilst fast twitch (type II) fibres typically have fewer mitochondria and perform anaerobic glycolysis (Voet and Voet, 1995). Type II fibres are capable of a short burst of rapid activity whereas type I fibres participate in more sustained activity.

Histochemical analysis of skeletal muscle reveals the presence of three fibre types (Armstrong and Phelps, 1984): fast twitch oxidative glycolytic (FOG, type IIA), fast twitch glycolytic (FG, type IIB) and slow twitch oxidative (SO, type I). Whole muscles typically contain these fibres in varying quantities, for example rat soleus muscle was reported to consist of 87% SO, 13% FOG and 0% FG fibres, whereas rat EDL muscle was reported to contain 2% SO, 42% FOG and 56% FG fibres (Armstrong and Phelps, 1984). However, it is known that changes in fibre type composition can occur in skeletal muscle in the presence of changes in innervation, electrical stimulation or mechanical factors (Daugaard and Richter, 2001).

One protein whose expression is shown to differ in skeletal muscle fibre types is the insulin responsive glucose transporter, GLUT 4. GLUT 4 protein is expressed at highest levels in type I compared to type II fibres (Daugaard and Richter, 2001). GLUT 4 expression in muscle has also been shown to correlate with the ability of a particular muscle to increase glucose uptake in response to insulin and contraction (Henriksen et al., 1990). GLUT 4 expression in skeletal muscle has been reported to correlate with physical activity, with inactivity reducing GLUT 4 content and exercise increasing GLUT 4 content in various muscle fibre types (reviewed in Daugaard and Richter, 2001).

1.3.2 Role of the T-tubule system in skeletal muscle glucose transport

Skeletal muscle fibres are covered in a membrane known as the sarcolemma. The T-tubule system is continuous with the sarcolemma and forms invaginations, which penetrate deep into the centre of the muscle. T-tubules are suggested to function in transmission of membrane depolarisation to the central part of the muscle and are also hypothesised to function in delivering nutrients, such as glucose, deep into the muscle body (Dohm and Dudek, 1998).

GLUT 4 has been reportedly localised to the T-tubule membrane using a variety of techniques including immunogold labelling, using cell impermeable photolabels and cell fractionation and membrane isolation techniques (reviewed in Dohm and Dudek, 1998). Furthermore, as shown in figure 1.9, GLUT 4 is reportedly recruited to the T-tubule membrane in response to insulin and contraction (Munoz et al., 1995, Roy and Marette, 1996), suggesting this organelle may indeed be the site of glucose uptake in skeletal muscle.

1.3.3 Exercise-stimulated glucose transport

It is generally accepted that both insulin and exercise/contraction of skeletal muscle cause an increase in glucose uptake into the muscle. However, it is believed that these processes act independently and utilise distinct signalling pathways in order to promote glucose uptake. It has been demonstrated that stimulation of skeletal muscle with insulin and exercise/contraction produces additive effects on glucose transport (Ploug et al., 1987, Wallberg-Henriksson et al., 1988). Insulin and contraction are also reported to recruit GLUT 4 from distinct intracellular pools (Douen et al., 1990), however the exact nature of these intracellular GLUT 4 compartments is not well defined. Furthermore, contraction-stimulated glucose transport, unlike insulin-stimulated glucose transport, is reported to be PI3-kinase independent. It has been demonstrated that no change in skeletal muscle insulin receptor and IRS-1 tyrosine phosphorylation or PI3-kinase activity occurs in response to exercise/contraction (reviewed in Hayashi et al., 1997 and Sakamoto and Goodyear, 2002). Additionally, wortmannin (a PI3-kinase inhibitor) does not inhibit contraction-induced glucose transport in skeletal muscle (Yeh et al., 1995). Therefore, studies of contraction

induced glucose transport have focused on delineating the mechanisms responsible for this process.

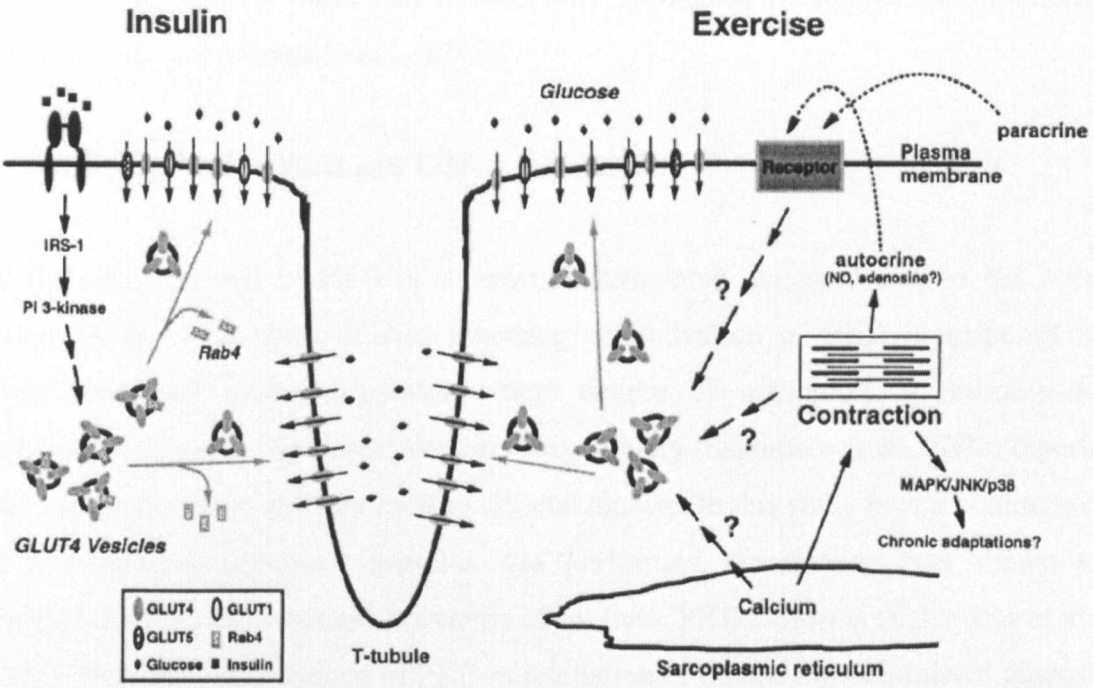

Figure 1.9 The T-tubule system of skeletal muscle (taken from Hayashi et al., 1997)

GLUT 4 is recruited to the T-tubules and the sacrolemma/plasma membrane in response to exercise/contraction and insulin

1.3.3.1 Role of calcium in exercise-stimulated glucose transport

Calcium has a role in muscle contraction, in that on release from the sarcoplasmic reticulum in response to membrane depolarisation, the concentration of intracellular calcium increases causing stimulation of the contractile filaments, and the onset of muscle contraction. Hence, calcium has been postulated to function in contraction-stimulated glucose transport. It has been reported that agents which increase intracellular calcium promote increased skeletal muscle glucose transport, whilst agents that decrease intracellular calcium concentration prevent increases in muscle glucose transport (reviewed in Hayashi et al., 1997 and Wojtaszewski and Richter, 1998). However, it is suggested that calcium ions do not directly activate glucose

transport as increases in intracellular calcium concentration occur for only a very short time, but increased glucose transport in response to contraction is sustained over longer periods. Hence it is postulated that calcium acts to activate other factors which will function over a prolonged period to increase glucose transport, for example calcium-dependent PKCs have been implicated in contraction-stimulated glucose transport (Hayashi et al., 1997).

1.3.3.2 Regulation of PKB and GSK-3 by exercise

Historically, the role of PKB in contraction-stimulated glucose transport has been controversial, with some studies reporting no activation of PKB in response to contraction and others suggesting some degree of activation in response to contraction/exercise. However, one very recent study (Sakamoto et al., 2002) reports that contraction does activate PKB in skeletal muscle. In this study *in situ* contraction of five different hindlimb muscles was performed. Contraction was shown to promote a rapid and transient activation of all three PKB isoforms (Sakamoto et al., 2002). However, the function of PKB in regulation of contraction-stimulated glucose transport is not known.

Like insulin, exercise has also been reported to inhibit the activity of GSK-3 (Markuns et al., 1999), but the mechanism of GSK-3 inhibition by insulin and contraction is reportedly different. Insulin was reported to inhibit GSK-3 activity by promoting its phosphorylation by PKB. Exercise was also reported to decrease GSK-3 activity, but it did so without promoting phosphorylation of the protein (Markuns et al., 1999). Again the function of GSK-3 inhibition by exercise is uncertain, but likely involves increasing glycogen synthase activity (Sakamoto and Goodyear, 2002).

1.3.3.3 Role of AMPK in exercise-stimulated glucose transport

AMP-activated protein kinase (AMPK) has been postulated to act as a 'fuel gauge' in monitoring cellular energy levels. When AMPK senses decreased energy levels in cells it acts to switch off ATP-consuming process and switch on pathways of ATP generation (reviewed in Winder, 2001). AMPK is comprised of 3 subunits (α, β and γ), with two known α (α_1 and α_2) subunits, two β (β_1 and β_2) subunits and three γ (γ_1,

γ_2, and γ_3) subunits having been identified. All three subunits are required for expression of full AMPK activity, and the various α, β and γ subunits have been found in a variety of combinations in different cell types. The α subunit is the catalytic subunit and contains the protein kinase domain, whilst the β and γ subunits are regulatory components. In skeletal muscle the α_2 isoform is more abundant than the α_1 isoform and whilst β_1 and β_2 are both expressed in EDL muscle, only β_1 is found in soleus muscle (Winder, 2001).

AMPK is activated allosterically by increasing concentrations of AMP and is inhibited by ATP and creatine phosphate. In addition, AMPK is activated by phosphorylation by the upstream kinase, AMPK kinase (Hawley et al., 1996), which is also allosterically activated by AMP. AMPK and AMPKK can be artificially activated using the compound 5-aminoimidazole-4-carboxamide-riboside (AICAR). AICAR is taken up into cells and phosphorylated, thus forming the AMP analogue ZMP, which activates AMPK and AMPKK without affecting the AMP:ATP ratio of the cell.

AMPK is rapidly activated in skeletal muscle in response to various conditions of metabolic stress, including contraction, hypoxia, and hyperosmolarity (Hayashi et al., 2000) which are all likely to alter the fuel status of the muscle. Specifically, contraction has been reported to stimulate AMPK activity in rat skeletal muscle using a variety of protocols including treadmill running and *in situ* muscle contraction. The activation of AMPK in skeletal muscle has been suggested to be dependent on work rate/load in that the greater the force generated by contraction or the greater the intensity of the treadmill run, the greater the activation of AMPK is observed (Sakamoto and Goodyear, 2002). Studies in human skeletal muscle have also demonstrated activation of AMPK in response to exercise/contraction (Fujii et al., 2000, Wojtaszewski et al., 2000).

AMPK was first suggested to have a role in contraction-stimulated glucose transport in studies using AICAR, in which AICAR was shown to stimulate glucose transport in perfused hindlimb skeletal muscle (Merrill et al., 1997). Since then various studies have implicated AMPK in regulation of contraction-stimulated glucose transport by

activation of AMPK using AICAR. For example AICAR has been shown to promote glucose uptake in a manner similar to contraction in that the effects of insulin and AICAR are partially additive in promoting the glucose transport response, while the effects of AICAR and contraction are not (Hayashi et al., 1998). Furthermore, wortmannin was shown not to inhibit AICAR stimulated glucose transport (Hayashi et al., 1998). AICAR has been shown to promote GLUT 4 translocation in skeletal muscle (Kurth-Kraczek et al., 1999). However, no selective inhibitors of AMPK are available, and it is possible that AICAR has other deleterious effects, in addition to activation of AMPK. To address these issues studies have been undertaken using dominant negative forms of AMPK. Expression of a dominant negative AMPK in mouse skeletal muscle prevented the action of AICAR to increase glucose uptake (Mu et al., 2001). This dominant negative AMPK also reduced contraction-stimulated glucose transport, but only partially, which the authors suggested implies the presence of an AMPK-independent pathway leading to glucose uptake, which is activated by contraction. The molecules that are downstream of AMPK in contraction-stimulated glucose transport are unknown, however endothelial nitric oxide synthase (eNOS) has been proposed as a target for AMPK (Fryer et al., 2000). As discussed below, NO may have a role in regulation of contraction-stimulated glucose transport in skeletal muscle.

1.3.3.4 Role of nitric oxide and eNOS in exercise-stimulated glucose transport

Nitric oxide (NO) functions in a range of cellular processes including neural signalling, vasoregulation and the immune response (Reid, 1998). One of the main actions of NO is activation of soluble guanylyl cyclase, resulting in production of cGMP, leading to activation of a range of physiological responses (reviewed in Schmidt et al., 1993), including vasodilation. Studies in the 1970's reported that nitrite containing compounds (for example, nitroglycerin) stimulated guanylate cyclase, promoting an increase in cGMP production, leading to vascular relaxation, a phenomenon which was suggested to occur via the formation of NO (Katsuki et al., 1977). Later studies suggested that vessel relaxation, in response to a variety of agonists, occurred due to the release of an endothelial derived relaxing factor (EDRF) (Cherry et al., 1982). Subsequently, two groups independently identified EDRF and NO as being the same molecule (Palmer et al., 1987, Ignarro et al., 1987).

NO is produced by nitric oxide synthases (NOSs) with the net overall reaction being conversion of L-arginine and molecular oxygen to form NO and L-citrulline. The reaction occurs in the presence of the cosubstrate nicotinamide adenine dinucleotide phosphate (NADPH) and the cofactors flavin mono-nucleotide (FMN), flavin adenine nucleotide (FAD), tetrahydrobiopterin (BH_4), haem and calmodulin (Reid, 1998). Three NOS isoforms have been identified. These include two proteins that are expressed constitutively: neuronal NOS (nNOS), so called because it is highly expressed in neuronal cells and endothelial NOS (eNOS), originally identified in endothelial cells. The final enzyme (iNOS) is induced by various stimuli including inflammatory cytokines. Each NOS isoform has a similar structure, shown in figure 1.10. They consist of a C-terminal reductase domain, containing binding sites for FMN, FAD and NADPH and an N-terminal oxygenase domain, which contains binding sites for L-arginine, BH_4 and haem (Mayer and Hemmens, 1997). The calmodulin-binding region is at the interface of the oxygenase and reductase domains. The extreme N-terminal regions of the proteins are different and are thought to be important for intracellular targeting (Mayer and Hemmens, 1997). NOS proteins are reported to function as dimers and BH_4 has been suggested to be required for dimer formation (Fleming and Busse, 1999). Calcium-dependent calmodulin binding is the primary regulator of NO synthesis by nNOS and eNOS, whereas iNOS binds calmodulin with high affinity and is not regulated by calcium, rather it is regulated primarily at the level of transcription (Reid, 1998). Once calcium-calmodulin binds eNOS/nNOS, NADPH donates electrons to the reductase domain. The electrons are subsequently shuttled through the calmodulin-binding domain, towards the oxygenase domain, which may result in formation of NO (Govers and Rabelink, 2001).

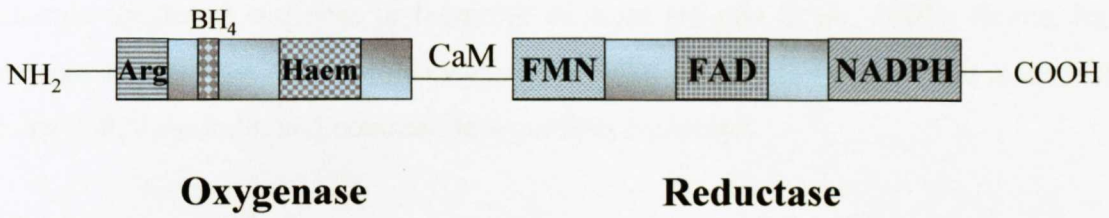

Figure 1.10 Schematic diagram of nitric oxide synthase structure

The diagram depicts regions where substrates and cofactors bind the NOS proteins CaM = calmodulin, Arg = L-arginine.

Each of the NOS isoforms are reported to be expressed in skeletal muscle. nNOS is expressed at highest levels in type II muscle fibres, whereas eNOS expression is found in all fibre types and although iNOS is not expressed constitutively in skeletal muscle it can be induced during the immune response (Reid, 1998). Skeletal muscle was first reported to release NO by Balon and Nadler in 1994. They showed that electrical stimulation of skeletal muscle increased this NO release and that a NOS inhibitor, L-NMMA (N^G-monomethyl-L-arginine monoacetate), decreased NO release and glucose uptake. A role for NO in regulation of glucose transport was further suggested by subsequent studies showing NOS inhibition reduced basal and exercise-stimulated glucose transport, but was without effect on insulin-stimulated glucose transport (Balon and Nadler, 1997). In addition, the use of sodium nitroprusside (SNP, a nitric oxide donor) increased glucose uptake in a dose-dependent manner and chronic treadmill training of rats resulted in increased expression of both eNOS and nNOS (Balon and Nadler, 1997). Studies in treadmill run rats also demonstrated that an acute bout of exercise promoted increased NOS activity (Roberts et al., 1999).

It has been suggested that increased NO production in skeletal muscle in response contraction may involve AMPK (Fryer et al., 2000) through AMPK-mediated phosphorylation and activation of eNOS, leading to NO production. In this study NOS inhibitors were shown to block increased glucose transport in response to AMPK activation. However, recent studies have cast some doubt over the involvement of NO in contraction-stimulated glucose transport. In one study, the effects of insulin and the NO donor SNP were shown to be fully additive in respect to glucose uptake. However, addition of the NOS inhibitor L-NAME (N^G-nitro-L-arginine methyl ester) to the drinking water of rats for two days had no effect on glucose uptake in response to treadmill exercise (Higaki et al., 2001). Hence, the authors suggest that NO stimulates glucose uptake using a mechanism that is distinct from both the insulin and contraction signalling pathways.

1.3.3.5 Exercise effects insulin sensitivity in skeletal muscle

After a single bout of exercise insulin action is increased in the muscles which had previously been active during the exercise period (reviewed in Wojtaszewski et al.,

2002). Using one-legged exercising, it has been shown that this is a local response and is restricted to the exercised muscles (Hayashi et al., 1997). The increase in insulin action is reported to involve glucose transport, glycogen synthesis and amino acid transport. This increased insulin sensitivity appears to be due to glycogen depletion, which occurs in skeletal muscle during exercise (Wojtaszewski et al., 2002). While the underlying mechanisms behind this phenomenon are not understood, it is important due to the fact that physical activity will improve the insulin sensitivity of insulin resistant/diabetic patients.

1.4 Diabetes, hypertension and insulin resistance

1.4.1 Diabetes

Diabetes is a disease that was once believed to be of minor importance to world health, however diabetes is now considered to be a major cause of morbidity and mortality worldwide. In the year 2000 it was estimated that around 150 million people were affected by diabetes, a figure which is expected to double by the year 2025 (Zimmet et al., 2001).

There are two main forms of diabetes. Type 1 (insulin dependent) diabetes is an autoimmune disorder in which the β-cells of the pancreas are destroyed, resulting in loss of insulin secretion. People with type 1 diabetes require daily insulin injections to regulate blood glucose levels and promote survival. Type 2 (non-insulin dependent) diabetes is characterised by insulin resistance and/or abnormal insulin secretion and is associated with a sedentary lifestyle and obesity. In type 2 diabetic individuals, blood glucose concentration may be controlled by diet and exercise, but where this is not the case, exogenous insulin may be required. The frequency of type 1 diabetes is low compared to type 2 diabetes, which accounts for around 90% of cases (Zimmet et al., 2001). Development of type 2 diabetes accounts for the large increase in diabetes observed in recent years and is primarily due to environmental and behavioural factors including the sedentary lifestyle, fast-food culture and increasing prevalence of obesity.

Adults with diabetes have an increased mortality rate and their life expectancy is decreased by around 5-10 years, which is due to development of microvascular (retinopathy, nephropathy and neuropathy) and macrovascular (heart disease, stroke and peripheral vascular disease) complications (Donnelly et al., 2000). Type 2 diabetes is also associated with the metabolic syndrome (or syndrome X), which is a multifactorial disease that includes conditions such as glucose intolerance, hyperinsulinaemia, dyslipidaemia, hypertension and obesity (Zimmet et al., 2001). However, the primary cause leading to development of type 2 diabetes and metabolic syndrome is unknown.

1.4.2 Hypertension in diabetes

Diabetes and hypertension are inter-related diseases which are frequently found to coexist and it has been reported that type 2 diabetes is almost 2.5 times more likely to develop in hypertensive patients, compared to normotensive subjects (Sowers et al., 2001). The use of anti-hypertensive agents to lower blood pressure in diabetic individuals was reported to reduce cardiovascular disease-related morbidity and mortality in type 2 diabetic patients and in lowering microvascular and macrovascular diabetic complications (Sowers et al., 2001). Furthermore, reducing blood pressure in hypertensive individuals is also suggested to prevent the development of diabetes (Sowers et al., 2001). The mechanisms by which hypertension, and subsequently, diabetes develop are not understood, however it is probable that genetic as well as environmental factors are involved (Donnelly and Connell, 1992).

1.4.3 Molecular mechanisms of insulin resistance and diabetes

Insulin resistance can be described as a condition in which insulin's actions at the peripheral tissues are impaired (Hunter and Garvey, 1998). Whilst this definition could be applied to any of insulin's actions it is generally used to describe resistance to insulin's effects on glucose transport. Insulin resistance is frequently accompanied by hyperinsulinaemia, which occurs as the pancreatic β cells attempt to compensate for reduced insulin sensitivity in the peripheral tissues. Insulin resistance is reported to be the primary defect in type 2 diabetes and can lead to a variety of abnormalities

that lead to development of obesity, hypertension, polycystic ovarian syndrome (PCOS) and dyslipidaemia and atherosclerosis (Saltiel, 2000).

Various studies have been undertaken in order to determine the cellular basis of insulin resistance. It has been suggested that any defect is likely to occur in the insulin signal transduction pathway, or in the trafficking, docking or fusion of the GLUT 4 vesicle, with the plasma membrane (Hunter and Garvey, 1998). A number of studies have identified genetic defects that are causes of human insulin resistance syndromes. For example in many patients with type A severe insulin resistance, mutations in the insulin receptor have been identified, leading to reduced tyrosine kinase activity of the receptor (Hunter and Garvey, 1998). In contrast, mutations in the insulin receptor, leading to reduced insulin binding have been reported to cause leprechaunism, a syndrome that is also characterised by severe insulin resistance. The hyperinsulinaemia associated with insulin resistance is suggested to have a role in insulin-induced insulin resistance (Pessin and Saltiel, 2000). The high concentration of circulating insulin is suggested to stimulate serine phosphorylation of the insulin receptor β subunits, thus decreasing insulin receptor tyrosine kinase activity. PKC is a kinase implicated in the process, as PKCs are activated in a number of insulin resistant models (Pessin and Saltiel, 2000). Insulin resistance in PCOS is associated with hyperphosphorylation of the insulin receptor and a decrease in insulin-stimulated tyrosine autophosphorylation and tyrosine kinase activity of the receptor (Hunter and Garvey, 1998).

Defects in downstream signalling events have also been reported in insulin resistant states. For example reduced IRS-1 tyrosine phosphorylation and PI3-kinase activity was observed in lean to moderately obese type 2 diabetics (Zierath et al., 2000) and decreased association of PI3-kinase with IRS proteins in insulin resistant skeletal muscle has also been reported (Pessin and Saltiel, 2000). Some reports also suggest PKB phosphorylation is reduced in skeletal muscle from type 2 diabetic patients however, other reports suggest this is not the case (Zierath et al., 2000), therefore a role for PKB in insulin resistance has still to be confirmed.

Defects in GLUT 4 are also reported to result in insulin resistance. In adipocytes, GLUT 4 expression at both the protein and mRNA level was reported to be reduced

by up to 80% in type 2 diabetes (Hunter and Garvey, 1998), resulting in reduced basal and insulin-stimulated glucose uptake in this tissue. Conversely, in skeletal muscle from type 2 diabetic patients, expression of GLUT 4 was reported to be normal. However, in these patients, GLUT 4 translocation in response to insulin was reduced (Hunter and Garvey, 1998). Fractionation of skeletal muscle determined that in the type 2 diabetic patients, more GLUT 4 was residing in dense membrane vesicles, as opposed to low-density vesicles, suggesting subcellular localisation of GLUT 4 is altered in insulin resistant skeletal muscle (Hunter and Garvey, 1998) and further studies suggest this may also be the case in adipocytes.

1.5 Animal models of insulin resistance/diabetes and hypertension

Whilst various observations have been made pertaining to insulin resistance in human tissue, the underlying biochemical mechanisms are not known due to the difficulty in performing many studies on the small amounts of biopsy material available. For this reason many animal models of insulin resistance, diabetes and hypertension are useful in studying these diseases.

1.5.1 The Zucker rat

The Zucker rat is a model of obesity and insulin resistance. Initially the peripheral tissues of these animals are hyper-responsive to insulin's action on glucose transport, however this response declines with age until the animals become insulin resistant in skeletal muscle at around 70 days of age. Adipose tissue remains hyper-responsive to insulin for a prolonged period, but insulin resistance also affects adipose tissue of older animals (Abel et al., 1996). Insulin resistance in skeletal muscle of Zucker rats is not associated with changes in expression of GLUT 4 mRNA or proteins. Conversely, in adipose tissue the hypersensitive response to insulin is associated with increased expression of GLUT 4 protein, which declines to levels lower than in lean controls, when the adipose tissue becomes insulin resistant (Abel et al., 1996). The major cause of insulin resistance in skeletal muscle of the Zucker rat is suggested to be a defect in GLUT 4 translocation to the plasma membrane (Abel et al., 1996).

1.5.2 The spontaneously hypertensive rat (SHR)

The spontaneously hypertensive rat (SHR) is an animal model of hypertension, which has also been proposed as a model of human insulin resistance syndromes. Studies by Mondon and Reaven (1988) and Reaven et al. (1989), reported the existence of insulin resistance in this strain. The SHR has also been reported to have elevated triglycerides and free fatty acids (Iritani et al., 1977, Aitman et al., 1997). Using genetic mapping techniques Aitman and colleagues identified a gene, Cd36 (or Fat, fatty acid translocase), that was reported to have peak linkage to the defects of glucose and fatty acid metabolism in the SHR (Aitman et al., 1999). The Cd36 gene was deleted in the SHR and was suggested to underlie the insulin resistance, hypertriglyceridaemia and defective fatty acid metabolism observed in this animal.

1.5.3 The stroke-prone spontaneously hypertensive rat (SHRSP)

The stroke-prone spontaneously hypertensive rat (SHRSP) was established by Okamoto and colleagues by selective breeding of the SHR (Okamoto et al., 1974). However, the SHR and the SHRSP (as well as the Wistar-Kyoto (WKY) rat, the normotensive control strain) were imported by the National Institute of Health (NIH) in the United States before the strains were inbred. This resulted in the existence of genetic differences between all the colonies that were separated before full inbreeding (Kurtz et al., 1989, Kurtz and Morris, Jr., 1987, Samani et al., 1989, Matsumoto et al., 1991) (see figure 1.11). Therefore, direct comparison of experimental data produced using different colonies can be difficult.

The SHRSP exhibits elevated blood pressure compared to control strains and in males stroke is reported to develop around 40 weeks of age (Okamoto et al., 1974). During the course of this work, studies in this laboratory (Collison et al., 2000) showed that like the SHR, the SHRSP also exhibited insulin resistance. Adipocytes from the SHRSP showed reduced insulin-stimulated glucose uptake and a reduced ability of insulin to inhibit catecholamine mediated lipolysis, compared to adipocytes from the WKY. This defect could not be explained by expression of a defective Cd36 gene, as the deletion mutation observed in the SHR was not present in the SHRSP (Collison et al., 2000). These results suggested that while the Cd36 gene may have a

role in the defective fatty acid metabolism reported in the SHR, the defect in insulin action in the SHR/SHRSP is likely due to other factors.

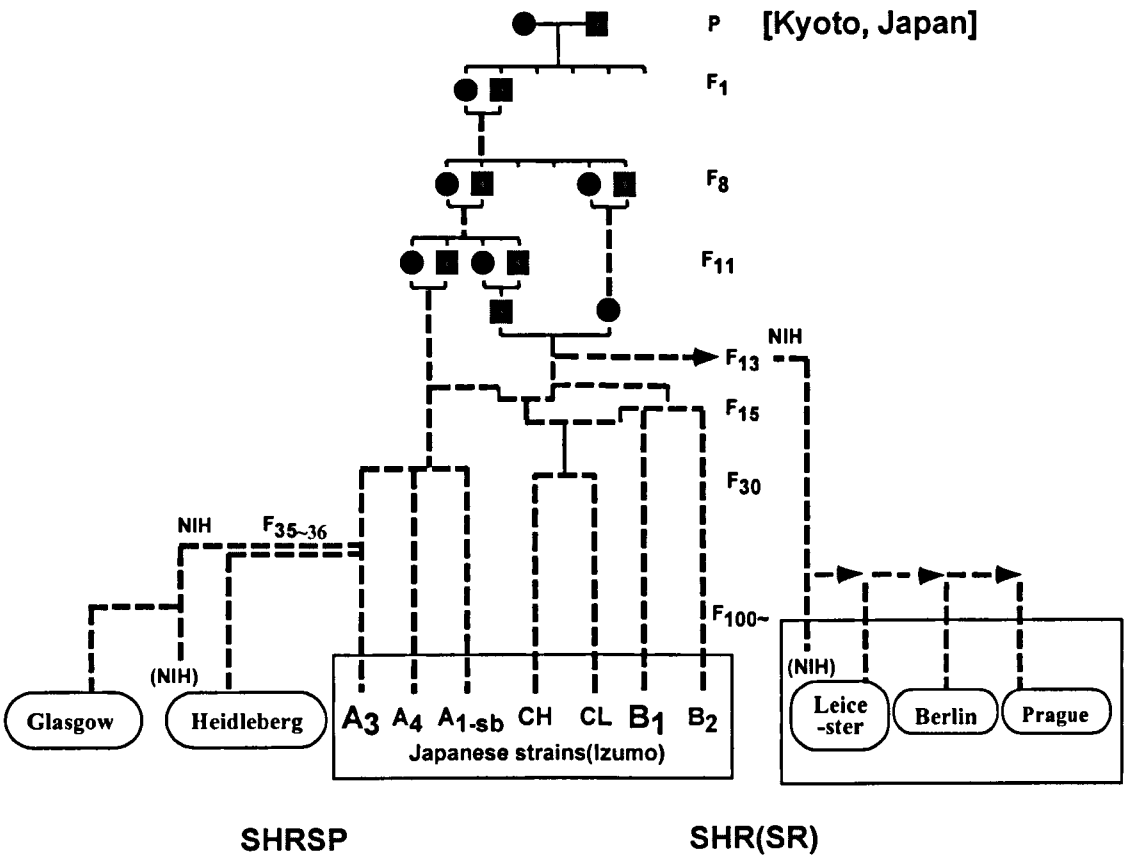

Figure 1.11 Genealogical origin of the SHR and the SHRSP

The SHRSP strain, maintained at Glasgow, was obtained from colonies maintained at the University of Michigan, whose breeding stocks had been obtained from NIH (Davidson et al., 1995, Jeffs et al., 1997).

Work in this laboratory (James et al., 2001), confirmed that the SHRSP also exhibited insulin resistance in skeletal muscle, the major site of post-prandial glucose disposal. This defect was shown to be specific for the insulin-signalling pathway, as in the SHRSP, glucose transport was decreased in response to insulin, but was similar in response to activation of AMPK (which is suggested to have a role in mediating exercise-stimulated transport), compared to the control WKY muscle.

1.6 Aims of this study

The aim of the current study was to investigate the possible causes of the observed insulin resistance in skeletal muscle of the SHRSP. This was examined using three approaches. Firstly, antibodies specific for eNOS protein, phosphorylated or dephosphorylated at residue 1177, were raised and characterised in order to study regulation of eNOS in skeletal muscle from SHRSP and WKY. Secondly, various aspects of the insulin signalling cascade were studied in order to determine if any defects were present which may account for altered insulin signalling in skeletal muscle from the SHRSP. Finally a yeast two-hybrid screen was carried out using the protein flotillin. This protein is known to be localised in lipid rafts and is reported to localise molecules involved in insulin signalling to glucose transport in these lipid raft domains (see section 1.2.7.3). During the course of this work, studies in our laboratory illustrated over-expression of flotillin skeletal muscle from SHRSP (James et al., 2001). A yeast two-hybrid screen was undertaken to identify flotillin interacting proteins, which may be involved in regulation of glucose transport.

CHAPTER 2

MATERIALS AND METHODS

2.1 Materials

All reagents used were of the highest quality available and were obtained from the following suppliers:

2.1.1 General Reagents

Anachem Ltd, Luton, Bedfordshire, UK

30% acrylamide/bisacrylamide

Complete supplement mixture (-Ade/-His/-Leu/-Trp)

Amersham Pharmacia Biotech, Little Chalfont, Buckinghamshire, UK

Activated CH Sepharose 4B

PD 10 disposable columns

Protein G Sepharose

Bio-Rad Laboratories Ltd, Hemel Hempstead, Hertfordshire, UK

Electroporation cuvettes

'Econo-pak' disposable columns

BDH Laboratory Supplies, Poole, Dorset, UK

Acetic acid

Ammonium persulphate

Calcium chloride solution

di-Potassium hydrogen orthophosphate

Magnesium acetate

Magnesium chloride

Magnesium sulphate

Methanol

Orthophosphoric acid

Potassium chloride

Potassium dihydrogen orthophosphate

Sodium acetate

Sodium azide

Sodium dihydrogen orthophosphate

Sodium hydrogen carbonate

Tetra-Sodium pyrophosphate

Calbiochem (CN Bio-sciences) Beeston, Nottingham, UK

Calmodulin

Hepes

Keyhole limpet haemocyanin

MOPS

Okadaic acid

Clontech, Palo Alto, California, USA

Human muscle Matchmaker™ II library in pACT2

Human testis Matchmaker™ II library in pACT2

Human testis Protein Medley™ lysate

Difco Laboratories, Detroit, USA

Yeast nitrogen base (without amino acids)

Bacto agar (for yeast agar plates)

Fisher Scientific, Loughborough, Leicestershire, UK

Dimethyl sulphoxide (DMSO)

Glycine

Hydrochloric acid

Potassium hydroxide

Sodium dodecyl sulphate (SDS)

Sodium diaminoethanetetra-acetic acid (EDTA)

Sodium hydroxide

Sucrose

Fisons Chemicals, Leicestershire, UK

OptiFlow Safe1 scintillation fluid

Invitrogen, Groningen, The Netherlands

pCRII-TOPO™ TA cloning kit

OneShot TOP10 competent *Escherichia coli*

Konica Europe, GmbH, Hohenbrunn, Germany

Konica medical film

Melford Laboratories Ltd, Ipswich, UK

Dithiothreitol

Merck Pharmaceuticals, West Drayton, UK

Aquamount

Disodium succinate

Isopentane

Millipore Corporation, Bedford, MA

Microcon YM-10 centrifugal filters

MWG Biotech, Germany

Oligonucleotide primers

New England Biolabs (UK) Ltd, Hitchin, Herfordshire, UK

Prestained protein marker, broad range (6-175)

NovoNordisk, DK-2880, Bagsvaerd, Denmark

Human Actrapid® Insulin solution - 100 IU/ml

Oxoid Ltd, Hampshire, UK

Bacteriological Agar

Yeast extract

Tryptone

Premier Brands UK, Knighton Adbaston, Staffordshire, UK

Marvel powdered milk

Promega, Southampton, UK

All restriction enzymes

Alkaline phosphatase

Pfu polymerase

Taq polymerase

Nuclease-free water

Deoxynucleotide triphosphates (dNTPs)

Qiagen Ltd, Crawley, West Sussex, UK

QIAprep spin miniprep kit

QIAprep gel extraction kit

Plasmid maxi kit

Roche Diagnostics, GmbH, Mannheim, Germany

Complete™ Protease Inhibitor Tablets

Hexokinase

Glucose-6-phosphate dehydrogenase

Schleicher & Schuell UK Ltd, Brunswick Park, London, UK

Nitrocellulose membrane (0.45 μM)

Sigma Chemical Company Ltd., Poole, Dorset, UK

2-deoxy-D-glucose

3-amino-1,2,4-triazole (3-AT)

3-maleimidobenzoic acid N-hyroxysuccinimide ester (MBS)

5-amino-imidazolecarboxamide riboside (AICAR)

Adenosine 5'-triphosphate (ATP)

Adenosine monophosphate (AMP)

Amino acids

Ampicillin

Amyloglucosidase

Benzamidine

Bovine serum albumin (BSA)

Bromophenol blue

Cobalt chloride

Coomassie G

Ethylene glycol-bis (β-aminoethylether) -N,N,N',N'-tetra acetic acid (EGTA)

D-glucose

Glycerol

Glycogen

Kanamycin

β-Nicotinamide adenine dinucleotide phosphate (NADP)

N, N, N', N',-tetramethylethylenediamine (TEMED)

Nitro blue tetrazolium (Nitro BT)

Phenazine methosulphate (PMS)

Phenylmethylsulfonyl fluoride

Polyethylene glycol (PEG) 3,350

Poly-l-lysine

Ponceau S solution

Potassium fluoride

Protein A Sepharose

Sodium chloride

Sodium fluoride

Sodium orthovanadate

Tris Base

Triton X-100

Trypsin inhibitor, from soyabean (SBTI)

Tween 20

YPD Powder

TCS Cellworks, Botolph Claydon, Buckinghamshire, UK

Human aortic endothelial cells

Large vessel endothelial cell medium

Whatman International Ltd., Maidstone, Kent, UK

Whatman 3mm filter paper

Whatman number 1 filter paper

Phosphocellulose (P-81) paper

2.1.2 Antibodies

Amersham Pharmacia Biotech, Little Chalfont, Buckinghamshire, UK

Horseradish peroxidase (HRP)-conjugated donkey anti rabbit IgG antibody

HRP-conjugated donkey anti mouse IgG antibody

ECL western blotting detection system

BD Transduction Laboratories

Anti-GSK-3β (mouse monoclonal IgG) - raised against the N-terminal 160 residues of rat GSK-3β

Anti-caveolin-1 (mouse monoclonal IgG) - raised against N-terminal 97 residues of human caveolin-1

Anti-flotllin-1 (mouse monoclonal IgG) - raised against C-terminal region, amino acids 312-428, of mouse flotillin

Anti-PKC α (mouse monoclonal IgG) - raised against a protein fragment corresponding to amino acids 270-427 of rat brain PKC α

Anti-PKC β (mouse monoclonal IgG) - raised against a protein fragment corresponding to residues 126-324 of human PKC β

Anti-PKC δ (mouse monoclonal IgG) - raised against a protein fragment corresponding to amino acids 114-289 of rat PKC δ

Anti-PKC ε (mouse monoclonal IgG) - raised against protein fragment corresponding to N-terminal residues 1-175 of rat PKC ε

Anti-PKC θ (mouse monoclonal IgG) - raised against a protein fragment corresponding to residues 21-217 of mouse PKC θ

Anti-PKC ι (mouse monoclonal IgG) - raised against a protein fragment corresponding to C-terminal amino acids 404-587 of human PKC ι

New England Biolabs (UK) Ltd, Hitchin, Herfordshire, UK

Anti-PKB, phospho Thr 308 (rabbit polyclonal antibody) - raised against a phospho-Thr 308 synthetic peptide

Sigma Chemical Company Ltd., Poole, Dorset, UK

HRP-conjugated donkey anti sheep IgG

Anti-eNOS (sheep polyclonal IgG) - raised against the synthetic peptide SGPYNSSPRPEQHK corresponding to amino acids 594-607 of bovine eNOS

FITC-linked goat anti-rabbit IgG

Upstate Biotechnology UK, Botolph Claydon, Buckinham, UK

Anti-IRS-1 (rabbit immunoaffinity purified IgG) - raised against C-terminal 14 amino acid peptide ([C]YASINFQKQPEDRQ) of rat liver IRS-1

Anti-IRS-2 (rabbit polyclonal IgG) - raised against a GST fusion protein corresponding to amino acids 976-1094 of mouse IRS-2

Anti-PI3-kinase, p85 (rabbit polyclonal IgG)

Anti-Akt/PKB, PH domain, clone SKB1 (mouse monoclonal IgG) - raised against a GST fusion protein corresponding to residues 1-149 of human Akt 1

Anti-phospho Akt1/PKBα (Ser 473) (sheep immunoaffinity purified IgG) – raised against a synthetic peptide corresponding to C-terminal residues 467-477 of rat Akt1 (KHFPQF[pS]YSAS)

Anti-GSK-3α (sheep immunoaffinity purified IgG) - raised against a 13 residue synthetic peptide [QAPDATPTLTNSS] corresponding to residues 471-483 of rat GSK-3α

Anti-phospho-eNOS (Thr 495) (rabbit immunoaffinity purified IgG) - raised against a synthetic peptide corresponding to amino acids 489-501 of human eNOS (GITRKK[pT]FKEVAN)

Anti-GLUT 4 (rabbit affinity purified polyclonal IgG) directed against the C-terminal 14 amino acids of human GLUT 4 was prepared in-house (Brant et al., 1992).

Anti-phospho eNOS (Ser-1177) was a generous gift from Prof. D.G. Hardie, University of Dundee, Dundee, UK.

2.1.3 Radioactive Materials

Amersham Pharmacia Biotech, Little Chalfont, Buckinghamshire, UK

Adenosine 5′ [γ–^{32}P] triphosphate

D-[U-^{14}C] glucose

α-D-[U-^{14}C] glucose-1-phosphate

NEN DuPont (UK) Ltd., Stevenage, Herts, UK

2-[^{3}H(G)] deoxy-D-glucose

[U-^{14}C] Sucrose

2.1.4 Peptides

PKB substrate peptide (RPRAATF) was a generous gift from Dr. R. Plevin, University of Strathclyde, Glasgow, UK.

GSK-3 substrate peptide, phospho-glycogen synthase peptide-2 (YRRAAVPPSPSLSRHSSPHQ(pS)EDEEE), and the GSK-3 non-substrate peptide, glycogen synthase peptide-2 (Ala 21) (YRRAAVPPSPSLSRHSSPHQAEDEEE), were both from Upstate Biotechnology UK, Buckingham, UK.

For anti-eNOS antibody production, peptides corresponding to residues 1172 to 1183 of human eNOS, CR_{1172}IRTQSFSLQER$_{1183}$ (dephosphorylated) and CR_{1172}IRTQSpFSLQER$_{1183}$ (phosphorylated) were produced by Dr G. Bloomberg, University of Bristol, Bristol, UK.

2.1.5 *Escherichia coli* strains

DH5α

XL1-blue

KC8 (all from lab stocks)

2.1.6 *Saccharomyces cerevisiae* strain for yeast 2 hybrid

PJ69-2A was the only yeast strain used in this study (James et al., 1996). It has the following genotype:

MATa, trp1-901, leu2-3,112, ura3-52, his3-200, gal4Δ, gal80Δ, LYS::$GAL1_{UAS}$-$GAL1_{TATA}$-HIS3, $GAL2_{UAS}$-$GAL2_{TATA}$-ADE2

2.1.7 Miscellaneous

Purified AMPK was a generous gift from Prof. D.G. Hardie, University of Dundee, Dundee, UK.

2.2 General Buffers

Electrode Buffer	25 mM Tris, 192 mM glycine, 0.1% (w/v) SDS
HES buffer	20 mM Hepes, pH 7.4, 1 mM EDTA, 250 mM sucrose, 2 mM Na_3VO_4, 10 mM NaF, 1 mM $Na_4P_2O_7$
IP buffer	50 mM Tris-HCl, pH 7.4 at 4°C, 1% (v/v) Triton X-100, 1% (v/v) glycerol, 150 mM NaCl, 50 mM NaF, 5 mM $Na_4P_2O_7$, 1 mM Na_3VO_4, 1 mM EDTA, 1 mM EGTA, 1 mM DTT, 0.1 mM benzamidine, 0.1 mM PMSF, 5 μg/ml SBTI
KH (Krebs Henseleit) buffer	118 mM NaCl, 4.7 mM KCl, 1.2 mM K_2HPO_4, 1.2 mM $MgSO_4.7\ H_2O$, 25 mM $NaHCO_3$, 2.5 mM $CaCl_2$, pH 7.4, supplemented with 25 mM D-glucose and 0.1% (w/v) BSA
KRH	20 mM Hepes, pH 7.4, 119 mM NaCl, 5 mM $NaHCO_3$, 4.75 mM KCl, 1.3 mM $CaCl_2$, 1.2 mM $MgSO_4.7$ H2O
LB (Luria-Bertani Broth)	10% (w/v) NaCl, 10% (w/v) tryptone, 5% (w/v) yeast extract
Lysis buffer	50 mM Tris-HCl pH 7.4 at 4°C, 50 mM NaF, 1 % (v/v) Triton X-100, 250 mM mannitol, 1 mM $Na_4P_2O_7$, 1 mM Na_3VO_4, 1 mM EDTA, 1 mM EGTA, 1 mM DTT, 0.1 mM benzamidine, 0.1 mM PMSF, 5 μg/ml SBTI
PBS	137 mM NaCl, 2.7 mM KCl, 10 mM Na_2HPO_4, 1.8 mM KH_2PO_4

TAE	40 mM Tris-acetate, 1 mM EDTA
TBS	20 mM Tris-HCl, pH 7.4, 150 mM NaCl
TBST	20 mM Tris-HCl, pH 7.4, 150 mM NaCl, 0.02% (v/v) Tween-20
TE	10 mM Tris, pH 8.0, 1 mM EDTA
Transfer Buffer	25 mM Tris, 192 mM glycine, 20% (v/v) methanol
2X sample buffer	4% (w/v) SDS, 20% (v/v) glycerol, 125 mM Tris, pH 6.8, bromophenol blue

2.3 Methods

2.3.1 General Methods

2.3.1.1 Gel electrophoresis

SDS-polyacrylamide gel electrophoresis (SDS-PAGE) was carried out using Bio-Rad mini-protean II gel kits. The resolving gel consisted of 8%-15% acrylamide (depending on the mass of the proteins to be studied), 375 mM Tris, pH 8.0, 0.1% (w/v) SDS, polymerised with 0.1% (w/v) $(NH_4)_2S_2O_8$ and 0.08% (v/v) TEMED. The stacking gels consisted of 5% acrylamide, 125 mM Tris, pH 6.8, 0.1% (w/v) SDS, polymerised with 0.1% (w/v) $(NH_4)_2S_2O_8$ and 0.1% (v/v) TEMED. Sample buffer (2X) was added to samples before boiling for 5 min and loading onto the gel. Gels were electrophoresed at a constant voltage, typically 80 V, until the proteins had passed through the stacking gel, and then 120-180 V (depending on the percentage of acrylamide in the resolving gel) to resolve the proteins.

2.3.1.2 Western blotting

After gel electrophoresis, proteins were transferred to nitrocellulose, using Bio-Rad trans-blot apparatus. Briefly, nitrocellulose was cut to size and equilibrated in transfer buffer. The gel was then laid on the nitrocellulose, and sandwiched between two pieces of Whatman 3MM filter paper. This was then placed in a transfer cassette, in the trans-blot apparatus. Transfer of proteins was achieved at a constant current of 220 mA for 2 hr, or 40 mA overnight. Protein transfer was confirmed by immersing nitrocellulose in Ponceau S solution for 1 min.

2.3.1.3 Coomassie staining of SDS-PAGE gels

To allow visualisation of proteins separated by SDS-PAGE a Coomassie blue stain was used. This consisted of 5% glacial acetic acid, 45% methanol and 0.25 g/l Coomassie Brilliant Blue R and was filtered through Whatman No. 1 filter paper. The gel was submerged in stain for around 15 min before rinsing and destaining in the same acetic acid, methanol, H_2O mixture, without the Coomassie dye. Destaining

was for at least 3 hrs or overnight with a number of changes of destain buffer. The gel was then placed between clear polythene sheets and scanned to provide digital records, or layered between two sheets of cellophane and dried overnight at 37°C.

2.3.1.4 Immunodetection of proteins

Nitrocellulose was incubated with antibodies, as per manufacturer's instructions. Typically, nitrocellulose was incubated for 1 hr at room temperature (or overnight at 4°C) in TBST containing 5% (w/v) non-fat milk powder, to promote blocking of non-specific binding. Nitrocellulose was then incubated with antibody, diluted to the required concentration in TBST containing 1% (w/v) non-fat milk powder. Nitrocellulose was washed 3 times for 10 min in TBST, before incubation with secondary antibody. Secondary antibodies were typically HRP (horseradish peroxidase) conjugated and used at a 1:1000 dilution in TBST containing 1% (w/v) non-fat milk powder. Nitrocellulose was again washed 3 times for 10 min in TBST. Immuno-labelled proteins were visualised using the ECL (enhanced chemi-luminescence) system according to the manufacturers instructions. The nitrocellulose was then exposed to film and developed using an X-Omat processor.

2.3.1.5 Immunoprecipitation of proteins

Antibody was bound to Sepharose beads (Protein A-Sepharose, for mouse and rabbit antibodies, Protein G-Sepharose for sheep antibodies) by incubation in IP buffer for 1 hr at 4°C. Beads were washed 3 times in IP buffer, before addition of muscle lysate. Beads and lysate were incubated for 2 hr at 4°C. Beads were again washed 3 times in lysis buffer. For gel electrophoresis beads were boiled in 2X SDS sample buffer and for kinase assays beads were washed 3 times in kinase assay buffer (see below).

2.3.1.6 Preparation of Bradford reagent and protein assays

Protein concentration of samples was determined by the method of Bradford (Bradford, 1976). Bradford reagent was prepared in house (5% (v/v) ethanol, 5.5%

(v/v) phosphoric acid, 40 mg/l Coomassie G) and filtered through Whatman No. 1 filter paper and stored protected from light. For protein determination, 1 ml of this reagent was added to 100 µl of sample and the absorbance measured against a reference sample which contained 1 ml Bradford reagent and 100 µl of water or buffer, as appropriate. Values obtained were compared to those of a standard curve prepared by analysing samples containing 1-6 µg BSA.

2.3.2 SHRSP

2.3.2.1 Animals

Rats were reared in-house, as described in (Jeffs et al., 1997, Davidson et al., 1995), and maintained under controlled conditions of temperature (21°C) and light (12 hr light-dark cycle). Rats were fed on normal rat chow (rat and mouse no.1 maintenance diet, Special Diet Services, UK) and had access to water *ad libitum* (as described in Jeffs et al., 1997).

2.3.2.2 Muscle dissection and tissue preparation

Male 12 week old rats were killed by CO_2 overdose. Muscles were carefully and quickly dissected and cleaned of connective tissue without stretching and with tendons intact. Muscles were allowed to recover for 30 min in KH buffer at 37°C with continuous gassing (95%O_2/5%CO_2). Muscles were pinned at resting length before performing stimulations.

2.3.2.3 Insulin stimulation of muscles

Muscles were quickly dissected, and allowed to recover, as described above, and incubated in the presence or absence of 1 µM insulin, in KH buffer containing 0.1% (w/v) BSA. Unless otherwise stated, muscles were quickly washed twice in 5 ml KH buffer without BSA, before being snap-frozen and stored at -80°C until required.

2.3.2.4 Glucose transport assays

Flexor digitorum brevis (FDB) muscles were placed in KH Buffer and were allowed to recover as described above. Muscles were incubated for 30 min in the presence or absence of 1 μM insulin. Muscles were then rapidly washed 3 times with glucose-free KH Buffer supplemented with 1% BSA and incubated for 10 min at 37°C in uptake buffer (KH buffer containing 1μM insulin, 10 μM deGlc (1 μCi/ml) and [^{14}C]-Sucrose (0.2 μCi/ml; used as an extracellular marker)). Muscles were washed 3 times with 5 ml ice-cold PBS, blotted on filter paper, weighed and solubilised in 1 ml 0.5 N NaOH at 60°C for 45 min. Tissue associated radioactivity was determined by liquid scintillation counting.

2.3.2.5 Preparation of muscle lysates

Muscles were prepared as described in section 2.3.2.3. Muscles were pulverised in liquid nitrogen using a mortar and pestle on dry ice. The powdered muscle was then homogenised using a Polytron hand-held homogeniser in 2.5-5 volumes ice cold lysis buffer. The homogenate was centrifuged at 14,000 x *g* for 10 min at 4°C to remove unsolubilised material.

2.3.2.6 Crude skeletal muscle fractionation

Muscles were prepared as described in section 2.3.2.3. Frozen tissue was then powdered in liquid nitrogen using a mortar and pestle on dry-ice and resuspended in HES buffer supplemented with proteinase inhibitor tablets, prior to homogenisation using a Teflon coated homogeniser. The homogenate was centrifuged at 12,000 x g for 20 min at 4°C and the pellet collected (heavy membrane fraction). The supernatant from this step was further centrifuged at 140,000 x g for 1 hr at 4°C and the pellet (light membrane fraction) and supernatant (soluble protein fraction) collected.

2.3.2.7 PKB assays

Soleus and EDL (extensor digitorum longus) muscle extracts were prepared as described in section 2.3.2.5. PKB (protein kinase B) immunoprecipitations were carried out using 200 μg soluble muscle extract and 2.5 μg anti-PKB-PH domain antibody, and assays performed on the immunoprecipitated protein. Reaction mixtures containing 20 μl HEPES-DTT (50 mM HEPES, pH 7.4, 1 mM DTT), 10 μl IP in HEPES-DTT and 10 μl 150 μM substrate peptide (RPRAATF) in HEPES-DTT were prepared on ice. The reaction was initiated by the addition of 10 μl ATP solution (250 μM [γ-^{32}P] ATP, specific activity 500,000-1,000,000 cpm/nmol, 50 mM $MgCl_2$). Blank reactions were prepared by substituting HEPES-DTT for substrate peptide. Reactions were allowed to proceed for 15 min at 30°C, at which time 40 μl of reaction mixture was spotted onto phosphocellulose paper and the paper dropped into 1% (v/v) phosphoric acid. The papers were washed, air-dried and the incorporation of ^{32}P into the substrate peptide determined in a scintillation counter.

2.3.2.8 GSK-3 assays

GSK (glycogen synthase kinase)-3 activity was assayed in immunoprecipitates obtained from muscle extracts, prepared as described in section 2.3.2.5, but in the absence of NaF. GSK-3α or GSK-3β immunoprecipitations were performed using 250 μg soluble muscle extract and 2.5 μg antibody. Reaction mixtures containing 20 μl IP in reaction buffer (8 mM MOPS, pH 7, 0.2 mM EDTA, 10 mM magnesium acetate) and 10 μl 400 μM substrate peptide (phospho-glycogen synthase peptide-2) were prepared on ice. The reaction was initiated by the addition of 10 μl ATP solution (450 μM [γ-^{32}P] ATP, specific activity 500,000-1,000,000 cpm/nmol, 75 mM $MgCl_2$). Blank reactions were prepared by substituting substrate peptide for an unphosphorylated form of the peptide, which cannot act as a substrate. When non-substrate peptide was not available H_2O was used, as it was found that the non-substrate peptide and H_2O resulted in similar values being obtained for blank reactions. Reactions were allowed to proceed for 30 min at 30°C, at which time 30 μl of reaction mixture was spotted onto phosphocellulose paper and the paper dropped

into 1% (v/v) phosphoric acid. The papers were washed, air-dried and the incorporation of ^{32}P into the substrate peptide determined in a scintillation counter.

2.3.2.9 Determination of muscle glycogen levels

Soleus and EDL muscles were prepared as described in sections 2.3.2.2 and 2.3.2.3. Muscles were pulverised in liquid nitrogen using a mortar and pestle on dry ice. The powdered muscle was then homogenised using a Polytron homogeniser in 2.5 volumes (w/v) 0.2 M sodium acetate, pH 4.8, containing 1% (v/v) Triton X-100. Extracts were then briefly sonicated, before addition of 250 mU amyloglucosidase (prior to addition of amyloglucosidase, 20 µl of sample was removed for protein determination). Extracts were incubated for 2 hr at 40°C and vortexed regularly, prior to incubation with assay cocktail (0.1 M Tris-HCl, pH 8.0, 0.3 mM ATP, 6 mM $MgCl_2$, 5 mM DTT, 1 mM NADP, 2.5 U/ml hexokinase, 1 µg/ml G6P-dehydrogenase) for 5 min at room temperature. Changes in fluorescence, as a result of NADPH production, were determined using an excitation wavelength of 355 nm and emission wavelength 460 nm. Reaction blanks were determined on samples that had not been treated with amyloglucosidase.

2.3.2.10 Glycogen synthesis

Glycogen synthesis was determined as [^{14}C]-glucose incorporation into glycogen. Freshly dissected and cleaned FDB muscles were incubated in KH buffer containing 5 mM glucose for 30 min at 37°C. Muscles were then pinned at resting length, and 3 ml KH buffer (containing 5 mM glucose) added. Muscles were incubated in the presence or absence of 1 µM insulin, with the addition of [U-^{14}C]-glucose (1 µCi/ml, final) for 1 hr at 37°C. At this time, muscles were rapidly washed 3 times with 5 ml of ice cold PBS. Muscles were blotted on filter paper, weighed and solubilised in 200 µl of 20% (w/v) KOH at 60°C for 30 min-1hr. Once fully dissolved, the lysate was neutralised by the addition of 200 µl 1M HCl and 400 µl water was added. Tubes were vortexed and 500 µl of the extract was transferred to screw cap eppendorfs and boiled for 8 min. Bovine glycogen (20 µl of 250 mg/ml) was added to give a final concentration of ~5 mg/ml. To precipitate glycogen 700 µl of ethanol was added, and

tubes were mixed overnight at 4°C. The samples were centrifuged at 2500 x g for 10 min and the pellets redissolved in 100 µl formic acid and 400 µl water, with warming of the tubes to 37°C. The radioactivity was determined by liquid scintillation counting.

2.3.2.11Glycogen Phosphorylase Assay

The activity of glycogen phosphorylase was measured in the direction of glycogen synthesis using a method adapted from (Gilboe et al., 1972) and (Halse et al., 2001). Soleus and EDL muscles were prepared as described in sections 2.3.2.2 and 2.3.2.3. Muscles were pulverised in liquid nitrogen using a mortar and pestle on dry ice. The powdered muscle was then homogenised in 2 volumes of glycogen phosphorylase extraction buffer (10 mM Tris-HCl, pH 7.8, 150 mM KF, 15 mM EDTA, 60 mM sucrose 1 mM DTT, 1 mM benzamidine, 1 mM PMSF, 5 µg/µl SBTI). Homogenates were then subject to sonication for 10 sec, amplitude 10. To 200-250 µg of protein (in 10 µl total volume extraction buffer) 190 µl of reaction cocktail (33 mM MES, pH 6.3, 20 mM EDTA, 100 mM KF, 1% (w/v) glycogen, 100 mM glucose-1-phosphate, 60 dpm/nmol ^{14}C glucose-1-phosphate; for phosphorylase A also 10 µM AMP and 5 mM caffeine, for phosphorylase A + B, 2 mM AMP) was added to start assay. Tubes were briefly vortexed and incubated at 30°C for 10 min. At this time point 175 µl was removed and spotted onto 3 cm x 3cm 3MM filter paper squares. Reactions were terminated by dropping filter paper into ice cold 60% ethanol. Filter papers were washed in 60% ethanol at room temperature for 2.5 hr, dried and subject to liquid scintillation counting.

2.3.2.12 Muscle fibre-typing

EDL muscles from WKY and SHRSP rats were dissected quickly and immediately prepared for cryotomy by freezing in iso-pentane cooled with liquid nitrogen. The frozen muscles were stored in a liquid nitrogen fridge until sectioning using a Bright cryostat. Sections were cut at 10µm and mounted on poly-l-lysine coated coverslips then stained using the following panel of histochemical reactions.

2.3.2.12.1 Staining sections for succinate dehydrogenase

Sections were stained for succinate dehydrogenase following the method of Martin et al. (1988). Sections were incubated in incubation medium (100 mM phosphate buffer, pH 7·6, 10 μM sodium azide, 1.5 mM Nitro B.T (Nitro blue tetrazolium), 5 mM EDTA, 48 mM disodium succinate, 20 μM PMS (Phenazine methosulphate)) at 37°C for 15-60 min (or until at least some fibres were strongly blue in colour) and then washed in water. Stained sections were mounted in aquamount.

2.3.2.12.2 Staining sections for myosin ATPase

Myosin ATPase staining was carried out using the method of Round et al. (1980). Briefly, for the routine pH 9.4 method, sections were incubated at 37°C for 30 minutes in the routine substrate incubation medium (1 mM ATP, 50 mM glycine, 50 mM NaCl, 100 mM $CaCl_2$, 2.5 μM DTT, pH 9.4) before performing three 2 min washes in 1% $CaCl_2$. Sections were incubated in 2% cobalt chloride for 2 min before washing thoroughly with water. Sections were then incubated in 1% ammonium sulphide (until specimens turn black, usually a few minutes), washed in water and mounted in aquamount. For the acid reverse method sections were pre-incubated in acetate buffer (20 mM sodium acetate, 66 mM acetic acid, pH 4.3 or 50 mM sodium acetate, 50 mM acetic acid, pH 4.6) at 37°C for 10 minutes. Sections were washed quickly in dilute buffered calcium chloride (10 mM glycine, 10 mM NaCl, 20 mM $CaCl_2$) before incubating in routine substrate incubation medium at 37°C for 30 minutes. Sections were washed three times for 2 min in 1% $CaCl_2$ before being incubated in 2% $CoCl_2$ for 2 min and then thoroughly washed with water. Sections were then incubated in 1% ammonium sulphide, washed in water and mounted in aquamount.

Stained sections were examined using a Zeiss Axiophot microscope and images captured with a JVC TK-1280E camera and Iomega Buz. These images came from the same area in each stained specimen and were representative of the overall fibre distribution.

2.3.3 Molecular Biology

2.3.3.1 Amplification of DNA by Polymerase Chain Reaction (PCR)

All PCRs were performed in thin-walled PCR tubes, in a Techne Progene thermocycler. Amplification of DNA was performed using *Pfu* polymerase enzyme. Reactions were typically set up as follows:

10X polymerase buffer	5 µl
forward primer (0.1mg/ml)	2.5 µl
reverse primer (0.1mg/ml)	2.5 µl
dNTPs (10 mM each dCTP, dGTP, dATP, dTTP)	2.5 µl
template DNA (50-100ng)	1 µl
polymerase	1 µl
nuclease-free water	to 50 µl

Tubes were then briefly vortexed before initiation of cycling. Typical cycling conditions were as follows:

95°C	2 min	
95°C	30 sec	30 cycles
55°C	30 sec	
68°C	2 min	
68°C	10 min	

Following PCR 20 µl of reaction mixture was analysed by agarose gel electrophoresis (see section 2.3.3.3).

2.3.3.2 Purification of PCR products

If a second round of PCR was to be performed, the first round PCR reaction was purified using a Qiagen PCR purification kit, according to the manufacturer's instructions, and using the buffers supplied. Briefly, 25 µl of the reaction was mixed

with 125 µl of buffer PB and placed in a QIAspin column and centrifuged in a microfuge at 14,000 rpm for 1 min. The column was then washed in 750 µl buffer PE containing ethanol, centrifuged again and the flow-through discarded. The column was centrifuged again to ensure complete removal of the buffer, placed in a sterile 1.5 ml microfuge tube and 50 µl of buffer EB (warmed to 40°C) was pipetted into the centre of the column and incubated for 1 min. The DNA was then collected by centrifugation in a microcentrifuge. For a further round of PCR 5 µl of this was used as a template.

2.3.3.3 Agarose gel electrophoresis

For standard small 1% agarose gels, 0.5 g agarose was dissolved in 50 ml TAE buffer in a microwave oven. This was allowed to cool, before addition of 1 µl ethidium bromide (10 mg/ml), giving a final concentration of 200 ng/ml. After mixing, the gel was poured into an electrophoresis cartridge and an appropriate comb inserted. The gel was allowed to set at room temperature, before being transferred to an electrophoresis tank containing TAE buffer. The comb was removed and samples in DNA loading buffer (5% (v/v) glycerol, 0.05% bromophenol blue) applied to the wells. 0.5-0.75 µg of a 1 kb DNA ladder was also used to allow determination of DNA size. Electrophoresis was carried out at 80 V for 45-60 min. Gels were visualised using an ultraviolet transilluminator and photographs were taken using a Mitsubishi video copy processor.

2.3.3.4 Gel purification of DNA

Required bands visualised under UV light were excised from agarose gels using a clean scalpel blade. Gel slices were transferred to sterile 1.5 ml microfuge tubes and DNA extraction was performed using a Qiagen gel purification kit, following the manufacturer's instructions, using the buffers supplied. Briefly, 600 µl of buffer QC was added to each gel slice and the tubes incubated at 37°C for 10-15 min, or until the agarose was completely dissolved. The solution was then applied to a QIAspin column, and centrifuged in a bench-top microfuge at 14,000 rpm for 1 min. The column was then washed with 750 µl buffer PE, the column centrifuged and the

flow-through discarded. The column was centrifuged again to ensure complete removal of the buffer, placed in a sterile 1.5 ml microfuge tube and 50 µl of buffer EB (warmed to 40°C) was pipetted into the centre of the column and incubated for 1 min. The DNA was collected in the microfuge tube by centrifugation for 1 min.

2.3.3.5 *Taq* polymerase treatment of *Pfu*-amplified products

If *Pfu*-amplified PCR products were to be cloned into pCRII-TOPO for sequencing or sub-cloning, they were first treated with *Taq* polymerase to add overhanging 'A' bases required for TA cloning. To do this 5 µl of Taq buffer, 1 µl dNTPs (10 mM each dCTP, dGTP, dATP, dTTP) and 1 µl *Taq* polymerase were added to gel purified PCR products (<50 µl). These were mixed thoroughly and incubated at 72°C for 20 min.

2.3.3.6 TA cloning of PCR products

TA cloning was performed using the pCRII-TOPO^{TM} kit, according to the manufacturer's instructions. Typically, 2 µl of *Taq* polymerase treated DNA was mixed with 0.5 µl pCRII-TOPO vector and incubated at room temperature for 5 min, before the addition of 0.5 µl salt solution (supplied with the kit). The 3 µl reaction mixture was gently added to a vial of OneShot TOP10 competent *Escherichia coli* cells (thawed on ice) and incubated on ice for 30 min. The cells were heat-shocked for 30 sec at 42°C in a water bath, chilled on ice for 1 min and then incubated in 250 µl SOC media (supplied with the kit) for 45 min at 37°C. The cells were plated onto LB agar plates containing 50 µg/ml kanamycin and incubated overnight at 37°C. Colonies were picked and cultured overnight in LB containing 50 µg/ml kanamycin. Small-scale DNA preparations were analysed by restriction digestion and sequencing (see below).

2.3.3.7 DNA restriction digests

Restriction digests were routinely performed in 20 µl volumes, containing 5 µl plasmid DNA, 2 µl of an appropriate 10X buffer, 1 µl of each restriction

endonuclease, and the remaining volume made up with sterile water. Digests were incubated at 37°C for 2-3 hrs. Following the addition of 6X DNA loading buffer, the digested DNA was subject to agarose gel electrophoresis, as described in section 2.3.3.3.

2.3.3.8 Ligations

Digested inserts and vectors were purified by agarose gel electrophoresis, followed by gel extraction, as described above. Ligation reactions were then set up in sterile microfuge tubes using approximately a 3:1 molar ratio of insert:vector. These were mixed together with 2 µl ligase buffer and 1 µl T4 ligase, in a final volume of 20 µl made up with sterile water. The ligation reactions were incubated overnight in an ice/water slurry. For transformation of *Escherichia coli* strain DH5α or XL1-blue 5 µl of the reaction was used.

2.3.3.9 Preparation of competent DH5α/ XL1-blue *Escherichia coli* cells

Sterile LB (10 ml) was inoculated with *E. coli* cells from a glycerol stock and cultured overnight at 37°C with shaking at 200 rpm. 0.5 ml of this was sub-cultured into 100 ml LB and further grown at 37°C with shaking until the optical density at 600 nm was 0.5-0.6 (typically this took around 2 hr). The cells were then chilled on ice for 10 min and harvested by centrifugation in sterile 50 ml tubes at 3000 rpm for 5 min at 4°C in a Beckman bench-top centrifuge. The supernatant was discarded and the cells gently resuspended in a total of 50 ml sterile 100 mM $CaCl_2$. The cells were incubated on ice for a further 30 min and were centrifuged as before. The supernatant was discarded and the cells were resuspended in a total of 5 ml 100 mM $CaCl_2$. The cells were divided into 250 µl aliquots in pre-chilled, sterile microfuge tubes and stored at -80°C until required.

2.3.3.10 Transformation of *Escherichia coli*

Competent *E. coli* cells, made as described in section 2.3.3.9, were thawed on ice and 50 µl per transformation were pipetted into pre-chilled sterile 1.5 ml microfuge

tubes. For each transformation, 5 µl of ligation reaction or 0.5 µl of purified plasmid DNA was added to the cells and gently mixed before incubation on ice for 15-30 min. The cells were then heat-shocked in a water bath at 42°C for 90 sec, then chilled on ice for 1 min. LB (450 µl) was added to each tube and incubated at 37°C for 45 min. The cells were pelleted by centrifugation for 10 sec at 14,000 rpm in a bench-top microfuge. Around 350 µl of LB was discarded and the cells resuspended in the remaining 150 µl. Cells were plated on to LB agar plates containing the appropriate antibiotic, and grown overnight at 37°C.

2.3.3.11 Small-scale DNA preparations

Bacterial colonies were picked from selective LB agar plates and transferred to 5 ml LB broth (containing 100 µg/ml ampicillin or 50 µg/ml kanamycin, as appropriate), and grown overnight at 37°C with shaking at 200 rpm. DNA purification was then performed using a Qiagen miniprep kit, according to the manufacturer's instructions and using the buffers supplied. Briefly, the cells from 1.5 ml of the culture were collected by centrifugation for 5 min at 14,000 rpm in a microfuge and resuspended in 250 µl buffer P1 (containing RNase A). Buffer P2 (250 µl) was added and the tubes mixed by inverting. Buffer N3 (350 µl) was added and the tubes mixed by inverting. The tubes were centrifuged for 10 min at 14,000 rpm in a microfuge and the supernatants were decanted into Qiagen miniprep spin columns and centrifuged for 1 min at 14,000 rpm in a microfuge. Buffer PE (750 µl), containing ethanol, was added to the column and the column was centrifuged again. The column was centrifuged again to ensure complete removal of the buffer. Buffer EB (50 µl), warmed to 40°C, was then pipetted into the centre of the column and incubated for 1 min. The DNA was then collected in a microcentrifuge, by centrifugation for 1 min.

2.3.3.12 Large-scale DNA preparations

Large-scale DNA preparations were performed using a Qiagen plasmid maxi kit, following the manufacturer's instructions and using the buffers supplied. Briefly, bacterial cultures of 100 ml were grown overnight in LB containing the appropriate antibiotic for selection. Cells were harvested by centrifugation at 3000 rpm for 10

min. The cells were resuspended in a total of 10 ml buffer P1 (containing RNase A). Buffer P2 (10 ml) was added and allowed to lyse the cells for 5 min. The reaction was neutralised by the addition of 10 ml chilled buffer P3. The precipitate formed was removed by centrifugation at 3000 rpm for 30 min, followed by filtration through 2 layers of muslin. The supernatant was then applied to a P100 Qiagen column, pre-equilibrated with 10 ml buffer QBT. The column was washed with 30 ml buffer QC (containing ethanol), before elution of DNA by the addition of 15 ml buffer QF. To precipitate DNA, 10.5 ml isopropanol was added to the eluted DNA and mixed well. The precipitated DNA was collected by centrifugation at 3000 rpm for 30 min. The pellet was washed in 4 ml 70% (v/v) ethanol. The ethanol was removed and the pellet air-dried prior to resuspension in 250 µl TE. The DNA concentration and purity were then assessed spectrophotometrically.

2.3.3.13 DNA sequencing

Initially, DNA sequencing was carried out by the University of Glasgow Molecular Biology Support Unit. Latterly, sequencing was carried out by MWG Biotech, Germany.

2.3.4 Yeast Two-Hybrid

2.3.4.1 Yeast media

YPD powder was dissolved in distilled water, according to manufacturer's instructions. The media was sterilised by autoclaving and allowed to cool. Sterile-filtered adenine hemisulphate (0.2% (w/v)) was added to give YPAD which had a final concentration of 0.003% adenine. For agar plates (containing 20g/l agar), the sterilised media was allowed to cool to 55-60°C before addition of adenine and subsequent pouring.

Quadruple dropout synthetic selection media consisted of 0.67% (w/v) yeast nitrogen base, 2% (w/v) glucose and 0.2% (w/v) complete supplement mixture (-Ade/-His/-Leu/-Trp). Triple (-Leu/-Trp/-His) and double (-Leu/Trp) dropout media were prepared by adding back the appropriate amino acids. Leucine and histidine were

added before autoclaving to give final concentrations of 0.002% and 0.001% respectively. The media was sterilised by autoclaving and allowed to cool. If required, sterile-filtered adenine hemisulphate (0.2% (w/v)) was added to give a final concentration of 0.003% adenine and sterile filtered tryptophan 1% (w/v) was added to give a final concentration of 0.002%.

2.3.4.2 Amplification of library DNA

MATCHMAKER™ cDNA libraries were purchased from Clontech. These consisted of *E. coli* cells expressing the pACT2 library and required amplification to obtain enough plasmid for yeast two-hybrid screening. Amplification was performed using agar plates, rather than in liquid media, to allow even representation of all the clones. Thus, cells were plated directly onto LB agar containing 100 μg/ml ampicillin and grown for 48 hr at 30°C. Cells were scraped into LB/glycerol (25% v/v), pooled and mixed thoroughly, and stored overnight at 4°C. Aliquots were prepared and stored at -70°C for future use. Around one third of the cells (equivalent to 3 litres of overnight culture) were used for plasmid preparation. DNA was prepared in a similar manner as described in section 2.3.3.12, large-scale DNA preparations.

2.3.4.3 Construction of the bait plasmid: pGBT9-flotillin 152-427

Human flotillin 152-427 was PCR amplified from skeletal muscle cDNA (a generous gift from Prof. K. Johnston, Molecular Genetics, University of Glasgow, Glasgow, UK) using *Pfu* polymerase and the following primers: 5′-GagatctGTAAGGACATTCACGATGACCAGG-3′ (*Bgl*II site in small letters) and 5′-ctcgag**TCA**GGCTGTTCTCAAAGGCTTG-3′ (*Xho*I site in small letters, STOP codon in bold). The resulting products were cloned into pCRII-TOPO, sequenced and subcloned into the *Bam*HI and *Sal*I sites of pGBT9, according to the methods in section 2.3.3.

2.3.4.4 Small-scale lithium acetate yeast transformations

A 25 ml overnight culture of PJ69-2A was used to inoculate 300 ml of YPAD to give a starting OD_{600} of between 0.2-0.3. This was further cultured at 30°C with shaking at 200 rpm, until the OD_{600} reached 0.4-0.6 (typically 3-4 hr). Cells were harvested by centrifugation at 2000 rpm for 5 min at room temperature in a bench-top Beckman centrifuge. The pelleted cells were resuspended and pooled in 25 ml sterile water and spun again. Cells were then resuspended in 1.5 ml freshly prepared sterile 100 mM lithium acetate in TE buffer. 100 µl of cells were transferred to a sterile 1.5 ml microfuge tube containing 10 µl salmon sperm carrier DNA (10 mg/ml) and 1 µl of each plasmid to be transformed. These were briefly vortexed and 0.6 ml freshly prepared sterile 5% (w/v) PEG-3350/100 mM LiAc solution was added to each tube. Tubes were vortexed for 10 sec and incubated at 30°C for 30 min with shaking at 200 rpm. DMSO (70 µl) was then added to each tube and mixed by inverting before being heat-shocked for 15 min at 42°C in a waterbath. The tubes were placed on ice for 1 min before being centrifuged for 5 sec in a microcentrifuge. The cell pellets were resuspended in 0.25 ml sterile TE and plated onto the appropriate synthetic medium selective for the transformed plasmids (lacking leucine and tryptophan if pGBT9 and pACT2 plasmids were co-transformed). After 3-4 days of growth at 30°C, colonies were picked and re-streaked onto selective media also lacking histidine (triple dropout, TDO) or histidine and adenine (quadruple dropout, QDO), to screen for the reconstitution of transcriptional activation and hence interactions.

2.3.4.5 Extraction of library plasmids from yeast cells

Yeast cells were grown overnight in liquid media lacking leucine and tryptophan. Cells were harvested from 1.5 ml of this overnight culture by centrifugation at 5000 rpm for 1 min in a bench-top microfuge. Cells were resuspended in 0.5 ml buffer S (10 mM K_2HPO_4, pH 7.2, 10 mM EDTA, 50 mM β-mercaptoethanol, 50 µg/ml zymolyase) and incubated at 37°C for 30 min, before addition of 100 µl lysis buffer (25 mM Tris-HCl, pH7.5, 25 mM EDTA, 2.5% (w/v) SDS). The tubes were vortexed and incubated for a further 30 min at 65°C before the addition of 166 µl of 3M potassium acetate, pH 5.5. Tubes were mixed by inverting and incubated on ice for

10 min. The tubes were centrifuged in a microfuge at 4°C for 10 min at 14,000 rpm. The supernatants were transferred to fresh tubes on ice containing 800 µl of 100% ethanol and incubated for 10 min. DNA was pelleted by centrifugation in a microfuge at 4°C for 10 min at 14,000 rpm, washed in 70% ethanol and allowed to air dry. The pellets were then resuspended in 40 µl distilled water. This DNA preparation contains both library and bait plasmid DNA, therefore to select for library plasmids, these preparations were transformed into elecrocompetent KC8 cells.

2.3.4.6 Preparation of electrocompetent KC8 cells

KC8 cells contain a *leuB* mutation resulting in a requirement for leucine to sustain growth which allows direct selection of the yeast LEU 2 gene, carried on the library plasmids.

KC8 cells were cultured overnight at 37°C by inoculating 5 ml of LB broth with cells scraped from an agar plate. 2 ml of this culture was used to inoculate another 200 ml of LB and incubated at 37°C with shaking at 200 rpm. When the OD_{600} of the culture had reached 0.5-0.6 (around 2-3 hr), cells were cooled on ice for 30 min, before harvesting in 50 ml tubes by centrifugation at 4°C for 10 min at 4000 rpm in a Beckman bench-top centrifuge. Cell pellets were resuspended in 50 ml ice cold, sterile water, mixed and centrifuged as before. This washing step was repeated again, and the cell pellets resuspended and pooled in 20 ml 10% (v/v) ice cold, sterile glycerol. Cells were harvested by centrifugation as before and the pellet resuspended in an equal volume of ice cold 10% glycerol. Cells were aliquoted (100 µl/transformation) into microcentrifuge tubes, and stored on ice until used.

2.3.4.7 Electroporation of KC8 cells (recovery of prey plasmids)

KC8 cells were prepared on day of use as described above. DNA extracted from yeast (1 µl) was added to 100 µl of KC8 cells before transferring to a pre-chilled sterile electroporation cuvette. Electroporation was carried out in a Bio-Rad Micropulser. The cells were gently recovered in 0.5 ml LB broth and incubated for 1

hr at 37°C. Cells were pelleted by centrifugation at 4000 rpm in a bench-top microfuge and 300 µl buffer was removed before resuspending and plating onto M9 minimal media agar plates lacking leucine. Plates were incubated at 37°C overnight. Colonies were picked and cultured overnight in LB broth containing 100 µg/ml ampicillin. Small-scale DNA preparations were then performed as described in section 2.3.3.11 and the purified plasmids were digested with *Bgl*II and *Eco*RI to verify that the correct plasmids had been rescued and also to verify the sizes of the inserts within those plasmids.

2.3.4.8 Re-transformation of recovered plasmids

Following the rescue of the pACT2 prey plasmids encoding the putative flotillin-1 interacting proteins, it was necessary to re-transform these back into the yeast with the bait pGBT9-flotillin 152-427 plasmid to ensure that the yeast were growing as a result of the plasmids and not due to mutation of the yeast. All transformations were carried out as described in section 2.3.4.4.

2.3.4.9 Sequence analysis

Prey plasmids that appeared to confer interactions with flotillin were digested with *Bgl*II to determine the sizes of the inserts, and subjected to sequencing. This was initially performed according to the procedure outlined in section 2.3.3.13 using a primer designed against the GAL4 activation domain sequence 5′-TACCACTACAATGGAT-3′. Sequences obtained were then analysed in Editview and by BLAST searching (Altschul et al., 1990).

2.3.4.10 Preparation of yeast lysates

A match-head sized ball of yeast was resuspended in 1 ml distilled H_2O. Prior to incubation on ice for 10 min, 150 µl of a 1.85 M NaOH, 7.5% β-mercaptoethanol solution was added. TCA (150 µl, 55%, w/v) was then added before a further 10 min incubation on ice. The precipitates were centrifuged for 15 min at 14,000 rpm, 4°C,

and the supernatant removed. Precipitated proteins were resuspended in 100 µl sample buffer.

2.3.5 eNOS Antibodies

2.3.5.1 Preparation of peptide-keyhole limpet haemocyanin conjugates

Peptides corresponding to residues 1172 to 1183 of human eNOS, CR_{1172}IRTQSFSLQER$_{1183}$ (dephosphorylated) and CR_{1172}IRTQSpFSLQER$_{1183}$ (phosphorylated) were linked to keyhole limpet haemocyanin (KLH), for use in rabbit immunisation. Briefly, 100 µl of 25 mg/ml 3-maleimidobenzoic acid N-hyroxysuccinimide ester (MBS) in dimethyl formamide was added to 1 ml KLH (15 mg/ml in PBS) drop wise in glass, with stirring at room temperature for 30 min. Free MBS was separated from that bound to KLH by gel filtration on Sephadex G25 (PD-10 disposable columns). The MBS-KLH was diluted to 2.5 ml in PBS and loaded onto a column pre-equilibrated in 25 ml PBS. The flow-through was discarded and elution of activated KLH was achieved using 3.5 ml PBS. The eluate was divided into 3 aliquots containing 5 mg activated KLH in each. Activated KLH (5 mg) was incubated with 250 µl of 20 mg/ml peptide with stirring for 3 hr at room temperature. The final mixes were divided into 5 aliquots, each containing 1 mg activated KLH and stored at -20°C.

2.3.5.2 Immunisation of rabbits with peptide-keyhole limpet haemocyanin conjugates

All of the immunisation and collection of sera was performed by the Scottish Antibody Production Unit (Diagnostics Scotland), Carluke, Lanarkshire, Scotland. One rabbit was immunised with one peptide and the immunisation schedule was as follows. Rabbits were initially immunised with 1 mg of peptide conjugate. They were re-immunised with the same amount of peptide conjugate one, two and three months after the initial immunisation. Blood was taken one week after the second and third immunisations and the animals were exanguinated after the fourth.

2.3.5.3 Preparation of antibody affinity columns

For each anti-peptide antibody, an affinity column was prepared using the same peptide. Activated CH Sepharose 4B (1 g) was placed into a Bio-Rad 'Econo-pak' disposable column and mixed with 15 ml of 1 mM HCl. This was eluted and the column washed with a further 200 ml of 1 mM HCl. The column was washed in 15 ml coupling buffer (0.1M $NaHCO_3$, pH 8.0), stoppered and 10 μmol peptide in 6 ml coupling buffer added. The peptide and CH Sepharose were then mixed for 4 hr on a rotating mixer at room temperature. The column was allowed to drain and the flow-through collected. The remaining active groups were blocked by the addition of 15 ml 0.1M Tris/HCl, pH 8.0. The column was stoppered and the CH Sepharose-peptide column resuspended and mixed for 1 hr on a rotating mixer at room temperature. The column was allowed to drain under gravity and the Sepharose resuspended in 15 ml TBS supplemented with 0.1% (v/v) Tween-20 and 0.02% sodium azide, and stored at 4°C.

2.3.5.4 Purification of anti-peptide antibodies

Peptide columns, prepared as described above, were used to purify anti-peptide antibodies from immunised rabbit serum. Columns were washed with 200 ml TBS supplemented with 0.1% (v/v) Tween-20. 5 ml rabbit serum was diluted three-fold in TBS/0.1% Tween and then loaded onto the column. Serum obtained from the rabbit immunised with phospho-peptide was first loaded 3 times onto the dephospho-peptide column, and then 3 times onto the phospho column. Conversely, serum obtained from the rabbit immunised with the dephospho peptide was loaded first 3 times onto the phospho-peptide column and then 3 times onto the dephospho-peptide column. Columns were washed with 300 ml TBS/0.1% Tween containing 0.4 M NaCl to remove non-specifically bound proteins. The column which had been the latter to be loaded with serum was the one from which specifically bound antibodies were eluted. This was achieved using 20 ml 50 mM glycine, pH 2.5 at 4°C. 1 ml fractions were collected and 50 μl of 1.5 M Tris/HCl, pH 8.0 at 4°C added to each fraction. The protein concentration of each fraction was assayed and the peak fractions pooled. Columns were recycled by washing with 100 ml 10X TBS and stored as described above.

2.3.5.5 Preparation of eNOS protein

For characterisation of the antibodies concentrated eNOS protein was prepared from homogenates of cell pellets, from cells infected with an eNOS adenovirus construct driving the level of eNOS expression (prepared by Dr. A. Frater, Department of Medicine and Therapeutics, University of Glasgow, Glasgow, UK). This cell debris still contained a large amount of eNOS protein. The cell pellet was solubilised in lysis buffer containing 1% (v/v) Triton X-100. The insoluble material was pelleted by centrifugation at 14,000 rpm in a bench top microfuge at 4°C for 10 min. Lysis buffer was again added to this insoluble fraction and was subject to sonication in a sonicating waterbath for 20 min.

2.3.5.6 Preparation of ^{32}P labelled eNOS

To specifically test the phospho-specific eNOS antibodies produced, eNOS was phosphorylated using AMPK in the presence of ^{32}P-labelled ATP. Soluble eNOS protein (200 μg), prepared as described above, was incubated with 35 units of AMPK, 200 μM AMP, 200 μM ATP (25 μCi), 3 μM $CaCl_2$, 1 μM calmodulin and 10 mM $MgCl_2$, for 30 min at room temperature. The phosphorylated protein was then resolved by SDS-PAGE, and subject to phosphorimage analysis or western blotting using the antibodies described in chapter 5.

2.3.5.7 Alkaline phosphatase treatment of eNOS

To specifically test the dephospho-specific eNOS antibodies produced, eNOS protein was subjected to treatment with alkaline phosphatase, to remove phosphates from phosphorylated residues. Phosphatase inhibitors (in the soluble eNOS protein described in section 2.3.4.5) were removed by concentrating the protein using a microconcentrator, and centrifuging at 14,000 rpm in a bench top microfuge for 15 min, adding 10 mM Tris/HCl, pH 8.0 (containing protease inhibitors) and centrifuging again. eNOS protein was then subjected to treatment with alkaline phosphatase. 250 μg protein was incubated with 50 units of alkaline phosphatase in the relevant volume of 10x reaction buffer (supplied by the manufacturer) for 30 min

at 30°C. At this time another 50 units of alkaline phosphatase was added to the reaction, which was allowed to proceed for a further 30 min at 30°C. eNOS protein was subject to gel electrophoresis, proteins transferred to nitrocellulose and antibodies tested.

2.3.5.8 Culture of Human Aortic Endothelial Cells (HAECs)

HAECs were grown in large vessel endothelial cell medium at 37°C in 5% CO_2 and passaged when 80% confluent. Cells were used for experiments between passages 3 and 6. Prior to use cells were maintained in serum free media for 4 hr. Incubations were performed in serum free media or KRH. Endothelial cell lysates were prepared by scraping cells into standard lysis buffer (section 2.2).

2.3.5.9 Methanol fixation and preparation of coverslips for confocal microscopy of HAECs

HAECs were grown on collagen-coated 22 mm diameter glass coverslips in large vessel endothelial cell medium at 37°C in 5% CO_2. Cells were fixed by the addition of 4 ml methanol for 5 min at -20°C. The coverslips were washed three times with 5 ml PBS, and blocked in goat serum diluted 1:10 in PBS for 30 min. Coverslips were washed a further three times with 5 ml PBS and incubated for 1 hour with primary antibody diluted appropriately in PBS. The coverslips were again thoroughly washed with PBS and then incubated for 1 hour with 1:100 FITC-linked goat anti-rabbit IgG. Coverslips were again thoroughly washed and then mounted on slides and stored at 4°C until viewed on the confocal microscope.

2.4 Statistical analysis

Statistical analysis was performed using the Student's t-test (2-tailed independent samples). A p value < 0.05 was taken as a significant difference between two groups.

CHAPTER 3

PREPARATION AND CHARACTERISATION OF ANTI-ENDOTHELIAL NITRIC OXIDE SYNTHASE ANTIBODIES, SPECIFIC FOR RESIDUE SERINE 1177 (PHOSPHORYLATED OR UNPHOSPHORYLATED)

3.1 Introduction

As described in Chapter 1, nitric oxide has been reported to have various effects on basal, contraction- and insulin-stimulated glucose transport in skeletal muscle. It has also been shown that insulin may have a role in endothelial cell nitric oxide production, via activation of endothelial nitric oxide synthase. eNOS is regulated in a number of ways, most notably by binding calmodulin at increased intracellular calcium concentrations. In addition, eNOS is also subject to post-translational modifications, including protein phosphorylation.

eNOS is phosphorylated on serine and threonine (Butt et al., 2000, Michell et al., 2001), and tyrosine (Fisslthaler et al., 2000) residues. However, research has focussed on the phosphorylation of eNOS at serine 1177 and threonine 495 (human sequence). Serine 1177 lies in the C-terminal reductase domain of the eNOS molecule and its phosphorylation results in eNOS activation. Some researchers (Chen et al., 1999) hypothesise that eNOS is auto-inhibited by its C-terminus and phosphorylation of Ser-1177 removes this auto-inhibition. Conversely, phosphorylation of threonine 495 is suggested to be an inhibitory phosphorylation, due to the fact that this residue lies within the calmodulin binding sequence (Fleming et al., 2001). Phosphorylation of Thr-495 is thought to prevent calmodulin binding and subsequent activation of the molecule.

Much of the research carried out to date on phosphorylation of eNOS has been carried out using a variety of endothelial cell cultures. A number of external signals have been identified which modulate the phosphorylation state of eNOS. These include shear stress (Corson et al., 1996, Fisslthaler et al., 2000), VEGF (Fulton et al., 2002), insulin (Montagnani et al., 2001), bradykinin (Harris et al., 2001), and hydrogen peroxide (Thomas et al., 2002). Various kinases have been identified which are reported to mediate these phosphorylations. These include AMPK (Chen et al., 1999), PKB/Akt (Fulton et al., 1999, Dimmeler et al., 1999, Michell et al., 1999), cAMP dependent protein kinase and cGMP dependent protein kinase (Butt et al., 2000) and calmodulin dependent kinase II (CaMKII) (Fleming et al., 2001), which all phosphorylate Ser-1177. In contrast, PKC phosphorylates eNOS on Thr-495 (Michell et al., 2001). A number of phosphatases have also been implicated in

regulating eNOS activity. Protein phosphatase 2A (PP2A) was reported to be responsible for Ser-1177 dephosphorylation (Michell et al., 2001) and PP1 was shown to dephosphorylate Thr-495 (Michell et al., 2001, Fleming et al., 2001), while another report implicated PP2B in Thr-495 dephosphorylation (Harris et al., 2001). It is likely that the specific protein kinase that phosphorylates eNOS on Ser-1177 will depend on the given stimulus, for example shear stress reportedly leads to activation of PKB and phosphorylation of eNOS Ser-1177, in a PI3-kinase dependent manner (Dimmeler et al., 1999). However, another study, (Boo et al., 2002), suggests that VEGF stimulates eNOS Ser-1177 phosphorylation via PKB, but shear stress acts through PKA-dependent and PKB-independent mechanisms. Additionally some stimuli, for example bradykinin, have been suggested to promote co-ordinate dephosphorylation of Thr-497 and phosphorylation of Ser-1179 (bovine sequence) (Harris et al., 2001). Thus, regulation of eNOS activity by phosphorylation is somewhat complex and specific tools are required to study this in more depth.

3.1.1 Aims of Chapter

As phosphorylation of serine 1177 plays a pivotal role in regulation of eNOS activity, anti-peptide antibodies specific for both the phosphorylated and unphosphorylated forms of the eNOS protein at this residue, were prepared and characterised. The aim was to use these antibodies to study eNOS activation/inactivation in skeletal muscle in response to various stimuli, allowing the role of eNOS activation and NO production to be explored in skeletal muscle.

3.2 Results

3.2.1 Preparation of anti-peptide antibodies

As described in Materials and Methods sections 2.3.5.1-2.3.5.4, rabbits were immunised with peptides corresponding to residues 1172 to 1183 of human eNOS, CR_{1172}IRTQSFSLQER$_{1183}$ (unphosphorylated) and CR_{1172}IRTQSpFSLQER$_{1183}$ (phosphorylated), serum collected and antibodies purified on peptide columns. Figure 3.1 shows Coomassie-stained gels of fractions collected from the affinity columns. Typically the antibodies eluted from the columns in the early fractions. The antibody fractions were then pooled and concentrated for later use.

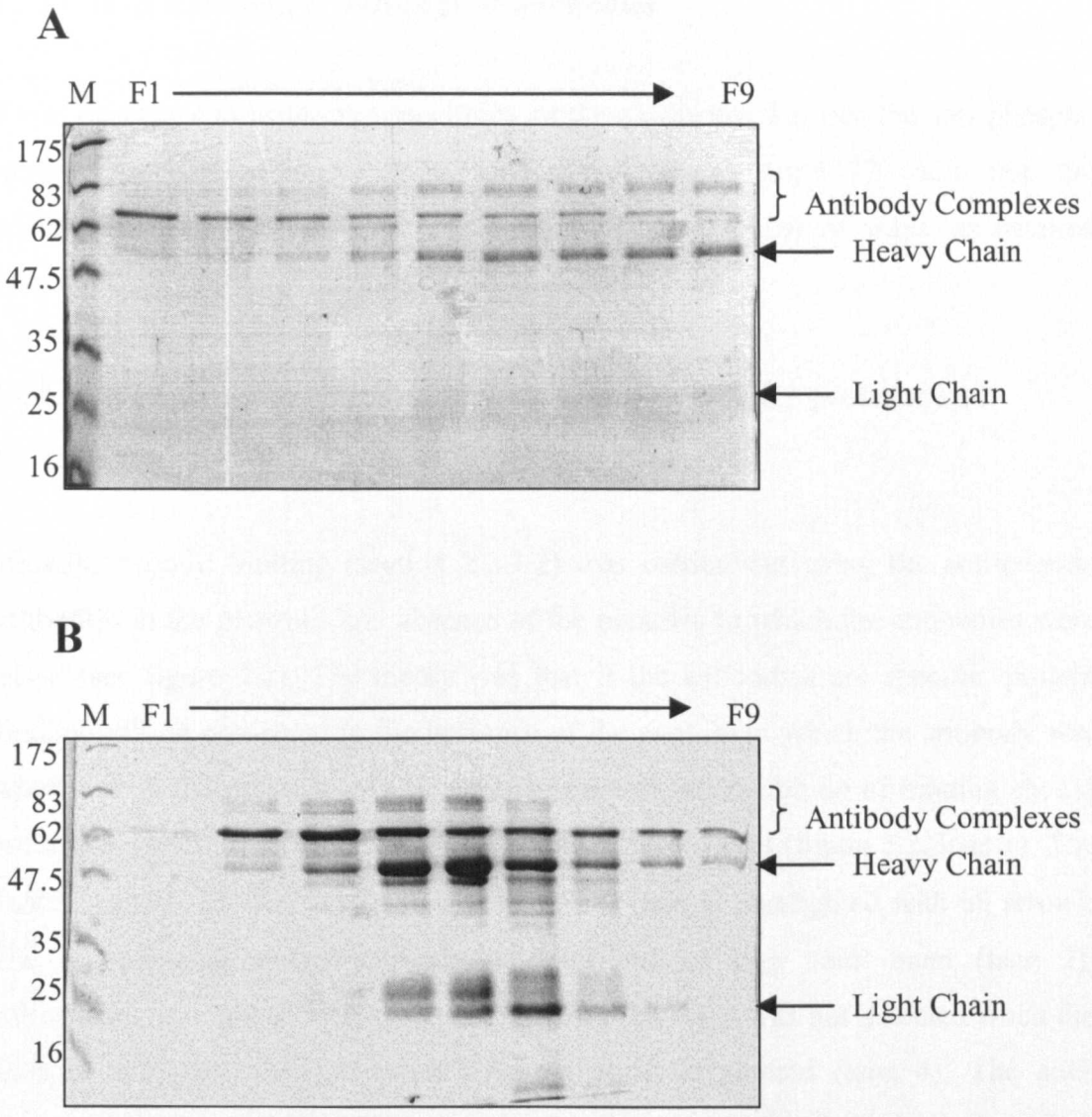

Figure 3.1 Preparation of anti-peptide antibodies

Antibody affinity columns were prepared as described in section 2.3.5.3. Purification of anti-peptide antibodies was carried out as described in section 2.3.5.4. 20 µl of each fraction was subjected to SDS-PAGE, and gels were stained with coomassie blue to visualise proteins. Panel A shows the first 9 fractions collected from purification of the anti-phospho eNOS antibody. Panel B shows the first 9 fractions collected from purification of the anti-dephospho eNOS antibody. The positions of the molecular weight standards are shown on the left of the figure.

3.2.2 Characterisation of anti-peptide antibodies

It was necessary to assess the specificity of the antibodies, i.e. that the anti-phospho antibody recognises only eNOS phosphorylated at Ser-1177, and not the unphosphorylated protein. This was performed in a number of ways, as detailed below.

3.2.2.1 Western blotting with anti-peptide antibodies in the presence and absence of blocking peptides

Initially, western blotting (section 2.3.1.2) was carried out using the anti-peptide antibodies in the presence and absence of the peptides to which the antibodies were raised (see figure 3.2). The theory was that if the antibodies are specific, protein binding will be prevented in the presence of the peptide to which the antibody was raised, but in the presence of the converse peptide, no inhibition of binding should occur. As a control, a commercial eNOS antibody was used (figure 3.2, lane 1). The darkest band (~130kD) is assumed to be eNOS (and is highlighted with an arrow). The anti-phospho eNOS antibody detected only a very faint band (lane 2), corresponding to phospho eNOS Ser-1177, and this band was not detected when the phospho antibody was incubated with the phospho peptide (lane 4). The anti-phospho eNOS antibody in the presence of dephospho peptide is shown in lane 5. A very faint band can be seen, similar to lane 2. The anti-dephospho eNOS antibody detects a strong signal at around 130 kDa. Incubation with the phospho peptide does not prevent the dephospho eNOS antibody recognising the eNOS protein (lane 6), but in the presence of dephospho peptide, binding is prevented completely (lane 7). These results suggest that the antibodies specifically recognise phosphorylated or dephosphorylated eNOS, corresponding to the peptides they were raised against.

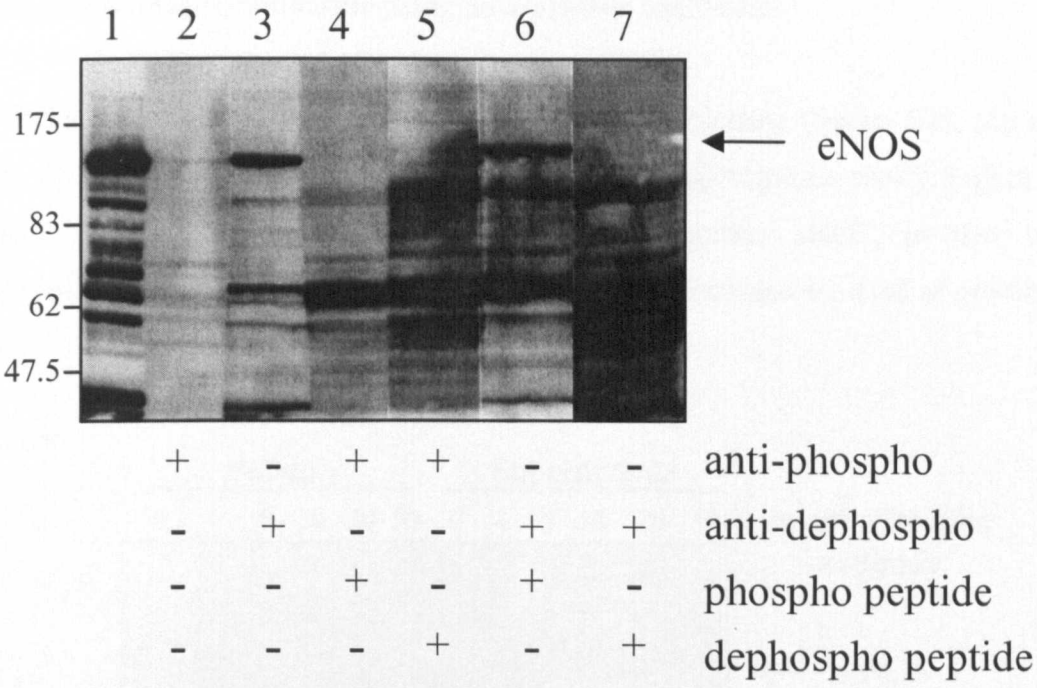

Figure 3.2 Western blotting using phospho and dephospho antibodies in the presence and absence of blocking peptides

Soluble eNOS protein (100 μg), prepared as described in section 2.3.5.5, was subjected to SDS-PAGE, and subsequent western blotting. The nitrocellulose was then cut into 7 strips and probed, as described below, with various antibodies in the presence or absence of blocking peptide. 1 = anti-eNOS from Sigma, 1:1000 dilution 2 = anti-phospho eNOS, 1:200 dilution, 3 = anti-dephospho eNOS, 1:200 dilution, 4 = anti-phospho eNOS, and 0.25 mg/ml phospho peptide, 5 = anti-phospho eNOS, and 0.25 mg/ml dephospho peptide, 6 = anti-dephospho eNOS, and 0.25 mg/ml phospho peptide, 7 = anti-dephospho eNOS, and 0.25 mg/ml dephospho peptide. The positions of molecular weight standards are shown on the left of the figure. The arrow indicates the position of eNOS.

3.2.2.2 Immunoprecipitations using anti-peptide antibodies

As the antibodies appeared to work well for western blotting (figure 3.2), the next step was to test the ability of the antibodies to immunoprecipitate eNOS. Figure 3.3 shows that the antibodies effectively immunoprecipitate eNOS, in that with increasing concentrations of antibody, the supernatant becomes depleted of protein.

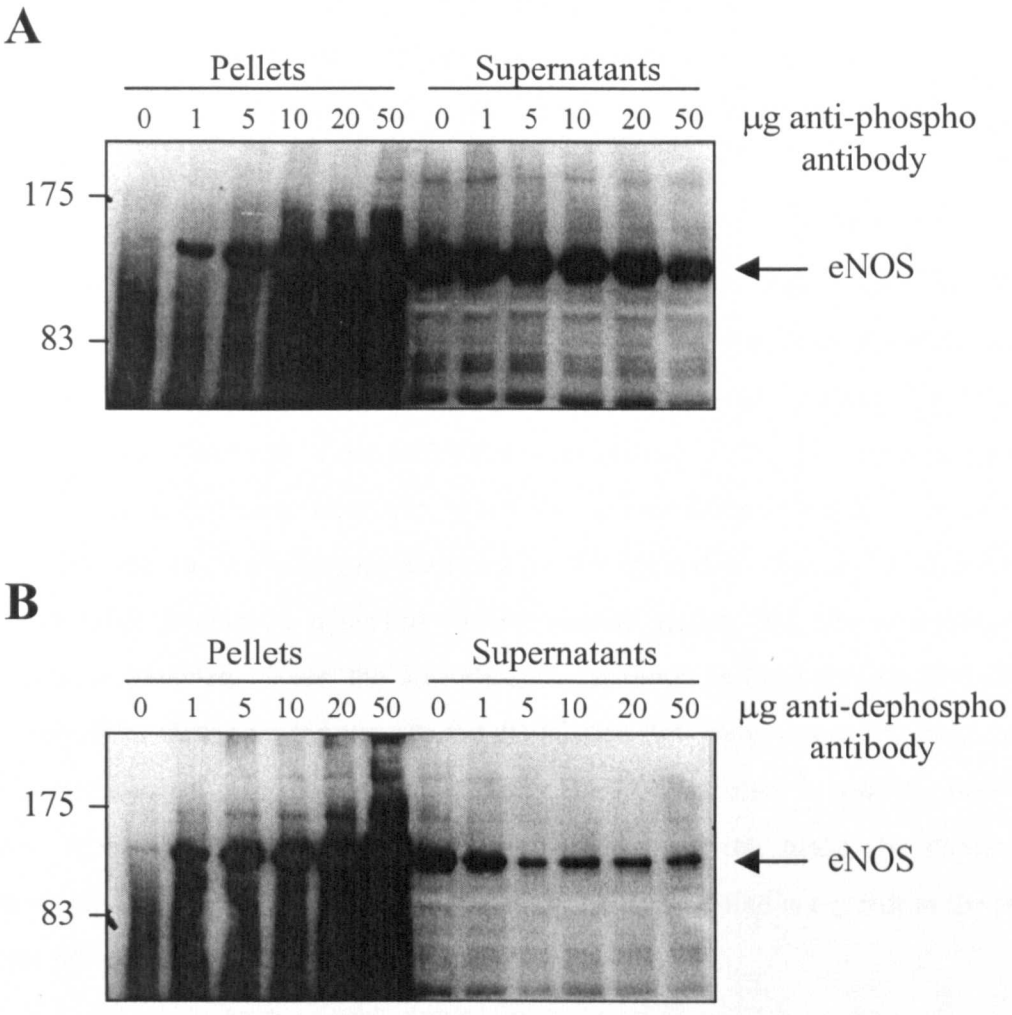

Figure 3.3 eNOS immunoprecipitations using antibodies prepared in-house
eNOS protein was prepared as described in section 2.3.5.5. eNOS protein (50 μg) was subjected to immunoprecipitation (see section 2.3.1.5) using increasing concentrations of antibodies as indicated. In panel A immunoprecipitations were carried out using the anti-phospho eNOS antibody. In panel B immunoprecipitations were carried out using the anti-dephospho eNOS antibody. Positions of molecular weight standards are shown on the left of the figure.

To analyse further the specificity of the antibodies, sequential immunoprecipitations were performed in which the immuno-depleted supernatant from an immunoprecipitation (IP) with one of the antibodies was subjected to immunoprecipitation using the other antibody. It would be expected, for example, that if an IP was carried out using the anti-phospho antibody, and the supernatant again used for an anti-phospho antibody IP, that little or no protein would be immunoprecipitated in the second instance, because the supernatant would have been essentially depleted of phospho eNOS during the first IP. However if the anti-dephospho antibody were used in the second instance, it would be expected that protein would be immunoprecipitated, due to the fact that dephospho eNOS had not previously been depleted.

The data from the sequential IP experiment is shown in figure 3.4. The results observed are somewhat confusing and not as expected. When both IPs were carried out using the anti-phospho antibody (figure 3.4, experiment 1) a small amount of eNOS protein is observed in the pellet from the second IP, but the supernatant does not appear to be depleted. However, when the anti-dephospho antibody is used for the first IP, and the anti-phospho antibody for the second IP (figure 3.4, experiment 2), very little protein is observed in the second pellet, but the supernatant is significantly depleted. When the anti-phospho antibody is used for the first IP the anti-dephospho antibody for the second IP (figure 3.4, experiment 3), much more protein is observed in the second pellet, and yet the supernatant is scarcely depleted. Finally, when both immunoprecipitations were carried out using the dephospho antibody (figure 3.4, experiment 4), no band of the correct size is present in the pellet and yet the supernatant is largely depleted.

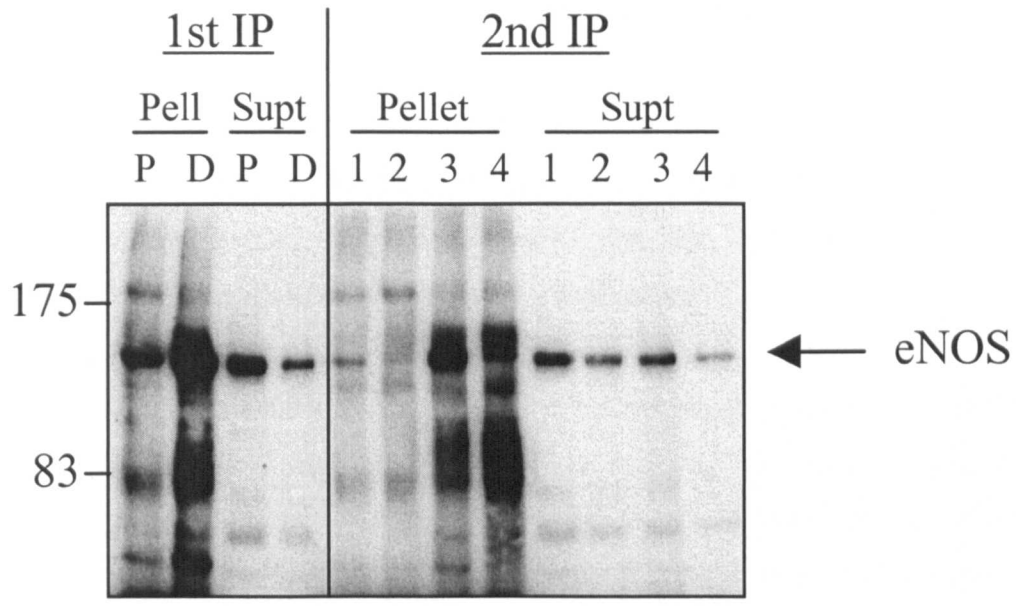

Figure 3.4 Sequential eNOS immunoprecipitation with phospho and dephospho antibodies

eNOS protein was prepared as described in section 2.3.5.5. Immunoprecipitations (section 2.3.1.5) were carried out using 25 μg eNOS protein and 10 μg of either anti-phopspho or -dephospho eNOS antibody. The supernatants from these immunoprecipitations were then used to immunoprecipitate with the converse antibody.

1 = IP with anti-phospho antibody first and anti-phospho antibody second

2 = IP with anti-dephospho antibody first and anti-phospho antibody second

3 = IP with anti-phospho antibody first and anti-dephospho antibody second

4 = IP with anti-dephospho antibody first and anti-dephospho antibody second.

The samples were subjected to SDS-PAGE, transferred to nitrocellulose and then probed with the anti-eNOS antibody from Sigma, which does not discriminate between the phospho and dephospho protein. P = phospho, D = dephospho, Pell = pellet, Supt = supernatant. Positions of molecular weight standards are shown on the left of the figure.

3.2.2.3 Phosphorylation and dephosphorylation of eNOS protein

The data in figure 3.4 cast some doubt over the specificity of the antibodies, therefore eNOS protein was treated with kinase or phosphatase (to promote phosphorylation or dephosphorylation, respectively), and then subjected to western blotting with the anti-phospho and dephospho antibodies.

eNOS protein was incubated with ^{32}P-ATP, in the presence or absence of AMPK (a kinase known to phosphorylate eNOS at Ser-1177) then subjected to immunoprecipitation with a commercially available anti-eNOS antibody (Sigma). Figure 3.5, panel A shows that in the presence of AMPK a band of eNOS size (130 kD) is phosphorylated to a greater extent than that in the absence of AMPK. The eNOS previously incubated with ^{32}P-ATP, in the presence or absence of AMPK was also analysed by western blotting using a number of antibodies (figure 3.5, B). An antibody that recognises both the phospho and dephospho eNOS (Sigma) demonstrated equal loading of protein (blot 1). In addition, a commercially available anti-phospho eNOS antibody (Thr-495) reacted to a far greater extent with eNOS pre-incubated with AMPK (blot 4). In contrast to the ability of the commercial antibody to specifically recognise phosphorylated eNOS, the anti-phospho and -dephospho antibodies prepared in this study showed no discrimination between phosphorylated and unphosphorylated protein (blots 2 and 3). Nevertheless, AMPK is known to phosphorylate eNOS at Thr-495 and Ser-1177 in the absence of calcium (Chen et al., 1999), so it may be that if the reaction conditions were not optimised for Ser-1177 phosphorylation, Thr-495 has been phosphorylated at the expense of Ser-1177.

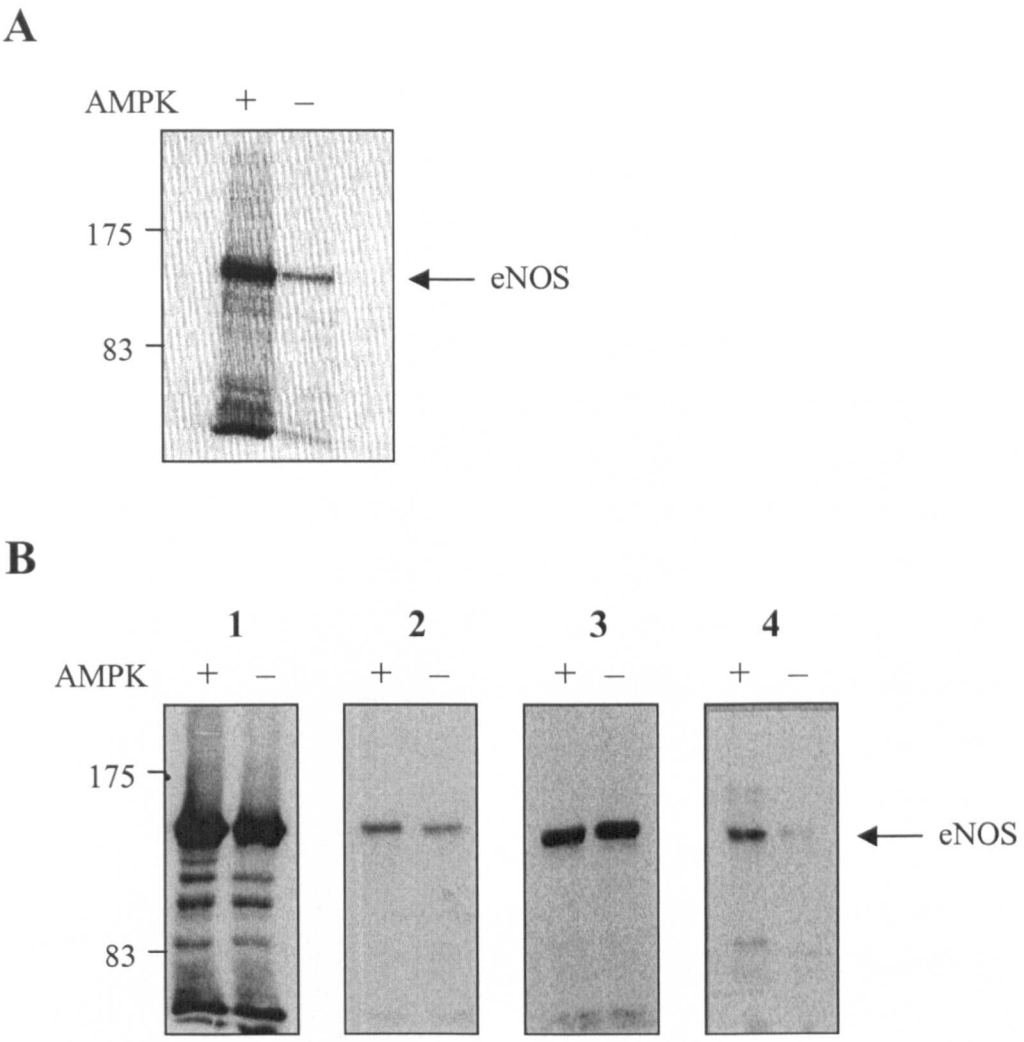

Figure 3.5 eNOS phosphorylation using ^{32}P ATP

eNOS (200 μg) protein was incubated in the absence or presence of 35 units AMPK as described in section 2.3.5.6. Around 70 μg protein was immunoprecipitated using the commercially available Sigma antibody, and subjected to SDS-PAGE and subsequent phospho-image analysis (panel A). Panel B shows protein treated in the same way (but without immunoprecipitation) subjected to SDS-PAGE (around 17 μg per lane). The nitrocellulose was probed with various antibodies: 1 = anti-eNOS from Sigma, 1:1000 dilution, 2 = anti-phospho eNOS, 1:200 dilution, 3 = anti-dephospho eNOS, 1:200 dilution, 4 = anti-phospho eNOS (Thr-495) from Upstate Biotechnology, 1:1000 dilution. Positions of molecular weight standards are shown on the left of the figure.

To further analyse the specificity of the antibodies, eNOS protein was subjected to dephosphorylation using the protein phosphatase PP1 (data not shown). No effect was observed using PP1, therefore eNOS protein was dephosphorylated using the broad-spectrum phosphatase, alkaline phosphatase. eNOS protein was incubated with or without alkaline phosphatase and analysed by western blotting using Sigma eNOS antibody, anti-phospho eNOS antibody, anti-dephospho eNOS antibody and also an anti-phospho eNOS Ser-1177 antibody donated by D.G. Hardie (figure 3.6, panel A). Protein loading of the treated and untreated samples was not equal in this experiment (see results using Sigma antibody) therefore the bands were quantified by densitometric analysis (panel B). The relative intensity of the alkaline phosphatase treated protein to that of the untreated protein detected by the Sigma antibody was calculated to be 87%. This is similar to the relative intensity using the anti-dephospho eNOS antibody (85%), indicating that increased amounts of dephospho eNOS Ser-1177 are not being detected by the dephospho antibody. However, relative intensities of alkaline phosphatase treated to untreated protein for the anti-phospho eNOS antibody and the anti-phospho eNOS from Dundee were 62% and 38% respectively. This suggests that alkaline phosphatase is dephosphorylating eNOS to some extent, which is detected by less binding of the anti-phospho eNOS antibodies to the alkaline phosphatase treated samples.

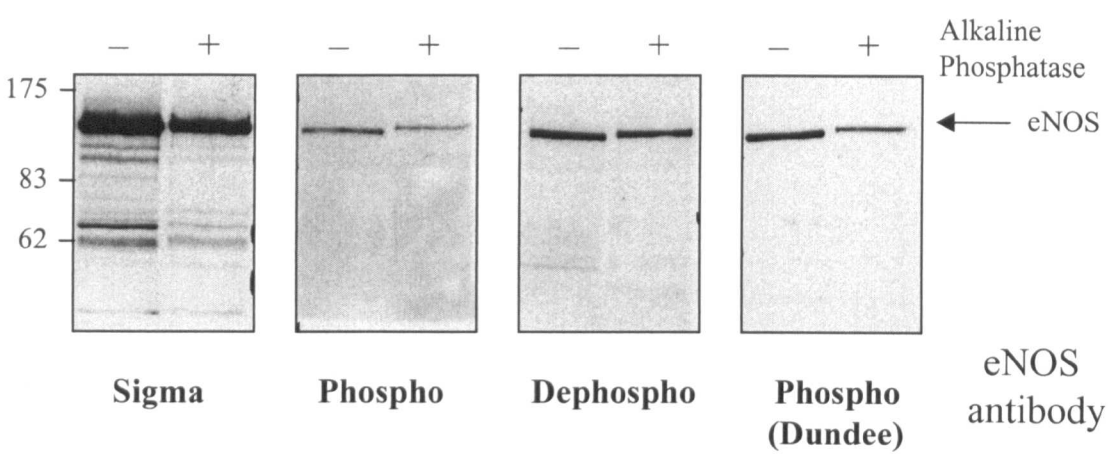
A
– + – + – + – +
Alkaline Phosphatase
175
83
62
eNOS
Sigma
Phospho
Dephospho
Phospho (Dundee)
eNOS antibody

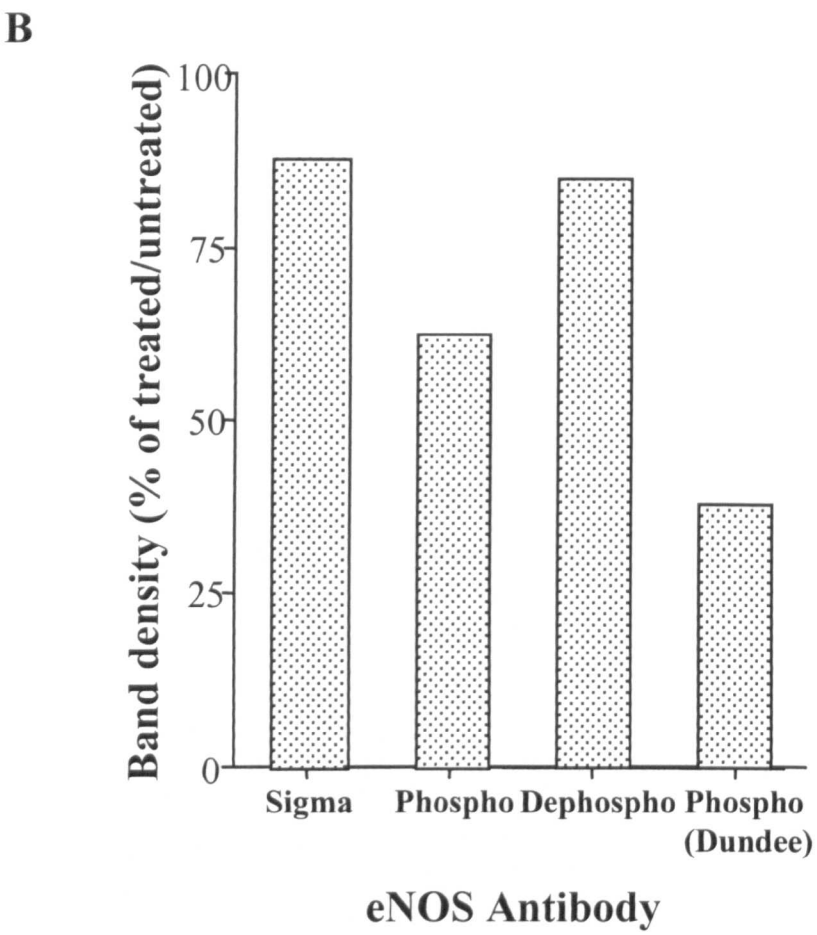
B
Band density (% of treated/untreated)
100
75
50
25
0
Sigma
Phospho
Dephospho
Phospho (Dundee)
eNOS Antibody

Figure 3.6 Alkaline phosphatase treatment of eNOS

eNOS protein (250 μg) was incubated in the presence or absence of alkaline phosphatase (a total of 100 units), as described in section 2.3.5.7. Proteins were then subjected to SDS-PAGE (25 μg/lane), transferred to nitrocellulose and probed with antibodies as described: anti-eNOS from Sigma, 1:1000 dilution, anti-phospho eNOS, 1:200 dilution, anti-dephospho eNOS, 1:200 dilution, anti-phospho eNOS from Dundee, 1:250 dilution (Panel A). Panel B shows desitometric analysis of the immunoblots from panel A. Positions of molecular weight standards are shown on the left of panel A.

3.2.2.4 Western blotting in endothelial cells

As much of the work on eNOS is undertaken in endothelial cells, the ability of the antibodies to detect eNOS phosphorylation in endothelial cells was assessed. Endothelial cells lysates were prepared from HAECs that had undergone various incubations (see figure 3.7). Lysates were probed with an anti-PKB antibody, and with the Sigma anti-eNOS antibody, and show equal loading of protein. Lysates were probed with anti-phospho PKB (Ser-473) antibody (figure 3.7). In the presence of IGF-1, but not insulin or EGF, PKB phosphorylation is increased. The samples were also probed with the phospho- and dephospho-eNOS antibodies, and with the phospho-eNOS antibody from Dundee. None of these antibodies appear to show any differences in eNOS phosphorylation state in response to any of the stimuli.

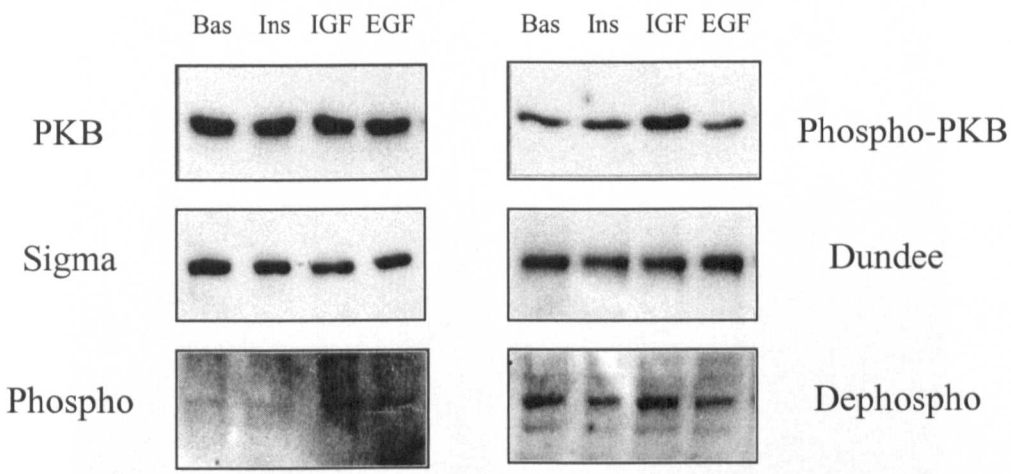

Figure 3.7 Western blotting of HAEC lysates

HAECs were cultured as described in section 2.3.5.8. HAEC lysates were prepared using standard lysis buffer (section 2.2) after the following treatments: basal, 1 μM insulin, 100 nM IGF-1, and 10 ng/ml EGF (all stimulations were for 10 min). 20 μg protein was subjected to SDS-PAGE and transferred to nitrocellulose. Nitrocellulose was incubated with antibodies as described: anti PKB, anti phospho-PKB (Ser-473), and Sigma anti-eNOS , all at 1:1000 dilution; Dundee anti-eNOS, 1:1000 dilution, anti phospho- and anti dephospho-eNOS at 1:200 dilution. Shown are representative data from three experiments. The cells used in these experiments were cultured by Dr. I. Salt/Mrs V. Morrow.

3.2.2.5 Confocal microscopy of endothelial cells

Studies were undertaken to test the efficiency of the antibodies for microscopy, in the event that their specificity could be confirmed. Figure 3.8 shows confocal microscope images of HAECs stained as described in section 2.3.5.9. Both the anti-phospho and dephospho-eNOS antibodies appear to be effective for confocal microscopy. Like the commercially available antibody they appear to show eNOS protein present in an intracellular, peri-nuclear location and to a lesser extent, around the plasma membrane.

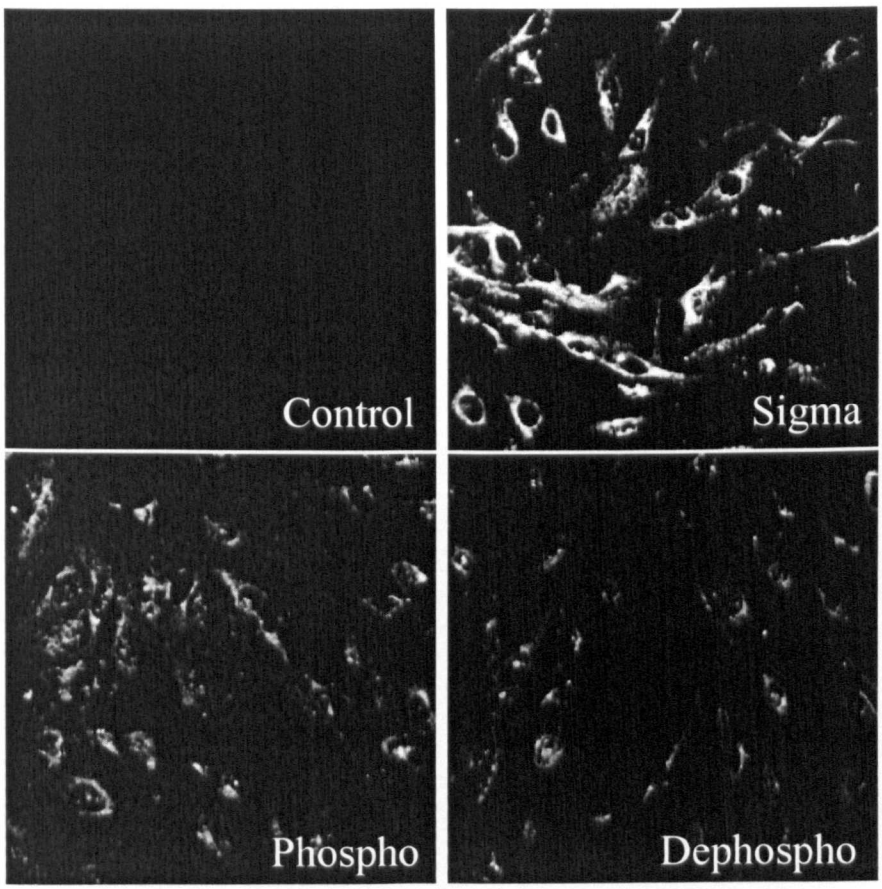

Figure 3.8 Confocal microscopy of endothelial cells

HAECs were cultured and coverslips were subjected to methanol fixation and stained with antibodies, as described in section 2.3.5.9. Dilutions of antibodies used were Sigma 1:50, anti-phospho eNOS 1:50, anti-dephospho eNOS 1:50. Control is with secondary antibody only. This experiment was performed by Dr. I. Salt.

3.3 Discussion

The phospho- and dephospho-specific eNOS Ser-1177 antibodies, prepared and characterised, as described above, are effective in detecting eNOS proetin for use in western blotting, immunoprecipitation and microscopy (figures 3.2, 3.3 and 3.8). They also recognise eNOS protein harvested from virally infected cells and in endothelial cells (figures 3.2 and 3.7). However, some doubts exist regarding their specificity for the phosphorylated/non-phosphorylated protein.

The data in figure 3.2, in which western blotting has been undertaken in the presence and absence of blocking peptides, suggests the antibodies are specific, in that, binding of protein is blocked only in the presence of the peptide to which the antibody was raised.

However, sequential immunoprecipitation experiments using the phospho- and dephospho-eNOS antibodies gave rather complex results, and the eNOS protein was not immunoprecipitated as expected, and this cast doubts as to the specificity of the antibodies. When the anti-dephospho antibody was used in the first instance, it appears to have depleted most of the eNOS from the supernatant, therefore when the second antibody was used (anti-phospho or -dephospho), there was little protein to immunoprecipitate. However in the pellet from the first anti-phospho IP, there appears to be a substantial amount of phospho protein. This suggests that when the anti-phospho antibody was used to IP from the dephospho immuno-depleted supernatant a substantial band of phospho eNOS should have been detected. However, this was not the case and only a very slight band was observed. Therefore it is possible that the anti-dephospho antibody has depleted the supernatant of both the phospho and dephospho protein. Conversely, it may be that in the presence of phospho and dephospho protein, the anti-phospho eNOS antibody has an affinity for the dephosphorylated protein.

To examine the specificity of the antibodies further eNOS protein that had been phosphorylated or dephosphorylated was prepared, the assumption being that only the anti-phospho eNOS antibody would recognise eNOS treated with kinase and only the anti-dephospho eNOS antibody would recognise phosphatase treated eNOS.

AMPK was used to phosphorylate eNOS (figure 3.5). It was expected that AMPK would phosphorylate all the serine and threonine residues (within consensus sequences) in the eNOS protein (including Thr-495 and Ser-1177), due to the high concentrations of kinase and substrate in the reaction. By phosphorimage analysis, it was determined that eNOS had been phosphorylated by AMPK, and using antibodies specific for phospho Thr-495, phosphorylation of this residue was detected. However, neither the phospho-specific or the dephospho-specific eNOS Ser-1177 antibodies discriminated against eNOS incubated with or without AMPK. These results suggest that the antibodies are not specifically recognising phosphorylated/unphosphorylated protein, or alternatively that the protein has not actually been phosphorylated on Ser-1177. However, (Chen et al., 1999), showed that AMPK can phosphorylate eNOS on Thr-495, as well as Ser-1177, in the absence of calcium-calmodulin, and the reaction conditions to detect preferential phosphorylation of Ser-1177 were similar to that used here. Therefore, phosphorylation of eNOS on Ser-1177 would have been expected to occur.

Alkaline phosphatase was used to dephosphorylate eNOS (figure 3.6). The protein sample treated with alkaline phosphatase contained less phospho-eNOS Ser-1177 (using both the antibody prepared in-house and the antibody gifted by D.G. Hardie). However no increase in dephospho-eNOS was detected using the dephospho-specific antibody. It would have been prudent to blot for phospho-Thr-495, to look for global dephosphorylation as this would provide a control for global dephosphorylation. However figure 3.5 shows untreated eNOS to have very low, almost undetectable levels of phospho-Thr-495. Therefore, it has not been determined whether alkaline phosphatase was efficient in dephosphorylating the eNOS protein, and whether any differences would have been likely to be identified using these antibodies. Dephosphorylation was also attempted using protein phosphatase 1 (PP1) (data not shown), but no changes in phosphorylation could be detected using the phospho- and dephospho-eNOS Ser-1177 antibodies. One recent study (Michell et al., 2001) suggests that PP2A is responsible for dephosphorylation of the Ser-1177 site, therefore it is possibly not surprising dephosphorylation was not detected in the presence of PP1.

Prof. D.G. Hardie, University of Dundee gifted an anti-eNOS, phospho Ser-1177 antibody. It is presumed that this antibody is indeed specific for the phosphorylated Ser-1177 residue, (although no evidence is available to support this). This antibody reacts similarly to the phospho-specific antibody prepared in-house.

Phosphorylation of eNOS Ser-1177 in response to insulin (Montagnani et al., 2001) and IGF-1 (Michell et al., 1999) has been observed in endothelial cells. However, this was not the case in this study. IGF-1, but not insulin, stimulated phosphorylation (and presumably activation) of PKB, but neither of the stimuli resulted in phosphorylation of eNOS Ser-1177 (figure 3.7) in HAECs, as determined by the antibody prepared in-house or that gifted by D.G. Hardie. As insulin did not result in activation of PKB, it would not be expected to cause eNOS activation, as it is well documented that eNOS is down-stream of PKB (Fulton et al., 1999, Dimmeler et al., 1999). It is possible that there was a problem with the cells, but this is unlikely, as the experiment was carried out on 3 separate occasions, or again it may be possible that the antibodies are not specific for the phosphorylated protein.

Confocal microscopy carried out using these phospho and dephospho eNOS antibodies and the commercially available antibody (figure 3.8) showed two pools of enzyme. The majority of staining was observed in a peri-nuclear region, with lesser amounts around the plasma membrane. This peri-nuclear staining is probably the Golgi, consistent with previous findings (Fulton et al., 2002).

At this stage, it cannot be stated conclusively whether the antibodies designed do specifically recognise eNOS phosphorylated/unphosphorylated at Ser-1177. Therefore they cannot at present be used for further studies of eNOS phosphorylation in skeletal muscle.

CHAPTER 4

EXAMINATION OF SKELETAL MUSCLE OF THE STROKE-PRONE SPONTANEOUSLY HYPERTENSIVE RAT FOR A DEFECT IN INSULIN SIGNALLING

4.1 Introduction

Reduced insulin-stimulated glucose uptake (insulin resistance) by skeletal muscle and adipose tissue is of major pathogenic importance in several common human disorders including type 2 diabetes, hypertension, obesity and combined hyperlipidaemia but the underlying mechanisms are unknown. For this reason animal models of insulin resistance are valuable tools for studying the phenotype and elucidating the mechanisms involved.

As described in section 1.5.3 the SHRSP is an animal model of hypertension, which also exhibits insulin resistance in adipose tissue and skeletal muscle. However, the underlying mechanisms leading to development of hypertension and insulin resistance in this animal have not been identified.

4.1.1 Aims of Chapter

The aim of the present study was to determine if any defects could be identified in the 'classical' insulin-signalling cascade (see introduction, section 1.2) in skeletal muscle of the SHRSP compared to the normotensive control WKY strain, and determine whether this accounted for the insulin resistance. This involved analysis of levels and localisation of a number of proteins by western blotting, and assessing activity levels of key components of the signalling pathway. Similarly, the possibility of a defect in the proteins involved in glycogen storage and metabolism was investigated.

4.2 Results

4.2.1 Skeletal muscle of SHRSP is insulin resistant

To confirm the results of James et al. (2001), the ability of insulin to stimulate glucose transport in skeletal muscle of SHRSP and WKY was determined. Figure 4.1 shows that in response to insulin, glucose transport in the SHRSP is lower than that observed in the WKY. Thus, SHRSP skeletal muscle exhibits insulin resistance compared to WKY.

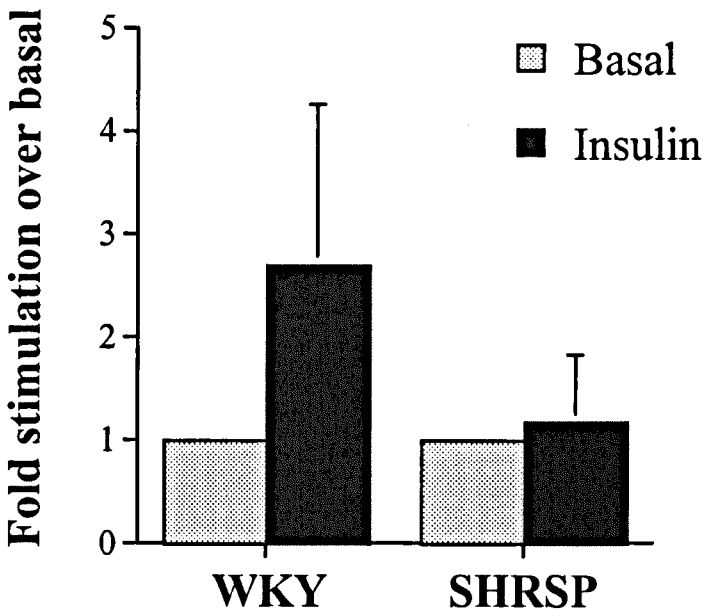

Figure 4.1 The effect of insulin on 2-deoxyglucose uptake in FDB muscle from SHRSP and WKY rats

Flexor digitorium brevis (FDB) muscles were incubated in KH buffer for 30 min in the presence or absence of 1 μM insulin in 95 % O_2/5 % CO_2 prior to assay of deGlc uptake as described in section 2.3.2.4. The results are expressed as fold stimulation over basal. The results shown are the mean ± S.E.M. for three experiments.

4.2.2 Analysis of the classical insulin-signalling pathway in WKY and SHRSP skeletal muscle

4.2.2.1 Analysis of the sub-cellular distribution of insulin-signalling pathway components

Many signalling pathways, including the insulin-signalling pathway, are subject to strict compartmentalisation within cells, to allow correct propagation of the signal and development of the appropriate response (Clark et al., 1998). Hence, the cellular content and distribution of molecules involved in insulin signalling and glucose uptake was characterised in skeletal muscle from SHRSP and control WKY rats, by performing sub-cellular fractionation of skeletal muscle.

Initially complex fractionation procedures were attempted, following protocols from (Bonen et al., 2000 and Dombrowski et al., 1996). These however, were unsuccessful and a crude fractionation procedure was therefore undertaken, in which a low speed centrifugation was first used to pellet heavy membranes and organelles. The supernatant from this spin was then subjected to a high-speed centrifugation in order to separate light membranes and cytosol (see section 2.3.2.6). Figure 4.2 panel A shows the results of this work. The light membrane fraction contains the majority of the intracellular membranes, as shown by the majority of the cellular GLUT 4 being present in this fraction. IRS-1 and IRS-2 are localised predominantly in the light and heavy membrane fractions, whilst PI3-kinase (p85 subunit) is localised predominantly in the light membrane and soluble protein fractions of skeletal muscle. Quantification of this data (figure 4.2, panel B) shows there are no significant differences between the protein levels and distribution of GLUT 4, IRS-1, IRS-2 and the p85α subunit of PI3-kinase in WKY and SHRSP skeletal muscle.

A

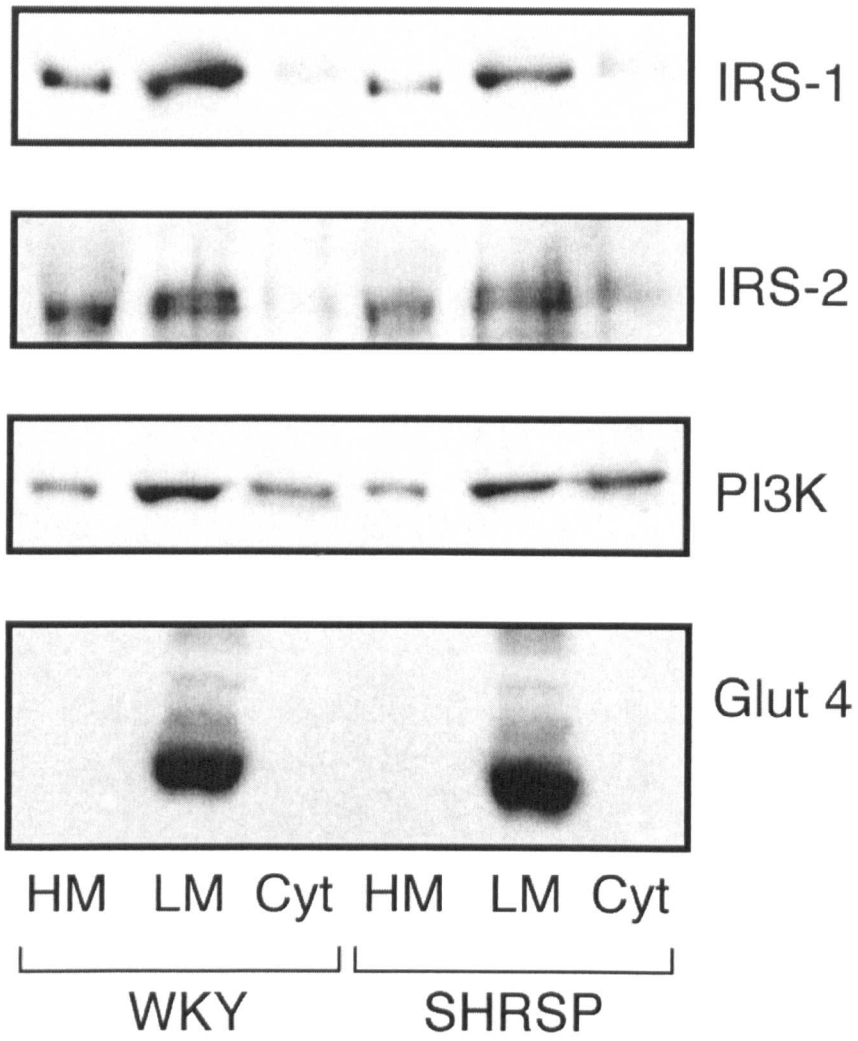

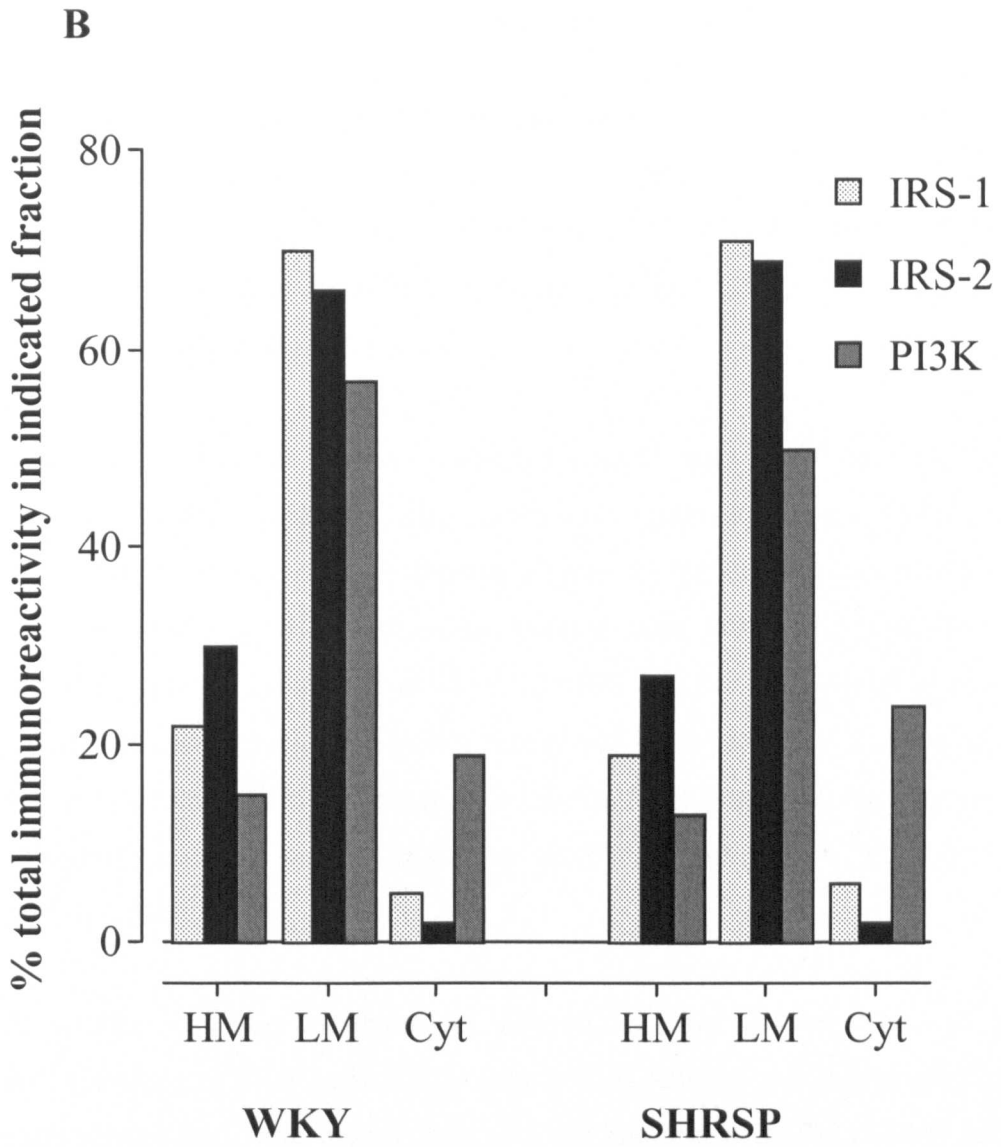

Figure 4.2 Immunoblot analysis of insulin signalling proteins in skeletal muscle from SHRSP and WKY rats

Crude skeletal muscle fractionation of soleus muscle was carried out as described in section 2.3.2.6. Fractions (20 μg protein) were subjected to SDS-PAGE and transferred to nitrocellulose (as described in sections 2.3.1.1 and 2.3.1.2). The distribution of IRS-1, IRS-2 and the p85α subunit of PI3-kinase in skeletal muscle fractions from SHRSP and WKY animals were analysed by immunoblotting (panel A), all antibodies were used at a dilution of 1:1000. LM = light membranes, HM = heavy membranes, Cyt = soluble protein fraction. The data presented are representative of three experiments of this type. Panel B shows quantification of data from three experiments of this type. No differences were observed in either expression level or sub-cellular distribution for any of the proteins studied.

4.2.2.2 Analysis of PKB protein levels and activity

PKB is activated in response to insulin and lies downstream of PI3-kinase in the insulin-signalling cascade. PKB activates a number of downstream signals in response to insulin (see introduction, section 1.2.4). Three isoforms of PKB are expressed in mammalian cells (PKB α, β and γ), with PKB α and β being the major isoforms expressed in skeletal muscle.

The total levels of PKB protein in skeletal muscle from WKY and SHRSP were examined. This was carried out using an antibody directed against the PH domain of PKB, which recognises all the isoforms. Figure 4.3 panel A shows levels of PKB protein are similar in EDL and soleus muscle from WKY and SHRSP. PKB is activated by phosphorylation at residues Thr-308 and Ser-473 (Alessi et al., 1996). Using an antibody which specifically recognises PKB phosphorylated at threonine 308 it was determined that in response to insulin, PKB from EDL and soleus muscle is phosphorylated to a similar extent on Thr-308, whether from WKY or SHRSP (Figure 4.3, panel B).

PKB activity was also measured, to determine if the cascade from the insulin receptor, leading to PKB activation is intact. PKB activity was determined on PKB immunoprecipitated from muscle lysates using the anti-PKB-PH domain antibody. Figure 4.3, panel C shows basal levels of PKB activity from EDL and soleus muscles to be similar between the two strains. In the presence of insulin a robust activation of PKB occurs in skeletal muscle from both WKY and SHRSP, and levels of PKB activity are similar in each strain. This suggests that the defect in the SHRSP causing insulin resistance does not occur in the 'classical' insulin-signalling cascade, due to the fact that the insulin-signalling pathway leading to PKB activation is intact.

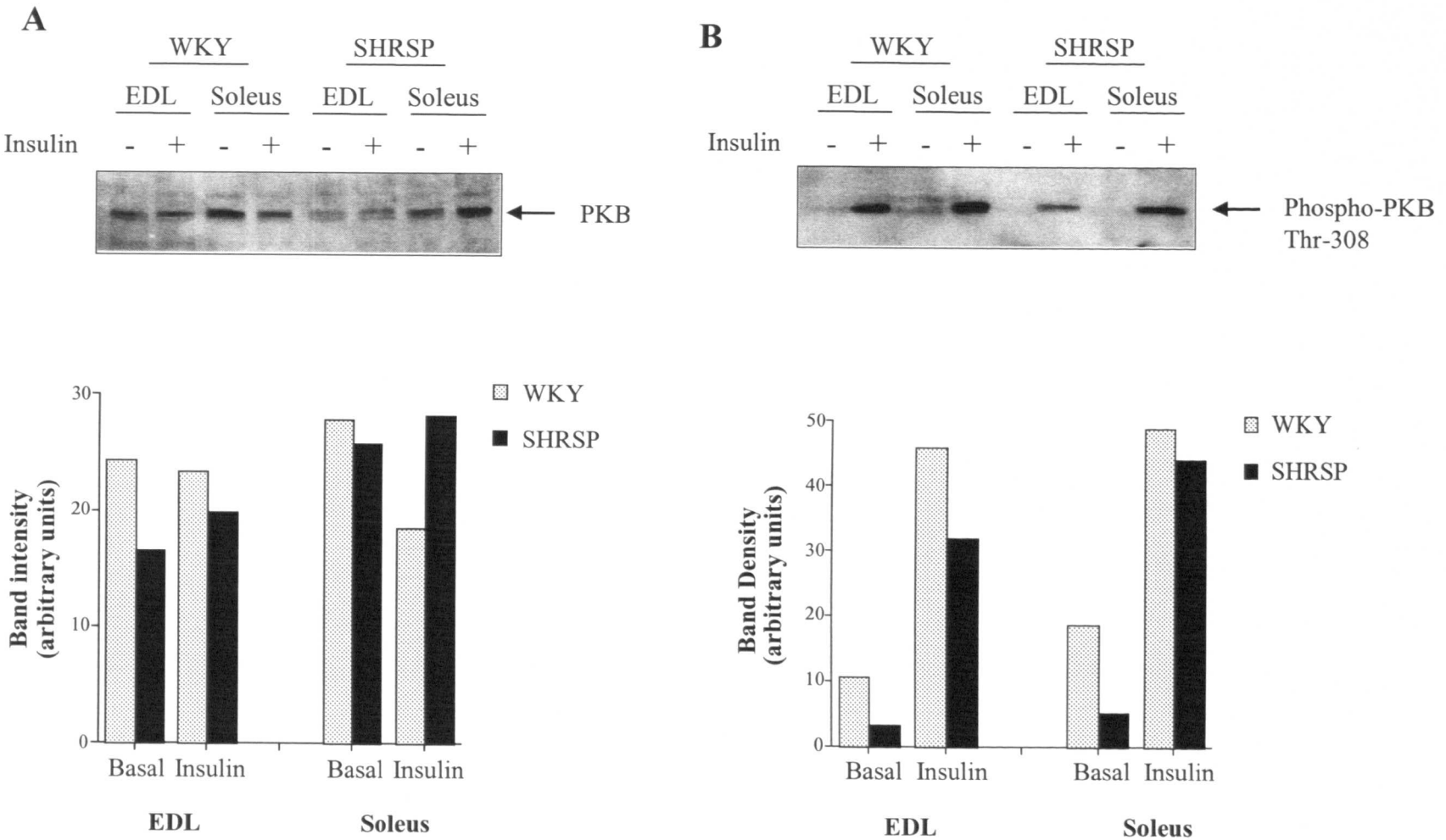
A
WKY
SHRSP
EDL
Soleus
EDL
Soleus
Insulin
- + - + - + - +
PKB
B
WKY
SHRSP
EDL
Soleus
EDL
Soleus
Insulin
- + - + - + - +
Phospho-PKB
Thr-308
Band intensity
(arbitrary units)
30
20
10
0
WKY
SHRSP
Basal Insulin
Basal Insulin
EDL
Soleus
Band Density
(arbitrary units)
50
40
30
20
10
0
WKY
SHRSP
Basal Insulin
Basal Insulin
EDL
Soleus

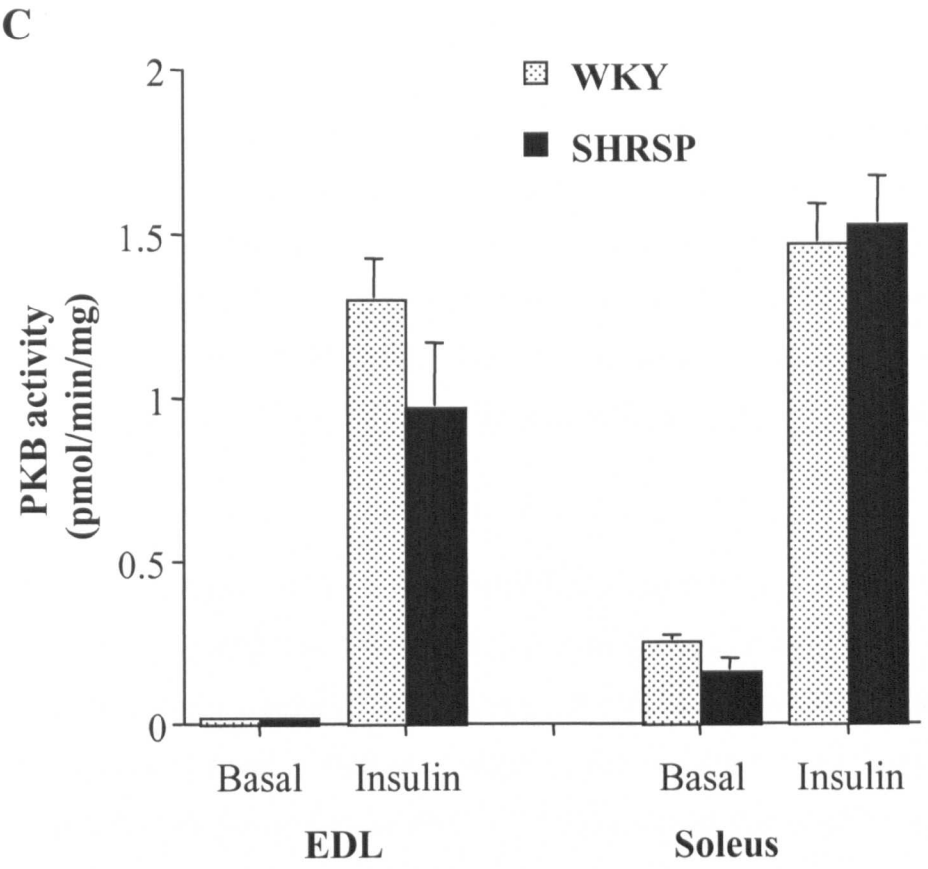

Figure 4.3 Analysis of PKB levels and activity in skeletal muscle from SHRSP and WKY

Panels A and B: skeletal muscle lysates were prepared as described in section 2.3.2.5. Protein (20 μg) was subjected to SDS-PAGE and western blotting (sections 2.3.1.1 and 2.3.1.2). Panel A: total PKB levels were determined by immunoblotting with an antibody specific for PKB-PH domain. Quantification of three experiments of this type shows PKB levels are similar in skeletal muscle from WKY and SHRSP. Panel B: levels of phosphorylated PKB were determined using an antibody that specifically recognises PKB phosphorylated at Thr-308. Quantification of three experiments of this type showed insulin induces similar levels of phosphorylation of PKB at Thr-308 in WKY and SHRSP skeletal muscle. Panel C: EDL and soleus muscles were incubated for 30 minutes in the presence or absence of 1 μM insulin. Muscle extracts were prepared as described in section 2.3.2.5. PKB activity was determined in PKB immunoprecipitates, by the ability of PKB to phosphorylate a substrate peptide, as described in section 2.3.2.7. The results are the mean ± S.E.M. for three experiments. The levels of PKB activity are similar in EDL and soleus muscle for WKY and SHRSP.

4.2.2.3 Analysis of protein levels of various PKC isoforms

A number of PKC isoforms have been implicated in insulin action (see introduction, section 1.2.5). For example, the conventional and novel PKCs have been implicated to function as negative feedback inhibitors of the insulin and IRS proteins, whilst the atypical PKCs are suggested to be downstream targets for signals generated by the insulin receptor (Farese, 2002). Therefore it was deemed prudent to analyse expression levels of a number of PKC isoforms in skeletal muscle from SHRSP and WKY.

Expression of the conventional PKC isoforms, PKC α and PKC β, was determined in skeletal muscle from SHRSP and WKY. PKC α is an 82 kDa protein whose level of expression appears to be similar in EDL, soleus and tibialis muscle from SHRSP and WKY (figure 4.4). A band is also recognised by the anti-PKC α antibody that is smaller in size than that expected for PKC α. The identity of this band has not been determined. Levels of expression of PKC β also appear to be similar in EDL, soleus and tibialis muscle from SHRSP and WKY (figure 4.4). PKC β is an 80 kDa protein, but again, the anti-PKC β antibody also recognises an additional band, smaller in size (around 70 kDa) than that expected for PKC β. Again the identity of this band is unknown. Expression of another conventional PKC was also examined in these skeletal muscles, however expression of PKC γ could not be detected in these rat skeletal muscle lysates.

Expression levels of the novel PKC isoforms (PKCs δ, ε and θ) was also assessed in WKY and SHRSP skeletal muscles. Of the muscles analysed, PKC δ expression is highest in soleus muscle with less in EDL and tibialis muscle (figure 4.4), however levels of PKC δ expression appears to be similar in WKY and SHRSP strains. PKC δ is an 80 kDa protein, and again the antibody raised against this protein recognises a non-specific band of lower molecular mass. PKC ε is a 90 kDa protein, whose expression is highest in tibialis muscle, followed by EDL muscle and is lowest in soleus muscle (figure 4.4), however PKC ε expression appears to be similar in the two strains. The anti-PKC ε antibody also recognises a non-specific band at around

70 kDa (data not shown). PKC θ is a 79 kDa protein which is expressed at similar levels in EDL, soleus and tibialis muscle. This protein is also expressed at similar levels in muscle from both WKY and SHRSP animals.

Expression of the atypical PKC isoforms was also studied in these muscles. PKC ι is a 74 kDa protein whose expression levels are similar in EDL, soleus and tibialis muscle and is also expressed at similar levels in muscle from both WKY and SHRSP animals (see figure 4.4). A number of bands are recognised by the antibody directed against this protein, the one that is PKC ι being determined using a positive control (not shown), but the identity of the non-specific bands is unknown. Expression of the other atypical PKC isoforms, PKCs λ and ζ, were also examined in these muscles. However, PKC λ could not be detected, and antibodies specific for PKC ζ did not prove effective when blotting skeletal muscle lysates.

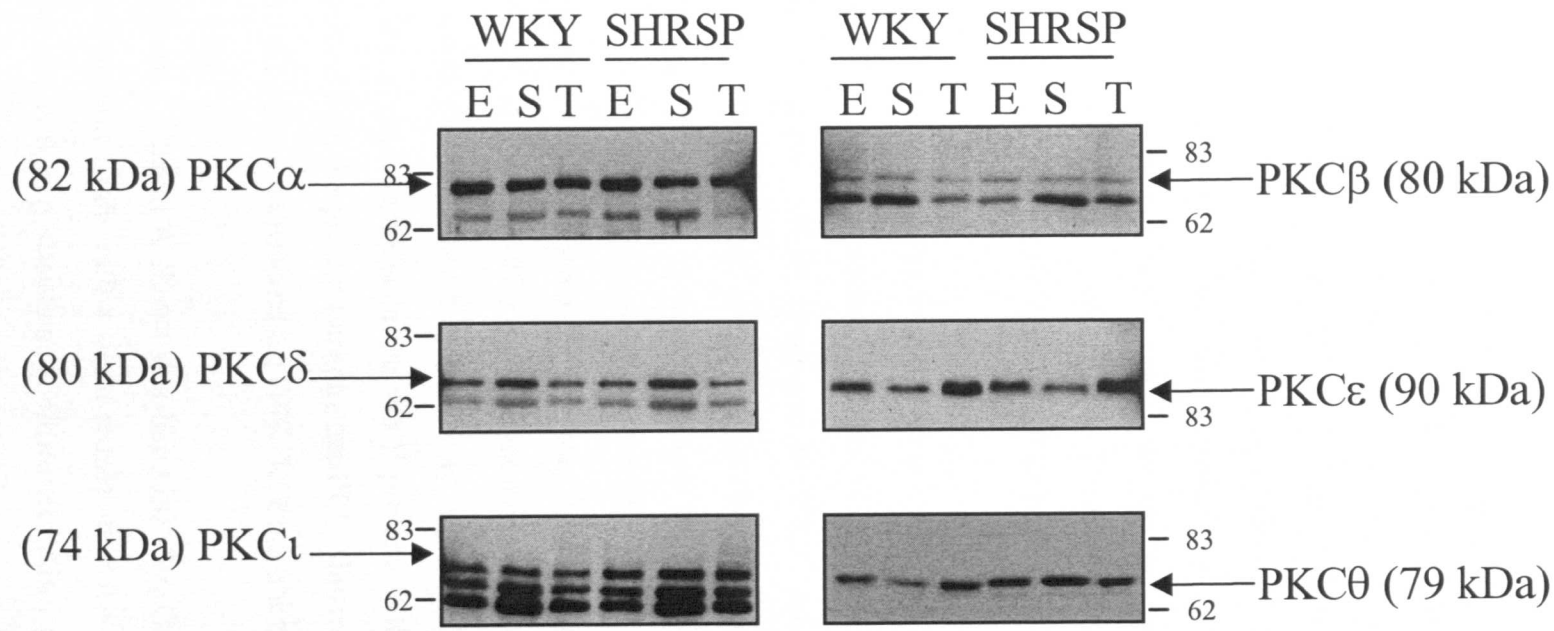

Figure 4.4 Analysis of PKC isoform expression in WKY and SHRSP skeletal muscle

Skeletal muscle lysates were prepared as described in section 2.3.2.5. Protein (20 μg) was subjected to SDS-gel electrophoresis and western blotting (sections 2.3.1.1 and 2.3.1.2). PKC levels were determined by immunoblotting with various antibodies. The dilutions of antibodies used were as follows: anti-PKC α and ε, at 1:1000 dilution; anti-PKC δ, at 1:500 and anti-PKC β, ι and θ all at 1:250 dilution. Blots of PKC α and β are representative of 1 experiment of this type. Blots of PKC δ, ε and ι are representative of 2 experiments of this type. The blot of PKC θ is representative of 3 experiments of this type. E = EDL, S = soleus, T = tibialis. Arrows indicate PKC isoform stated, as determined by migration of a protein standard on the SDS-PAGE gel (protein standards are not shown due to the high concentration on the gel and overexposure of the band in comparison to those of skeletal muscle samples).

4.2.3 Regulation of glycogen storage and metabolism in SHRSP skeletal muscle

4.2.3.1 Analysis of GSK-3 expression and activity

The major role of insulin in skeletal muscle is in regulating glycogen metabolism. This occurs via activation of PKB, which phosphorylates and inactivates GSK-3 (Cross et al., 1995). GSK-3, when active, phosphorylates and inactivates glycogen synthase. Therefore activation of PKB by insulin results in dephosphorylation of glycogen synthase due to inhibition of GSK-3. Two isoforms of GSK-3 exist (GSK-3α and GSK-3β), which are ubiquitously expressed. The proteins exhibit 97% sequence similarity in the kinase domain, but vary significantly outwith this region (see section 1.2.6.1). The levels and activity of both GSK-3 isoforms were studied in skeletal muscle from WKY and SHRSP.

Figure 4.5 panel A shows GSK-3α activity in basal and insulin-stimulated WKY and SHRSP EDL and soleus muscles. GSK-3α activity is slightly lower in skeletal muscle from SHRSP, compared to WKY, however this did not reach statistical significance. Of note is that inhibition of GSK-3α activity is not observed in the presence of insulin, in skeletal muscle from either strain. Panel B shows that in both EDL and soleus muscle from SHRSP, GSK-3α protein is greatly reduced in comparison to that from WKY. From the immunoblot it appears the protein which is expressed in the SHRSP has a lower molecular weight to that in the WKY and it was hypothesised that this may be due to dephosphorylation of the GSK-3α present. In order to dephosphorylate the WKY protein, WKY and SHRSP muscle lysates were treated with the protein phosphatase PP1. This treatment did not appear to change the banding pattern observed for GSK-3α from either WKY or SHRSP (data not shown).

Figure 4.6 panel A shows that like GSK-3α, GSK-3β activity is also similar in the two strains, again with a slight reduction in the activity of the protein from SHRSP, but not reaching statistical significance. Also, no inhibition of GSK-3β activity is observed in the presence of insulin. Figure 4.6, panel B shows the levels of GSK-3β protein to be similar in skeletal muscle from SHRSP and WKY, unlike the differences observed for GSK-3α.

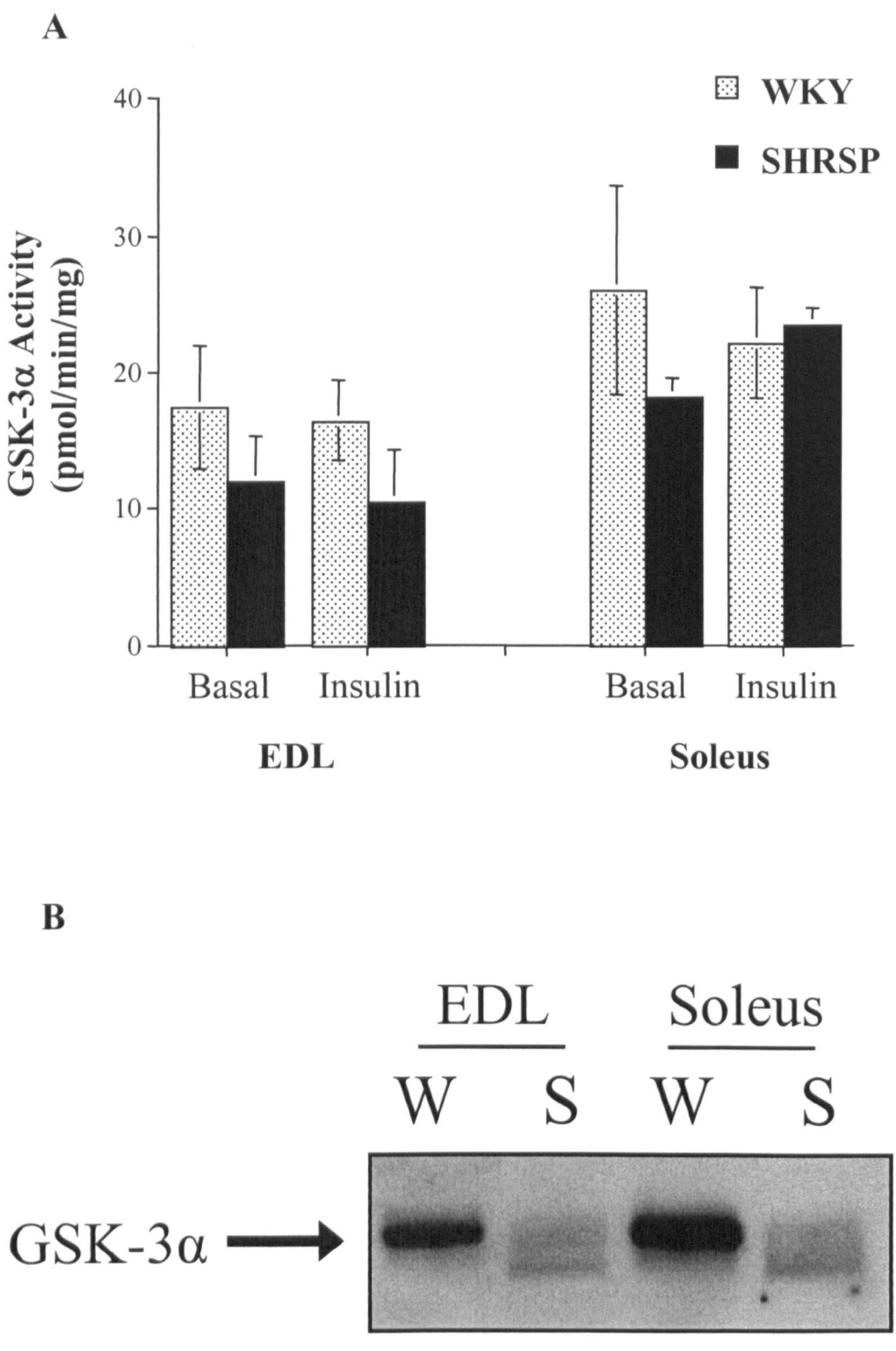
A
WKY
SHRSP
GSK-3α Activity
(pmol/min/mg)
40
30
20
10
0
Basal
Insulin
Basal
Insulin
EDL
Soleus
B
EDL
Soleus
W
S
W
S
GSK-3α

Figure 4.5 Analysis of GSK-3α levels and activity in skeletal muscle from SHRSP and WKY rats

EDL and soleus muscles were incubated for 30 minutes in the presence or absence of 1 μM insulin. Muscle extracts were prepared as described in section 2.3.2.5. GSK-3α activity was then determined as described in section 2.3.2.8 (panel A). The results are the mean ± S.E.M. for three experiments. GSK-3α activity in WKY and SHRSP is not significantly different. Shown in panel B is an immunoblot for GSK-3α. Skeletal muscle lysates were prepared as described in section 2.3.2.5. 20 μg protein was subjected to gel electrophoresis and western blotting (sections 2.3.1.1 and 2.3.1.2). The immunoblot shown is representative of data from 4 separate experiments. SHRSP expresses less GSK-3α than does the WKY.

A

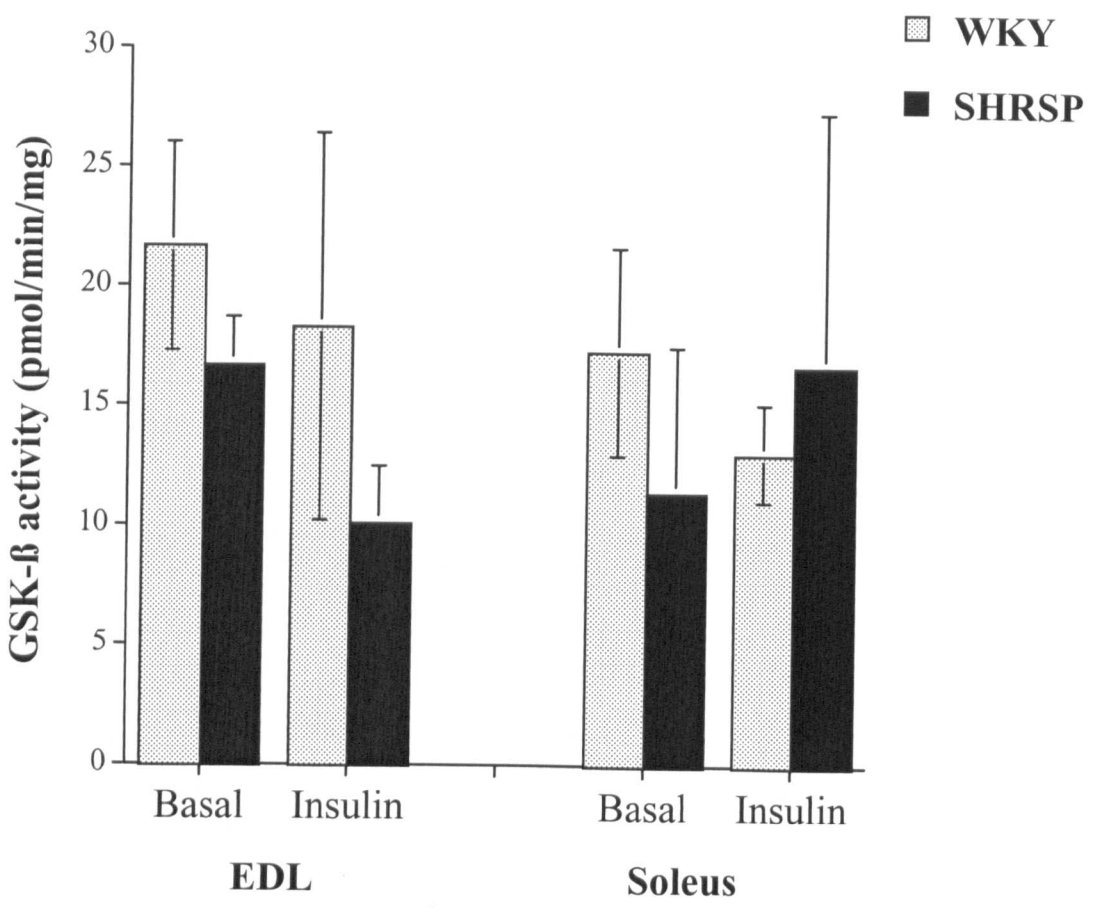
WKY
SHRSP
GSK-ß activity (pmol/min/mg)
30
25
20
15
10
5
0
Basal
Insulin
Basal
Insulin
EDL
Soleus

B

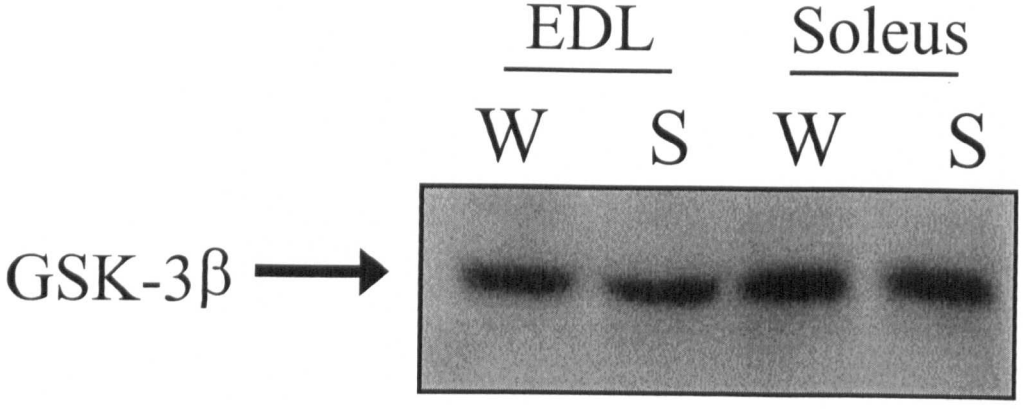
EDL
Soleus
W
S
W
S
GSK-3β

Figure 4.6 Analysis of GSK-3β levels and activity in skeletal muscle from SHRSP and WKY rats

EDL and soleus muscles were incubated for 30 minutes in the presence or absence of 1 μM insulin. Muscle extracts were prepared as described in section 2.3.2.5. GSK-3β activity was then determined as described in section 2.3.2.8 (panel A). The results are the mean ± S.E.M. for three sets of samples assayed three times each. GSK-3β activity is not significantly different in EDL and soleus muscle from SHRSP and WKY. Shown in panel B is an immunoblot for GSK-3β. Skeletal muscle lysates were prepared as described in section 2.3.2.5. 20 μg protein was subjected to gel electrophoresis and western blotting (sections 2.3.1.1 and 2.3.1.2). The immunoblot shown is representative of data from 3 separate experiments. GSK-3β protein levels are similar in SHRSP and WKY.

4.2.3.2 Determination of muscle glycogen levels in SHRSP and WKY

To determine if glycogen storage differed in WKY and SHRSP skeletal muscle, glycogen levels were analysed in EDL and soleus muscles. Glycogen was measured using a fluorescence-linked assay in which glucose is liberated from cellular glycogen using amyloglucosidase. Hexokinase is used to catalyse the conversion of glucose to glucose-6-phosphate (G6P), and G6P-deyhdrogenase is used to convert G6P to gluconate-6-phosphate, with the subsequent reduction of NADP. Production of NADPH is determined by changes in fluorescence.

Initial experiments (data not shown) suggested that SHRSP skeletal muscles had elevated glycogen levels compared to the WKY. However, refinement of the method, suggested that this was not the case and that the SHRSP has similar muscle glycogen levels to the WKY (figure 4.7). There is a tendency for SHRSP EDL to have less glycogen per milligram of protein, and soleus muscle to have more, compared to WKY. However, neither of these data were statistically significant. Again, insulin had little effect on glycogen levels in these samples.

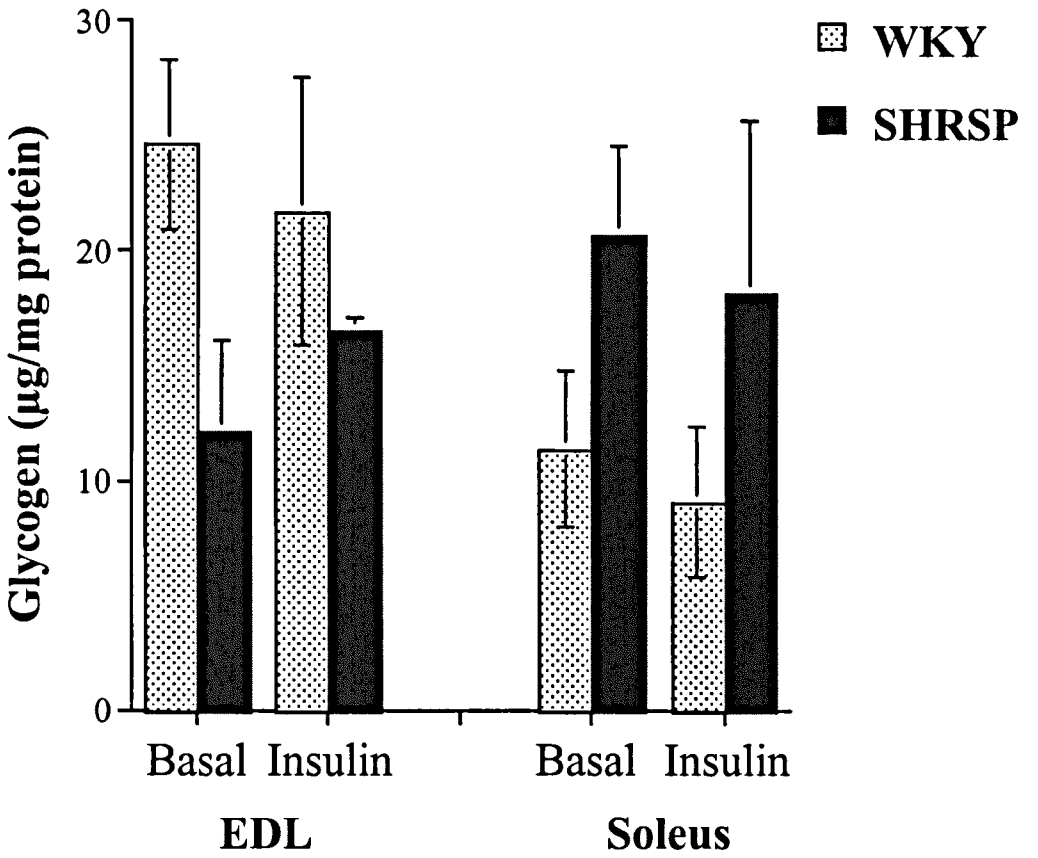

Figure 4.7 Analysis of glycogen levels in EDL and soleus muscle of SHRSP and WKY

Glycogen assays were performed on EDL and soleus muscle as described in section 2.3.2.9. The data presented are the mean ± S.E.M. of three independent experiments. Muscle glycogen levels are not statistically different between the two strains.

4.2.3.3 Analysis of glycogen metabolism in WKY and SHRSP muscle

To determine if any alterations in glycogen metabolism were present in SHRSP skeletal muscle, the processes of glycogen synthesis and breakdown were studied. Glycogen synthesis was measured as [^{14}C]-glucose incorporation into glycogen. Figure 4.8 shows that insulin stimulates glycogen synthesis in FBD muscle around 3-fold and levels of both basal and insulin-stimulated glycogen synthesis are similar in both strains.

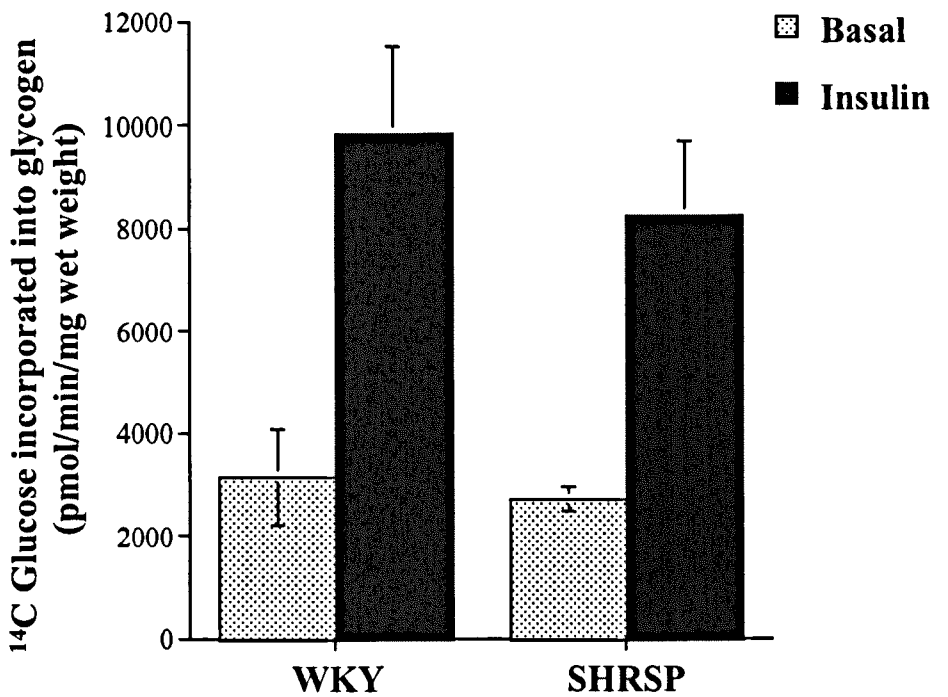

Figure 4.8 Comparison of glycogen synthesis in FDB muscle from WKY and SHRSP

FDB muscles were incubated in the presence or absence of 1 μM insulin for 1 hr at 37°C. Glycogen synthesis was measured as described in section 2.3.2.10. The results are the mean ± S.E.M. for three experiments. Basal and insulin-stimulated glycogen synthesis are not significantly different between WKY and SHRSP.

Glycogen is degraded by the action of phosphorylase and debranching enzyme (see section 1.2.6.3). Therefore, glycogen phosphorylase activity was measured to give an indirect measurement of glycogen breakdown in skeletal muscle from WKY and SHRSP animals. Phosphorylase exists in two forms: phosphorylase *a*, which is active and phosphorylase *b*, which is usually inactive. Phosphorylase *b* can be converted to phosphorylase *a* by phosphorylation by phosphorylase kinase. In muscle phosphorylase *b* is active only in the presence of high levels of AMP. Therefore when studying phosphorylase activity, the activity of both the isoforms are measured and phosphorylase activity is expressed as a ratio of the two.

Glycogen phosphorylase activity ratio is higher is EDL muscle, than in soleus muscle. However, glycogen phosphorylase activity ratio is not significantly different in EDL or soleus muscle from SHRSP and WKY (figure 4.9). Also, insulin did not produce any significant changes in the activity ratio of glycogen phosphorylase in muscles from either strain.

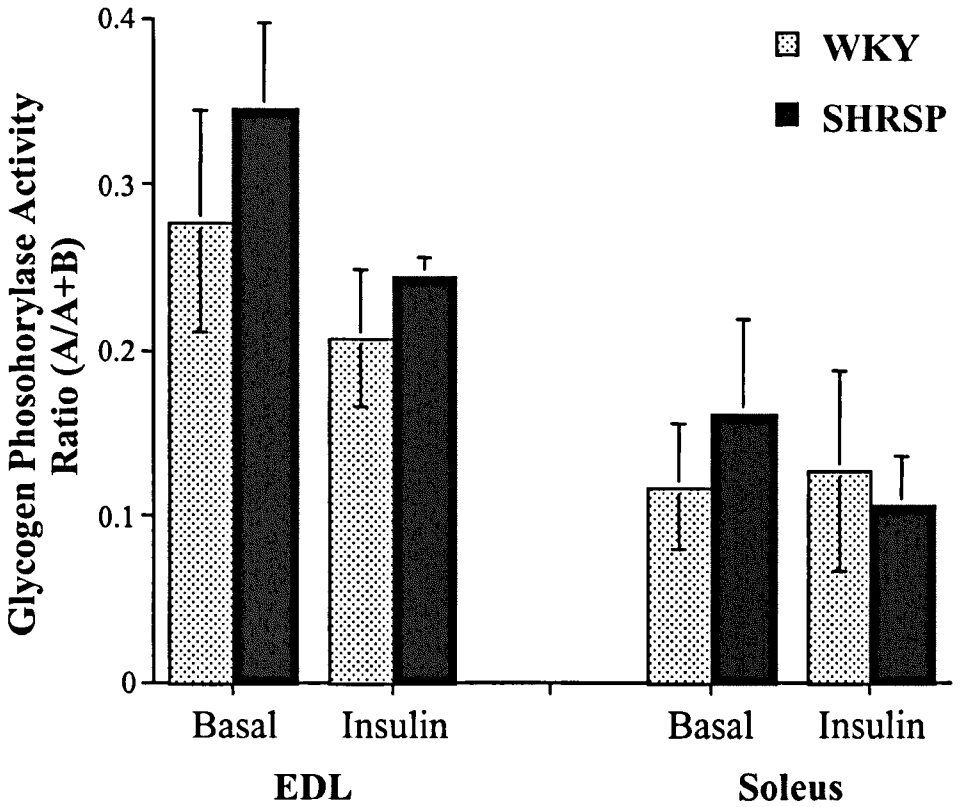

Figure 4.9 Analysis of glycogen phosphorylase activity in EDL and soleus muscle from WKY and SHRSP

EDL and soleus muscles were incubated in the presence or absence of 1 μM insulin for 30 min. Glycogen phosphorylase activity was determined (using 200-250 μg muscle extract) as described in section 2.3.2.11. The results are the mean ± S.E.M. of four experiments. Glycogen phosphorylase activity (basal and insulin-stimulated) is not significantly different in WKY and SHRSP skeletal muscle.

4.2.4 Skeletal muscle fibre-typing

Skeletal muscles consist of a variety of oxidative and glycolytic fibres that have specific roles in muscle metabolism (see introduction, section 1.3.1). Fibre type distribution is known to differ in various muscle types and different skeletal muscle fibre types have varying sensitivities to insulin and exercise. Therefore, skeletal muscle fibre-typing was performed (by Dr Ian Montgomery) to determine if any alterations in fibre type number or distribution were present in SHRSP skeletal muscle which could account for the insulin resistance observed.

Two different approaches are typically used when fibre typing skeletal muscles histochemically. These are determination of myosin ATPase activity and analysing reference enzymes of anaerobic and aerobic metabolism, for example succinate dehydrogenase and glycerol phosphate dehydrogenase (reviewed in Pette and Staron, 1990), which have been shown to differ in the various skeletal muscle fibre types.

Skeletal muscles from WKY and SHRSP were extensively fibre typed using these techniques. Shown are stains for succinate dehydrogenase and myosin ATPase, undertaken at pH 9.4 (figure 4.10). Fibre number and distribution appear to be similar in EDL muscle from WKY and SHRSP (figure 4.10). Similar results were also obtained in soleus and FDB muscle (data not shown).

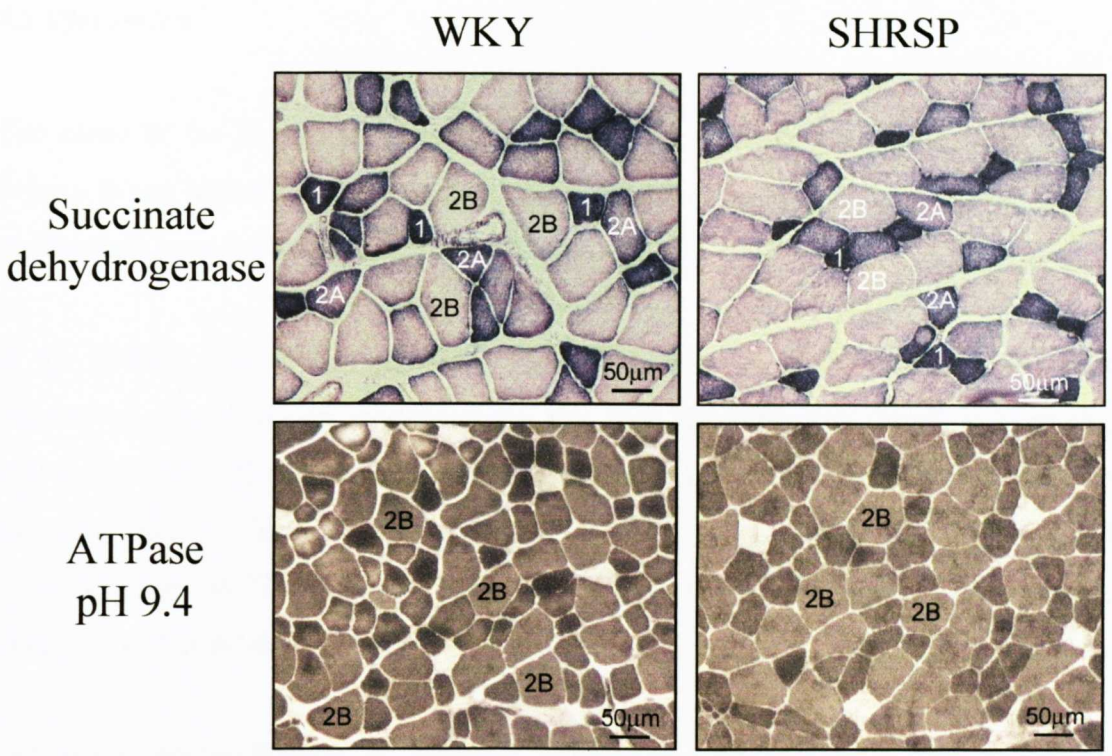

Figure 4.10 Fibre typing of EDL muscles

Upper panel: EDL muscles were sectioned and stained for succinate dehydrogenase as described in section 2.3.2.12.1. Type 1 fibres stain most intensively for succinate dehydrogenase, type 2A fibres have an intermediate staining pattern and type 2B fibres show low levels of staining for succinate dehydrogenase. Lower panel: EDL muscles were sectioned and stained for myosin ATPase as described in section 2.3.2.12.2. This experiment was performed by Dr I Montgomery.

4.3 Discussion

The cause of the insulin resistance observed in the SHRSP remains elusive, as no defects in the 'classical' insulin-signalling cascade, or in insulin-regulated glycogen metabolism have been identified in this study.

In the SHRSP, the insulin-signalling cascade leading to PKB activation is intact (figure 4.3, panel B) as evidenced by the data showing that basal and insulin stimulated PKB activity is similar in magnitude in both WKY and SHRSP skeletal muscle. This is further shown by the presence of similar levels of PKB phosphorylated on Thr-308 (a phosphorylation required for activation of the protein), in response to insulin.

The compartmentalisation of proteins downstream of insulin in the signalling pathway is likely to be important in regulation of signal propagation. For example, the glucose transporter GLUT 4 is reported to reside predominantly in intracellular GLUT 4 storage vesicles in the basal state. It has also been suggested that localisation of IRS-1 and PI3-kinase to the cytoskeleton in adipocytes is important in activation of GLUT 4 translocation and increases in glucose transport in response to insulin (Clark et al., 1998). It was further suggested that release of IRS proteins from this compartment may lead to development of insulin resistance (Clark et al., 2000). Therefore, subcellular localisation of a number of proteins involved in insulin signalling was examined by subcellular fractionation of skeletal muscle. The data in figure 4.2 confirms that in the SHRSP, there are no alterations in expression or sub-cellular localisation of the insulin-signalling proteins, GLUT 4, the insulin receptor substrate proteins IRS-1 and IRS-2 and the p85α (regulatory) subunit of PI3-kinase. This further suggests that the 'classical' insulin-signalling pathway is intact. However, it should be noted that in one study, insulin activation of PKB was normal in skeletal muscle from obese and diabetic patients, despite decreases in insulin-stimulated PI3-kinase activity (Kim et al., 1999).

Another downstream target of insulin is PKC. A number of isoforms of PKCs exist, many of which are expressed in skeletal muscles (figure 4.4). The level of expression of all of the PKC isoforms examined was similar in WKY and SHRSP muscles.

However, expression of the atypical PKC isoforms (PKCs λ and ζ) which are most likely insulin effectors could not be determined. In the case of PKC ζ, this was due to the lack of a good positive control and the non-specific nature of the antibody. PKC λ is the mouse homologue of PKC ι therefore its expression may not be expected in rat skeletal muscle. A non-specific band of around 70 kDa was detected using a number of the antibodies (anti PKC α, β, δ, ε and ι). These antibodies were all raised against different regions of the proteins of interest, suggesting the non-specificity has not resulted due to the nature of the immunogen. The identity of the non-specific bands was not determined.

The primary role of insulin in skeletal muscle is the storage of elevated blood glucose as glycogen and muscle glycogen synthesis has been reported to be decreased by up to 50% in diabetic individuals (Shulman, 2000). Therefore, the role of insulin in regulating glycogen metabolism was studied in SHRSP skeletal muscle as in the presence of decreased glucose uptake into the skeletal muscle it might be expected that glycogen storage would be decreased. Glycogen metabolism in these muscles was examined by determining protein levels and activity of the glycogen synthase kinases GKS-3α and β, by analysing the processes of glycogen synthesis and breakdown in SHRSP skeletal muscle, and by determining muscle glycogen levels. No differences in the levels of glycogen synthesis, glycogen phosphorylase activity or GSK-3 activity were observed in skeletal muscle from SHRSP compared to that from WKY.

However, in this study insulin did not inhibit either GSK-3α or β activity (insulin incubation was 1 μM for 30 minutes at 37°C), figures 4.5 panel A and 4.6 panel A, in skeletal muscle from WKY or SHRSP. Neither did insulin affect cellular glycogen levels (figure 4.7), and only a minor effect was observed on glycogen phosphorylase activity (figure 4.9). This is surprising, as insulin is known to inhibit GSK-3 in skeletal muscle (Cross et al., 1997), and insulin was seen to activate PKB (figure 4.3) and glycogen synthesis (figure 4.8) in this study. One possibility may be that GSK-3 inhibition and glycogen phosphorylase activation occurs transiently in response to insulin. Hence, during the course of the 30 minute stimulation which has been chosen for these experiments, GSK-3 and phosphorylase activities may have returned to

basal levels, and thus inhibition/activation was not detected. This was not a problem when assaying glycogen synthesis, as radiolabelled product accumulates with time. Activation of PKB has also been reported to be transient with maximal activation in response to insulin being reported to occur within 5 minutes, and return to basal levels after around 30 minutes (Cross et al., 1997). However, in this study, a robust activation of PKB by insulin was observed (figure 4.3), using a method similar to that for GSK-3.

As previously stated, no significant differences in GSK-3α or β activity were observed in EDL or soleus muscle from SHRSP, as compared to WKY. However some problems were encountered on assaying GSK-3β as the samples showed intra- and inter-sample variation, as shown by the large error bars on the graph (figure 4.6, panel A). GSK-3β protein levels were similar between the two strains, however GSK-3α protein expression was shown to be decreased in SHRSP skeletal muscle (EDL and soleus), compared to WKY (figure 4.5, panel B). The presence of less GSK-3α protein in SHRSP skeletal muscle did not affect the levels of activity observed (figure 4.5, panel A), suggesting that the small amount of protein present in the SHRSP has a relatively high specific activity. From the immunoblot it appears the protein which is expressed in the SHRSP has a lower molecular weight to that in the WKY. The samples were prepared in the presence of the protease inhibitors SBTI, benzamidine and PMSF therefore it was presumed that the lower molecular weight species were not due to degradation of the protein. It was hypothesised that dephosphorylation of the GSK-3α protein may have resulted in the lower molecular weight observed, which would presumably make the protein more active. However, this again would not have been expected due to the prsence of phosphatase inhibitors in the lysis buffer. Treatment of muscle lysates from WKY and SHRSP with PP1 did not change the banding pattern observed for either of the strains, suggesting the change in molecular weight observed in the SHRSP protein was not due to dephosphorylation. However, no other phosphatase was utilised in this experiment and it may be that another phosphatase e.g. PP2A would bring about dephosphorylation of the protein.

Initial experiments on glycogen storage (data not shown) suggested that SHRSP muscle had elevated glycogen levels compared to the SHRSP. However, refinement of the method, suggested that this was not the case and that the SHRSP has similar muscle glycogen levels to the WKY (figure 4.7). However, the error bars on the graph are large in some cases. This is believed to be due to the technically challenging nature of the assay, and possibly due to some variation among animals.

As an alternative methodology, glycogen metabolism was investigated more fully by studying glycogen synthesis (figure 4.7) and glycogen phosphorylase activity (figure 4.8). No significant differences in glycogen synthesis or glycogen phosphorylase activity were detected in skeletal muscle from WKY and SHRSP skeletal muscle. This further supports the data suggesting there are no differences in glycogen storage in skeletal muscle from SHRSP and WKY. Skeletal muscle glycogen content in these two strains has also been analysed histochemically and by electron microscopy (Dr. I Montgomery, personal communication). Again no differences in glycogen storage were identified.

Skeletal muscle from WKY and SHRSP has been fibre-typed immuno-histochemically (figure 4.10). The results from this work show similar distribution and number of fibre types in skeletal muscle from SHRSP and WKY. Also, no gross morphological differences were apparent in the muscle from SHRSP, which could account for the insulin resistant, hypertensive phenotype observed in these animals.

Thus, the defect resulting in the insulin resistant phenotype in the SHRSP remains unidentified, although a number of possibilities exist which have not been clarified. A second pathway (involving the CAP-Cbl complex) that is modulated by insulin, and is required for GLUT 4 translocation, was recently identified (Baumann et al., 2000, see introduction). During the course of this study, two components of this pathway, caveolin-1 and flotillin, were observed to be over-expressed in SHRSP skeletal muscle (James et al., 2001). Various other components of this pathway have been studied, but the lack of good reagents made this somewhat difficult and unfruitful. Another possibility is that while GLUT 4 appears to be in the correct compartment in these muscles, translocation to the plasma membrane on insulin

stimulation may be in some way impaired. This has not yet been analysed due to the lack of a robust fractionation procedure.

CHAPTER 5

A YEAST TWO-HYBRID SCREEN WITH FLOTILLIN-1

5.1 Introduction

5.1.1 Flotillin is a protein found in lipid rafts

Flotillin-1 is a 47 kDa protein, which was originally isolated from murine lung tissue, and identified as a protein which resides in caveolae/lipid rafts (Bickel et al., 1997). Flotillin was predicted to be an integral membrane protein due to the presence of two hydrophobic regions in its N-terminus (amino acids 10-36 and 134-151) and its membrane localisation has been confirmed using a variety of methods (Bickel et al., 1997). Flotillin-1 was also reported to have two potential tyrosine phosphorylation sites and predicted sites for phosphorylation by PKC and PKA. Regions of the C-terminus were also reported to have the ability to form triple coiled-coils with other flotillin monomers (Bickel et al., 1997). Subsequently human flotillin-1 was cloned, and it was reported to have 98% identity with the mouse flotillin-1 (Edgar and Polak, 2001). The 42 kDa human flotillin-2 was also isolated (Hazarika et al., 1999) and the two human flotillin isoforms were reported to have 47% sequence identity (Edgar and Polak, 2001).

The flotillin proteins are expressed in a variety of tissues, with flotillin-2 being more widely expressed than flotillin-1 (Volonte et al., 1999). Co-immunoprecipitation studies have resulted in the suggestion that flotillins-1 and -2 form stable complexes with caveolins-1 and -2 (Volonte et al., 1999), with implications for a possible role for the flotillin proteins in caveolae structure. Flotillin-1 is highly expressed in brain and flotillin homologues have also been identified in Drosophila (Galbiati et al., 1998) and in goldfish (Schulte et al., 1997) and these studies suggested a role for flotillin in neural development. James et al. (2001) also reported the over-expression of flotillin-1 and caveolin-1 in skeletal muscle of the SHRSP, suggesting a possible role for these proteins in the insulin resistant/hypertensive phenotype observed in these animals.

5.1.2 The yeast two-hybrid system

The yeast two-hybrid system was first reported by Fields and Song (1989) and is a powerful tool for detecting protein-protein interactions. A reporter yeast strain is

used, containing inducible reporter genes fused to an upstream activator/promoter sequence (for example, the GAL 4 promoter). The yeast are transformed with plasmids containing gene fusions. The protein of interest (bait) is encoded as a gene fusion to the GAL 4 DNA binding domain, while the second plasmid contains the GAL 4 activation domain as a gene fusion to the library of proteins (termed the prey). Interaction of two proteins (in this case the bait with a protein expressed in the library) brings the activation domain into the proximity of the DNA, allowing activation of reporter gene transcription to occur (see figure 5.1). The reporter genes used are often nutritional genes, required for yeast growth. Hence, transformed yeast will grow on selection media (media lacking these nutrients) if an interaction occurs between two proteins that allows transcription of the reporter gene(s), and production of the required nutrients.

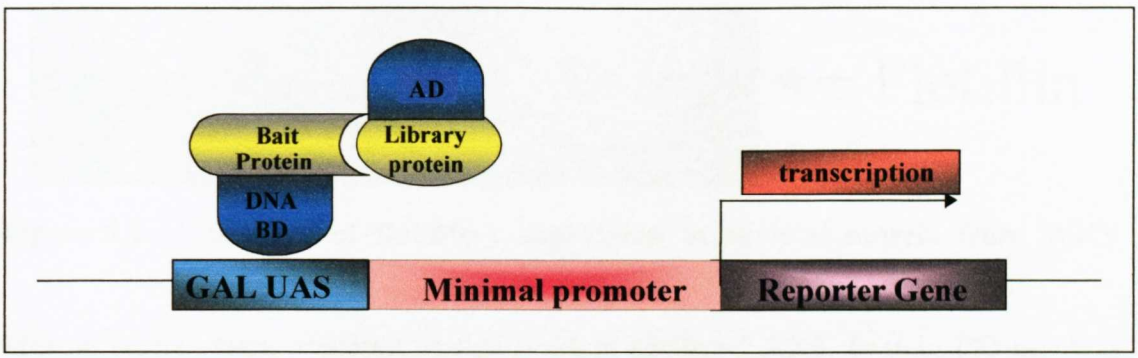

Figure 5.1 Schematic diagram of the principle of the yeast two-hybrid system

5.1.3 Aims of Chapter

The aim of this study was to identify novel flotillin-interacting proteins by the method of the yeast two-hybrid system and in so doing hopefully define more clearly the functional role of flotillin in insulin signalling. A further aim was to study these proteins with respect to the insulin resistance/hypertension observed in the SHRSP.

5.2 Results

5.2.1 Flotillin expression is increased in the SHRSP

To confirm the data of James et al. (2001) who reported increased expression of flotillin in skeletal muscle of SHRSP, skeletal muscle lysates from WKY and SHRSP were probed with an anti-flotillin antibody. In the three muscles tested, flotillin expression was greater in the SHRSP compared to the WKY (see figure 5.2).

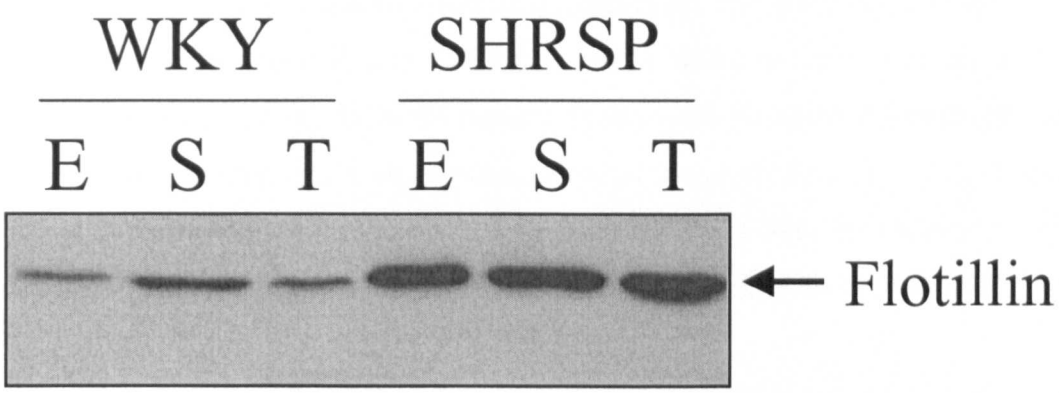

Figure 5.2 Analysis of flotillin-1 expression in skeletal muscle from WKY and SHRSP

Muscle lysates were prepared as described in section 2.3.2.5. Protein (20 μg) was subjected to SDS-PAGE and transferred to nitrocellulose, as described in sections 2.3.1.1 and 2.3.1.2. The nitrocellulose was probed with an anti-flotillin antibody (at 1:1000 dilution) following a similar protocol to that described in section 2.3.1.4. In the SHRSP flotillin protein expression is increased in all three muscles tested. E = EDL, S = soleus, T = tibialis. The data presented is representative of two experiments of this type. Quantification of the data from these two experiments (data not shown) revealed flotillin expression was increased on average 3-fold in EDL and tibialis muscle and 2-fold in soleus muscle from SHRSP compared to WKY.

5.2.2 Construction of the bait plasmid for the yeast two-hybrid screen

5.2.2.1 Cloning of human flotillin 152-427 from cDNA

When studying the interaction of proteins in the yeast two-hybrid system it is necessary that any potential transmembrane regions of the protein of interest be removed, to prevent the protein being targeted away from the yeast nucleus, where it is required to activate transcription of the reporter genes. Initial studies on murine flotillin-1 suggested the presence of two hydrophobic regions (shown in red in figure 5.3) which are suggested to be putative membrane spanning regions (Bickel et al., 1997). Later studies on human flotillin-1 suggested the presence of only one membrane-spanning region (Edgar and Polak, 2001). However, to be sure the protein would not be targeted away from the nucleus in the yeast two-hybrid screen, primers were designed to clone the DNA encoding only amino acids 152-427 of the human flotillin-1 protein (the human flotillin-1 is 1 residue shorter than the mouse isoform, as it lacks an asparagine residue close to the C-terminus (Edgar and Polak, 2001)).

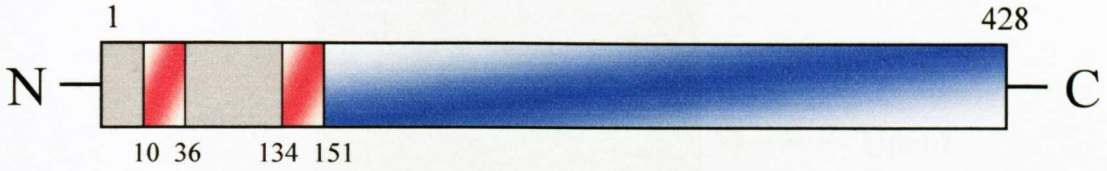

Figure 5.3 Schematic diagram of mouse flotillin-1 (adapted from Volonte et al., 1999)

Putative hydrophobic/membrane spanning regions are shown in red, the suggested cytosolic portion of the molecule is shown in blue. The numbers on the diagram correspond to the amino acids in the protein.

DNA corresponding to amino acids 152-427 of flotillin was PCR amplified from human heart and skeletal muscle cDNA using the following primers: 5′-GagatctGTAAGGACATTCACGATGACCAGG-3′ (*Bgl*II site in small letters) and 5′-ctcgag**TCA**GGCTGTTCTCAAAGGCTTG-3′ (*Xho*I site in small letters, STOP codon in bold), following the protocol described in section 2.3.3.1. Agarose gel

electrophoresis of the PCR products revealed a band of the expected size (figure 5.4, top panel), the flotillin 152-427 DNA fragment being 828 base pairs. Furthermore, digestion of the PCR product with the restriction enzyme *Sma*I should cut the DNA once producing two fragments of around 440 and 390 base pairs each. Figure 5.4, bottom panel shows such a digest and as expected two bands of the expected sizes are observed, suggesting that flotillin 152-427 has been amplified.

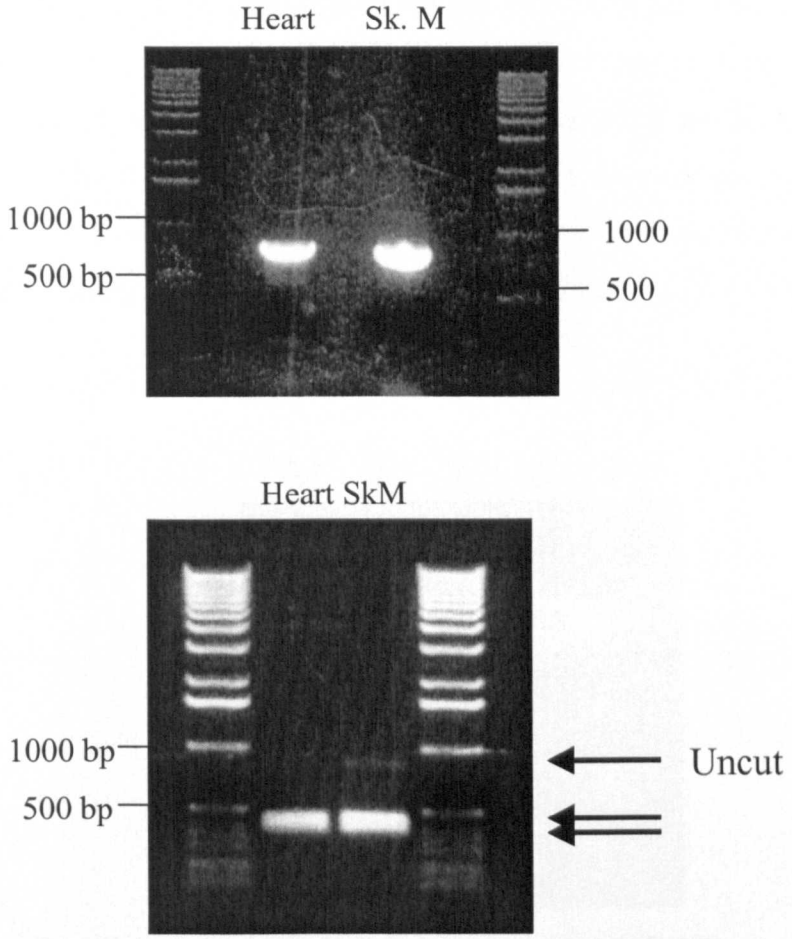

Figure 5.4 PCR amplification of flotillin 152-427 from heart and skeletal muscle cDNA

Flotillin 152-427 was PCR amplified as described in sections 2.3.3.1 and 2.3.4.3 from heart and skeletal muscle cDNA. Top panel: the PCR product was subjected to agarose gel electrophoresis as described in section 2.3.3.3. A band of around 850 base pairs is observed, as expected. Lower panel: the PCR product was subjected to restriction digestion with the enzyme *Sma*I as described in section 2.3.3.7, followed by agarose gel electrophoresis. Two bands of less than 500 base pairs are expected, these are not clearly resolved in the figure, but further electrophoresis did resolve two bands (data not shown).

5.2.2.2 TA cloning of flotillin 152-427

PCR amplified flotillin 152-427 (from muscle cDNA) was treated with *Taq* polymerase as described in section 2.3.3.5, to add 'A' base overhangs onto the DNA. This DNA was subsequently cloned into the pCRII vector, as described in section 2.3.3.6. As described, colonies were picked and small overnight cultures prepared. From these, DNA was extracted, as described in section 2.3.3.11. The DNA was then analysed by restriction digest using *Eco*RI (figure 5.5). No *Eco*RI sites are present in flotillin 152-427, therefore bands of around 850 bases, corresponding to the insert, and a larger band, corresponding to the vector, are expected. It can be seen in figure 5.5 that three of the four colonies picked contained an insert of the expected size. DNA from colony number 2 was sequenced to confirm the insert was flotillin 152-427, before any subsequent experimentation was carried out.

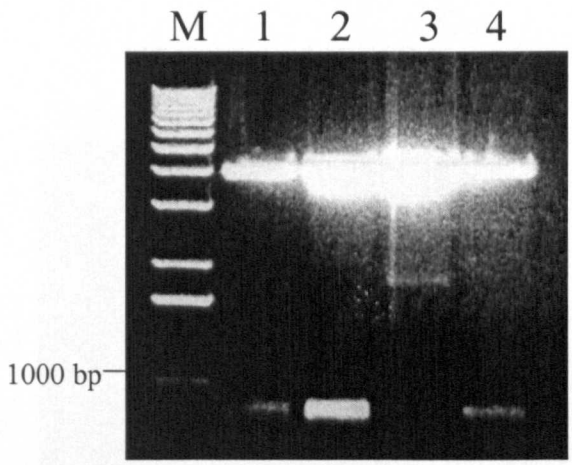

Figure 5.5 Restriction analysis of TA cloned flotillin 152-427

TA cloned flotillin 152-427 was prepared as described above, and in sections 2.3.3.5 and 2.3.3.6. Colonies were picked and grown overnight in liquid culture. DNA was extracted from these cultures as described in section 2.3.3.11. The DNA was subjected to restriction digest using *Eco*RI, as described in section 2.3.3.7, and subsequently subjected to agarose gel electrophoresis (section 2.3.3.3). In three out of the four colonies picked a band of around 850 bases is observed, as expected.

5.2.2.3 Sub-cloning of flotillin 152-427 into the yeast two-hybrid bait vector, pGBT9

The primers used for amplification of flotillin 152-427 had been designed to incorporate a restriction site for *Bgl*II in the forward primer and *Xho*I in the reverse primer, to allow cloning into the yeast two-hybrid vector using the complementary *Bam*HI and *Sal*I sites. The pCRII-flotillin 152-427 DNA was therefore digested with the restriction enzymes *Bgl*II and *Xho*I, as described in section 2.3.3.7. pCRII has an internal *Bgl*II site and thus three bands (of sizes around 3000, 926 and 850 bases) were expected on restriction with these enzymes. pGBT9 was digested with *Bam*HI and *Sal*I, which is expected only to linearise the plasmid, as these restriction sites are present only in the multiple cloning site of the plasmid (see appendix). Figure 5.6 shows the DNA was cut as expected by these enzymes.

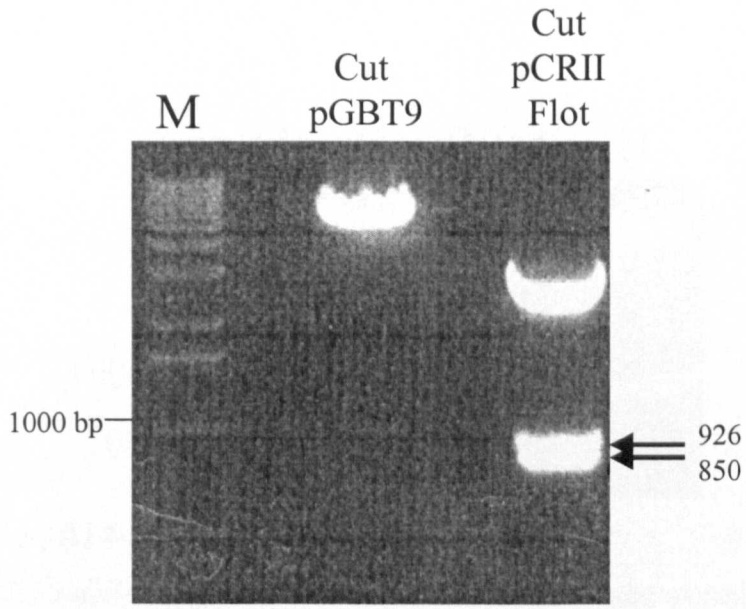

Figure 5.6 Restriction digests of pGBT9 and pCRII-flotillin 152-427

The pCRII-flotillin 152-427 DNA was digested with *Bgl*II and *Xho*I, as described in section 2.3.3.7. As expected three bands (of sizes around 3000, 926 and 850 bases) are observed, the lower band being flotillin 152-427. pGBT9 was digested with *Bam*HI and *Sal*I, which is seen to linearise the plasmid.

The linearised pGBT9 and the flotillin 152-427 bands were excised from the gel, and gel purified as described in section 2.3.3.4. The DNA was then ligated overnight (described in section 2.3.3.8) and the ligated DNA transformed into XL1-blue *E. coli* cells, as described in section 2.3.3.10. Colonies were picked and grown overnight in liquid culture. DNA was extracted from these cultures as described in section 2.3.3.11. Ligation of the pGBT9 vector and the flotillin 152-427 insert using the *Bam*H1/*Bgl*II and *Xho*I/*Sal*I sites described does not result in reconstitution of functional restriction sites. Therefore, the DNA was subjected to restriction digest using *Eco*RI and *Pst*I (as there are *Pst*I and *Eco*RI sites in the multiple cloning site of the vector, which will allow excision of the insert), as described in section 2.3.3.7, and subsequently subjected to agarose gel electrophoresis (section 2.3.3.3). Figure 5.7 shows restriction digests of DNA prepared form DNA isolated from 4 independent colonies. Each clone appears to contain the flotillin 152-427 DNA insert. This was confirmed by sequencing DNA from colony F. This DNA was used in all future experiments.

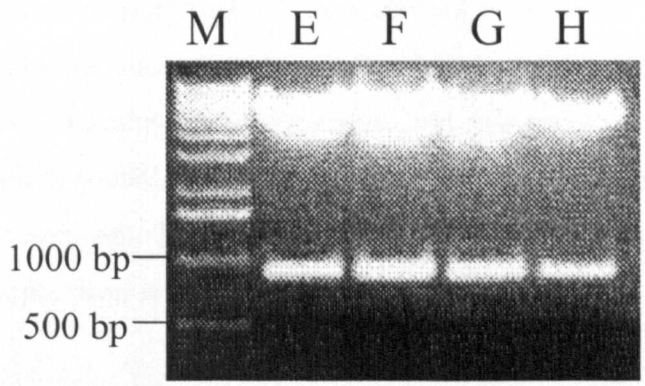

Figure 5.7 pGBT9-flotillin 152-427 restriction digests

Linearised pGBT9 and the flotillin 152-427 bands were ligated overnight (described in section 2.3.3.8) and the ligated DNA transformed into XL1-blue *E. coli* cells, as described in section 2.3.3.10. 4 colonies were picked and grown overnight in liquid culture. DNA was extracted from these cultures as described in section 2.3.3.11. The DNA was subjected to restriction digestion using *Eco*RI and *Pst*I as described in section 2.3.3.7, and subsequently subjected to agarose gel electrophoresis (section 2.3.3.3). Each clone appears to contain the flotillin 152-427 DNA insert.

5.2.3 Control yeast transformations

The genotype of the yeast strain (PJ692A) used in this screen is described in section 2.1.6. This yeast strain requires the presence of uracil, leucine, tryptophan, histidine and adenine in the growth medium. The bait plasmid used in the screen encodes expression of an enzyme required for tryptophan synthesis, and the library vector encodes for a protein required for synthesis of leucine. Thus, PJ692A transformed with both bait and library plasmids no longer require addition of tryptophan and leucine to the growth medium. The reporter genes in the strain encode the expression of histidine and adenine, therefore if bait and library proteins interact, leading to reporter gene expression, the need for histidine and adenine in the growth medium will also be subverted.

However, prior to performing the yeast two-hybrid screen it was necessary to check that the bait plasmid, containing the flotillin 152-427, and the library plasmid did not cause self-activation of reporter gene expression in the absence of an interaction occurring. Hence, wild-type yeast were transformed with the bait vector (pGBT9-flotillin 152-427) and the empty pACT2, as described in section 2.3.4.3. These were plated onto media lacking leucine and tryptophan to select for yeast which had taken up both plasmids. Six colonies were then picked and re-streaked onto media lacking leucine and tryptophan (double drop-out, DDO) media lacking leucine, tryptophan and histidine (triple drop-out, TDO) and media lacking leucine, tryptophan, histidine and adenine (quadruple drop-out, QDO).

As expected, the yeast (5 of 6 colonies selected) grew on the DDO media (figure 5.8). A small amount of growth was observed on the TDO plates and almost no growth was observed on the QDO plates (figure 5.8). No growth was expected on the TDO plates and to prevent this 3-AT (3-amino-1,2,4-triazole), which reduces leaky histidine expression, was included in the media at a concentration of 5 mM which was sufficient to reduce this background growth (data not shown).

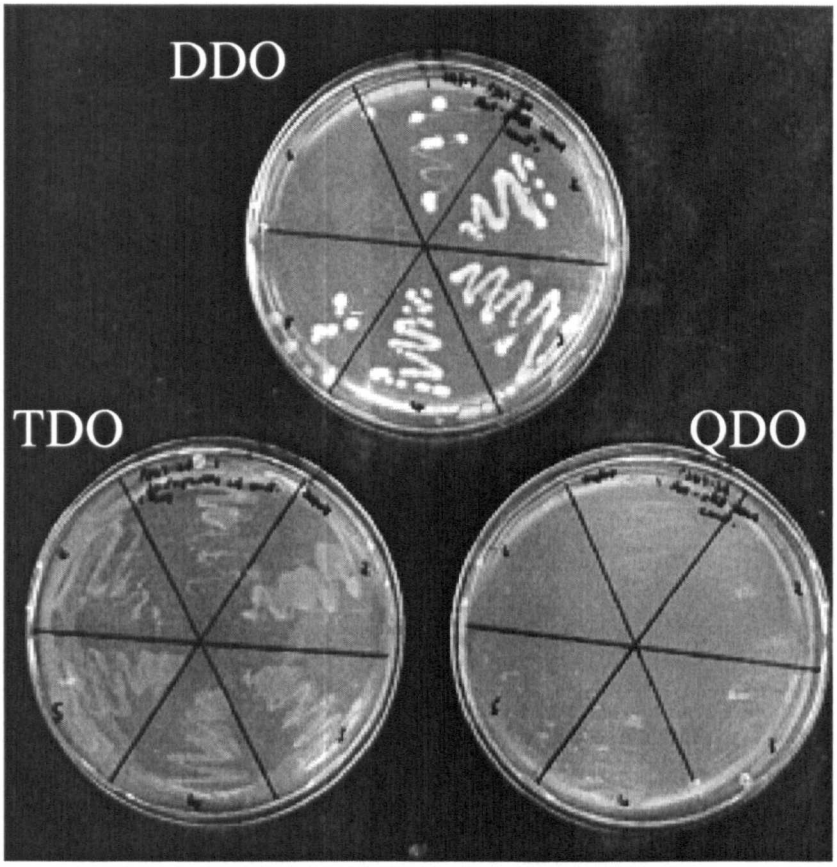

Figure 5.8 Analysis of growth requirement of control transfected yeast

PJ692A was transformed with the bait vector pGBT9-flotillin 152-427 and empty pACT2, as described in section 2.3.4.3. Yeast were plated onto DDO, TDO and QDO media and their growth monitored. 5 of 6 colonies picked grew well on DDO media. Some residual growth was observed on TDO media, which has since been resolved by including 3-AT in the media (data not shown).

5.2.3.1 Expression of flotillin/GAL 4 BD in control transformed yeast

Before performing the screen it was also necessary to check the bait protein was being expressed in the transformed yeast cells. Therefore yeast lysates were prepared and western blot analysis performed. Figure 5.9 shows a band of around 47 kDa is present in skeletal muscle, corresponding to flotillin-1. In 5 of the 6 yeast lysates a band of slightly smaller than 47 kDa is present, corresponding to flotillin 152-427/GAL 4 DNA binding domain fusion protein.

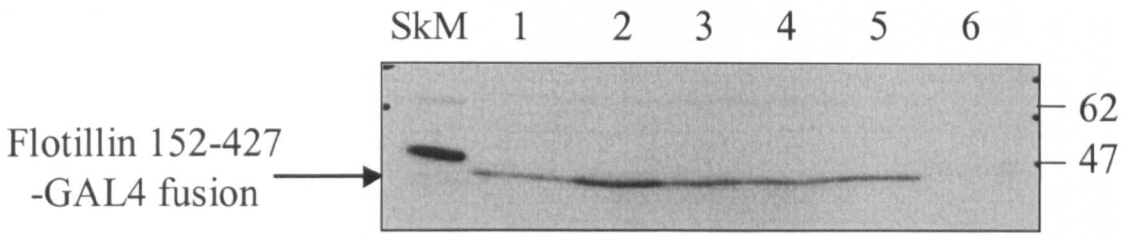

Figure 5.9 Western blots analysis of transfected yeast lysates

Yeast lysates and skeletal muscle lysates were prepared as described in sections 2.3.4.10 and 2.3.2.5. 20 μg muscle lysate and 20 μl yeast lysate was subject to gel electrophoresis as described in section 2.3.1.1. Proteins were transferred to nitrocellulose and detected by immunoblotting as described in section 2.3.1.2 and 2.3.1.4. Flotillin-1 protein is detected in 5 of the 6 yeast lysates.

5.2.4 The yeast two-hybrid screen

In the first instance a small-scale screen was performed using a skeletal muscle library from Clontech, amplified as described in section 2.3.4.2. However, this screen was unsuccessful with no flotillin interacting proteins being identified. It is believed there may be a problem with this library and therefore subsequent work was performed using a human testis cDNA library, also from Clontech and amplified in a similar manner as described for the skeletal muscle library.

Initially a small-scale screen was performed in which around 50,000 clones were screened. Yeast were sequentially transformed, initially with the bait plasmid followed by the library plasmid, as described in section 2.3.4.4, and plated onto TDO media. Colonies were picked over a 21 day period, and re-streaked onto TDO and QDO media (see figure 5.10), resulting in 95 positive clones. From the first 60 of these clones library plasmids were isolated as described in sections 2.3.4.5–2.3.4.7. These plasmids were subjected to sequence analysis and BLAST searching (Altschul et al., 1990) to determine the identity of the protein encoded. Of the 60 clones sequenced, 31 encoded regions of known or hypothetical proteins (see table 5.1).

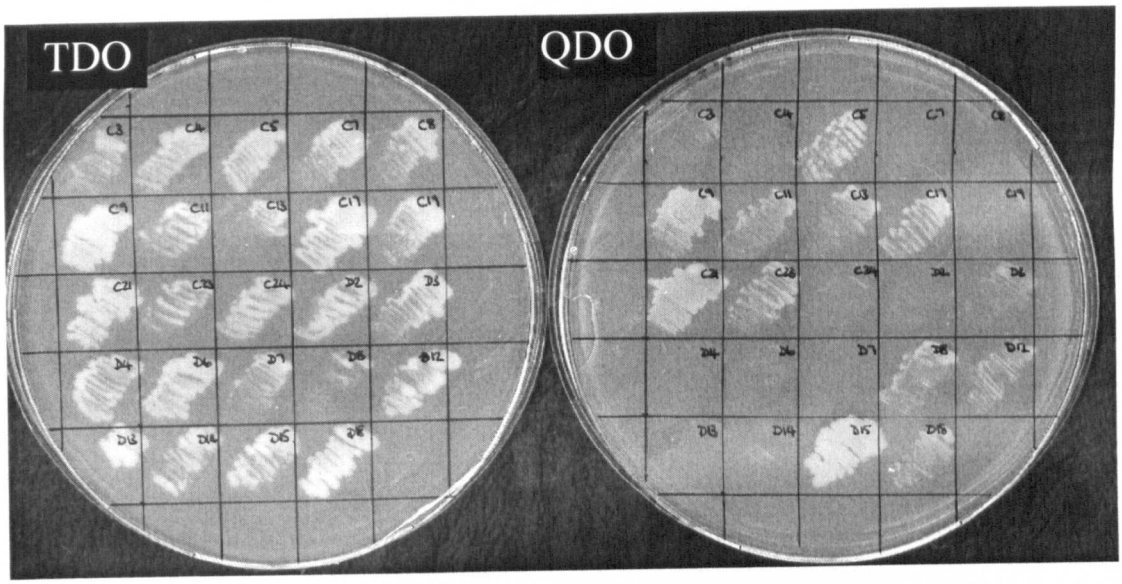

Figure 5.10 Yeast growth as a result of a protein interaction in a small-scale testis yeast two-hybrid screen

PJ692A were sequentially transformed with bait and library as described in section 2.3.4.4. Colonies were picked and re-streaked onto TDO and QDO as shown. Around 50% of the clones grew on the QDO media.

Clone ID	Protein encoded	Information from PIX analysis	
		Intracellular Localisation	Domains/Secondary Structure
A21	TACC1, transforming acidic coiled-coil containing protein 1	66% nuclear	Putative C-terminal coiled region
A25	HCR (a-helix coiled-coil rod homologue)	48% nuclear	Almost completely coiled, regions of homolgy to flotillin famliy, Ezrin/Radixin /Moesin family, tektin family and a Kbox
B7	KIAA0794 protein	40% nuclear, 36% cytoplasmic	N-terminal UBX domain
B11	TBL2, Transducin (beta)-like 2	44% nuclear, 28% cytoplasmic	Possibly 1 TM regions and 5 WD domains
B21	HSPC015 protein	56% nuclear	
B22	Hypothetical protein FLJ20396	36% ER, 24% mitochondrial	4 possible TM domains
B23	CDA017 protein	40% nuclear	Leucine rich repeats
B26	Membrane-spanning 4-domains, subfamily A, member 5	32% ER, 24% mitochondrial	4 TM domains, region of homology to Got1-like family
B29	Hypothetical protein FLJ20449	48% nuclear	Large putative coiled region, central helix-lool-helix DNA binding domain
B33	Ribosomal protein S16	84% cytoplasmic	
B39	Actinin, alpha 4 (non-muscle alpha actinin)	44% nuclear, 36% cytoplasmic	1 TM domain, large putative coil, dynamin central region, calponin homology, spectrin repeats and EF hand
B40	Poly(rC) binding protein 2 (alpha CP2)	64% cytoplasmic	One possible TM, 3 KH domains
B42	KIAA0193 gene product	32% nuclear, 28% cytoplasmic	
C4	Collagen, type I, alpha 1	60% extracellular	20 collagen triple helix repeats
C7	Ring finger protein 10	84% nuclear	C-terminal half is putatively coiled, zinc finger, 1 possible TM
C27	KIAA0185 protein	76% nuclear	Putative C-terminal coil, multiple S1 RNA binding domains
C30	Protamine 2 (Sperm histone P2 precursor)	76% nuclear	

D2	Thyroid autoantigen 70kD (Ku antigen)	24% nuclear, 20% ER, 20% cytoplasmic	Putative N-terminal coil, one possible TM
D6	Synaptosomal-associated protein, 29kD	48% cytoplasmic, 32% nuclear	Putative coiled regions
D12	Immunoglobulin superfamily, member 8	32% PM, 32% extracellular	Possible TM regions at each end, 4 immunoglobulin domains,
D13	Solute carrier family 9 (sodium/hydrogen exchanger), isoform 3 regulatory factor 1	60% cytoplasmic	Two PDZ domains
D14	Annexin A2	44% cytoplasmic, 24% nuclear	Possible C-terminal coiled region
D18	KIAA0376 protein	68% mitochondrial	Predicted to be largely coil forming
D25	Soggy-1	24 % cytoplasmic, 16% ER, 16% nuclear, 16% Golgi	One possible TM at N-terminal
D26	Similar to germ cell specific Y-box binding protein	52% nuclear	
E2	Hypothetical protein FLJ20036	52% cytoplasmic, 36% nuclear	Has double stranded RNA binding motif
E13	Heat shock transcription factor 2	48% nuclear, 36% cytoplasmic	Predicted to be largely coiled, HSF-type DNA binding, homeobox associated leucine zipper
E15	Tubulin, beta, 2	36% nuclear, 36% cyt	1possible TM, 1 putative coiled region at extreme C-terminus, tubulin domains
E16	Cystatin B (stefin B) (Liver thiol proteinase inhibitor)	48% cytoplasmic	
F14	Hypothetical protein BC014608	52% mitochondrial	Putative coiled regions, 3 calmodulin binding motifs
G1	Glycophorin E	32% ER, 32% mitochondrial	

Table 5.1 Putative flotillin interacting proteins identified in a small-scale testis yeast two-hybrid screen
TM = transmembrame, PM = plasma membrane, ER = endoplasmic reticulum

Subsequently a larger screen was performed in which around 500,000 clones were screened. Again yeast were sequentially transformed, but this time colonies were only picked for 10 days. This resulted in isolation of 256 positive clones (example plates from this screen are shown in figure 5.11). Library plasmids were isolated from the clones which grew on QDO media (102 clones) and of these 23 have been sequenced so far with 12 encoding known or hypothetical proteins (see table 5.2).

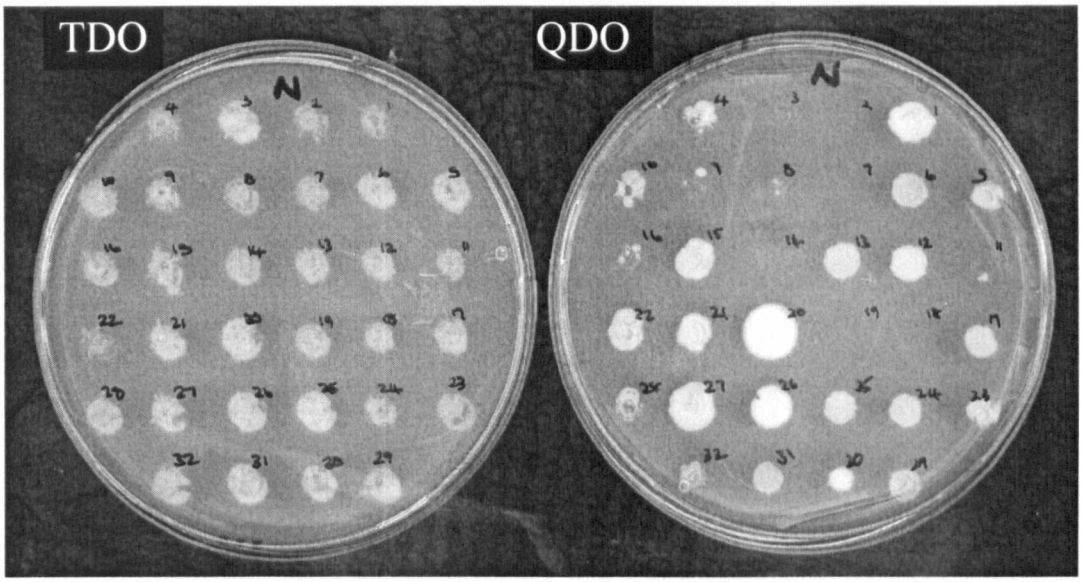

Figure 5.11 Yeast growth as a result of a protein interaction in a large-scale testis yeast two-hybrid screen

PJ692A were sequentially transformed with bait and library as described in section 2.3.4.4. Colonies were picked and re-streaked onto TDO and QDO as shown. Over 50% of the clones grew on the QDO media.

Clone ID	Protein encoded	Information from PIX analysis	
		Intracellular location	Domains/Secondary Structure
H5	Formin homology 2 domain containing 1	44% nuclear, 40% cytoplasmic	3 possible TM regions, 1 putative coiled region
H11	Hypothetical protein MGC2494	48% cytoplasmic	1 possible TM region
I24	Prostaglandin D2 synthase (21kD, brain)	60 % extracellular	1 possible TM domain, regions with triabain homology
I30	similar to HSF-type DNA-binding domain containing protein	52% nuclear	2 possible TM domains
K11	Binder of Arl Two (BART1)	56% cytoplasmic	
L4	NEDD8 ultimate buster-1	48 % nuclear	Predicts largely coil forming, regions of homology with ubiquitin family and predicts KRAB box and UBA TS-N domain
L9	Casein kinase 2, beta polypeptide	48% nuclear, 36% cytoplasmic	
L15	Nucleolar protein ANKT	56 % nuclear	SAP domain
N17	Hypothetical protein FLJ14225	24 % cytoplasmic, but also in nucleus, Golgi, vesicles etc	Possible fibronectin type III domain, PKD domain, REJ domain. 2 or 3 possible TM regions
N26	Proteaseome (prosome, macropain) 28 subunit, 3, clone	56% nuclear	proteosome activator pa28 alpha subunit, possible C-terminal coiled-coil
O3	ATP synthase, H+ transporting, mitochondrial F1 complex, O subunit	52% mitochondrial, 28% nuclear	ATP synthase delta subunit, predicts largely coil forming
O13	Similar to synaptomenal complex protein 3 (SCP-3)	68% nuclear	Possible C-terminal coiled region, CIP4 homology domain

Table 5.2 Putative flotillin interacting proteins identified in a large-scale yeast two-hybrid screen TM = transmembrane

The protein sequences of the putative flotillin interacting proteins were subjected to PIX analysis (http://www.hgmp.mrc.ac.uk/Registered/Webapp/pix/). This is a tool that runs a number of peptide analysis programs, allowing various predictions to be made about the peptide/protein of interest. It can be used to predict the secondary structure of a protein, detailing the presence of α-helices and β-sheets. The presence of transmembrane regions and various other structural and functional domains is also predicted, as well as the presence of any putative coiled-coil structure. The program will also predict the intracellular location of the protein of interest. The output from a PIX analysis of SNAP-29 (clone D6 is shown in figure 5.12). Details of the predictions made by PIX analysis of the putative flotillin interacting proteins are also detailed in tables 5.1 and 5.2.

While many interesting proteins have been identified as putatively interacting with flotillin, these results have to be viewed with caution. DNA from 18 of the positive clones (chosen at random) was used to re-transform the PJ692A-flotllin 152-427 yeast strain (as described in section 2.3.4.8), and each of these supported growth on triple drop out media (data not shown). This suggests that the yeast grew due to activation of the reporter genes, and not because a mutation had occurred. However, due to time constraints it has not been possible to do follow up bench work on any of these proteins and until such times as a biochemical interaction can be shown, these proteins must be viewed as putative flotillin-binding proteins.

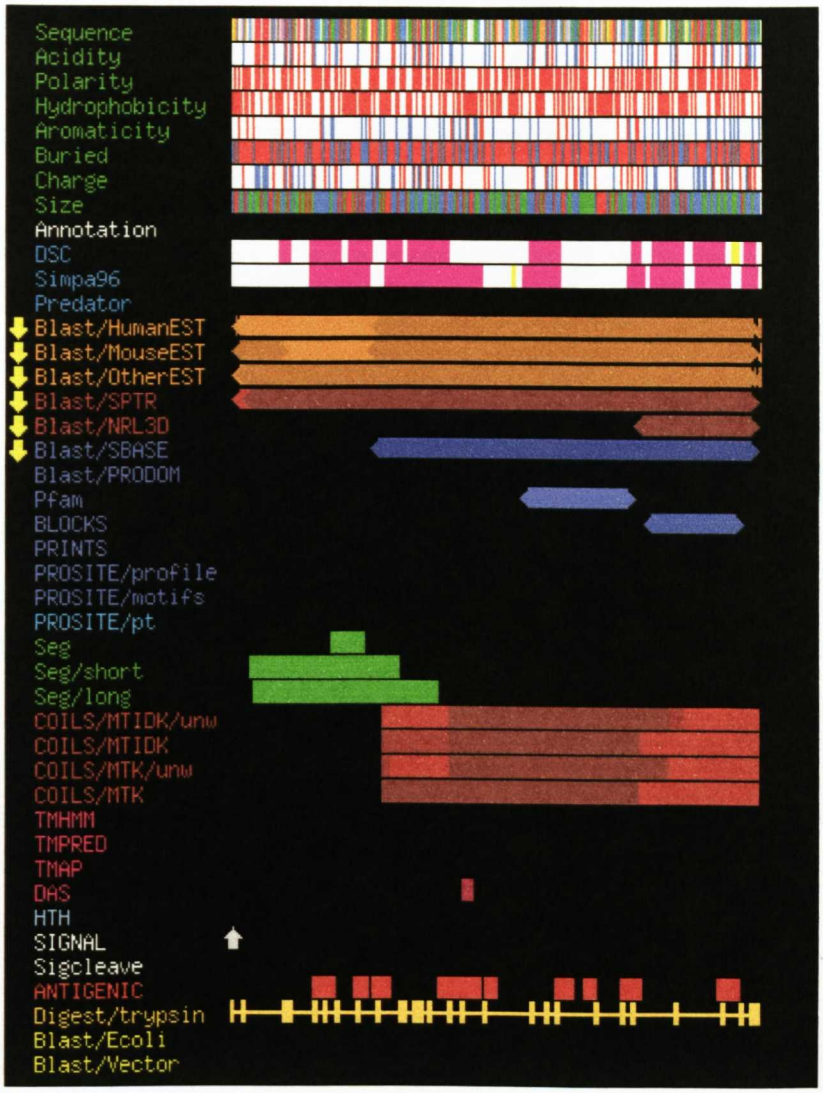

Figure 5.12 PIX analysis of SNAP-29 (clone D6)

Shown in red is the predicted coil structure of this protein. Transmembrane regions are shown in pink, none of which are present in this protein. In blue (Pfam) predicts a domain with homology to SNAP-25.

5.3 Discussion

A large number of proteins have been identified in this study by yeast-two hybrid screening, which may be flotillin interacting proteins. However as no biochemical analysis has been undertaken on these proteins, they must be viewed with some caution.

Flotillin has been reported to form triple coiled-coils with other flotillin monomers via interactions in the C-terminus (Bickel et al., 1997) and thus it is possible that positive interacting proteins, will also contain coil forming regions and interact with flotillin by forming coiled-coils. A number of proteins were identified in this yeast two-hybrid screen which by PIX analysis are predicted to contain coil-forming regions, for example, SNAP-29, annexin A2, HCR (a-helix coiled-coil rod homologue), TACC1 (transforming acidic coiled-coil containing protein 1). However it is also possible that coiled-coil interactions may occur non-specifically in the yeast two-hybrid system and these interactions would have to be analysed biochemically to be sure of their integrity.

Around half of the proteins identified are predicted to be localised predominantly to the nucleus by PIX analysis. Flotillin has previously been described as an integral membrane component of caveolae (Bickel et al., 1997), and therefore is not expected to have nuclear localisation. It is possible that a nuclear localisation signal is present on the molecule, but that this is overridden by the transmembrane domain, or it may be that flotillin is also present in nuclear membranes. However, the likelihood is that the flotillin 152-427 protein encoded in the screen, which is localised to the yeast nucleus with the Gal-4 binding domain has formed non-specific interactions with these nuclear proteins. Again this would need to be determined by the presence or absence of a biochemical interaction. It should be noted that PIX analysis also predicts the flotillin to be nuclear, therefore it is possible that this protein is nuclear and does interact with other nuclear proteins, or possibly more likely that the PIX analysis program tends to falsely predict nuclear localisation. Also the PIX program predicts a number of proteins to be localised to the cytoplasm whilst also predicting the somewhat contradictory presence of transmembrane domains. Therefore it must

be remembered that this program can only make predictions which really need to be followed up by bench work.

It was hypothesised that caveolin (the marker protein for caveolae) would have been identified as a flotillin interacting protein in this screen, as flotillin has been suggested to be present in caveolae. However this was not the case. This may possibly be due to the fact that the whole flotillin protein was not used in the screen. It is possible that an interaction between caveolin and flotillin may occur in the region of amino acids 1-151 of flotillin, which has been removed for the screen to prevent membrane targeting. It may also be a possibility that caveolin and flotillin do not actually participate in a protein-protein interaction. Caveolins and flotillins have been reported to form hetero-oligomeric complexes by co-immunoprecipitation of the proteins (Volonte et al., 1999). However a direct interaction of the two proteins was not shown and it may be possible that the proteins are complexed to another protein resident in caveolae.

Recently the sorbin homology domain has been suggested to be a flotillin-binding motif, as deletion of this region in the proteins CAP and vinexin prevented flotillin binding (Kimura et al., 2001). For this reason the PIX analyses of the putative flotillin interacting proteins were examined for the presence of sorbin homology domains. However, using PIX analysis, none of the proteins identified appear to contain this sorbin homology domain which has been reported to confer flotillin binding. Again it is possible that the region of flotillin which is bound by the sorbin homology domain has been removed in order to undertake the yeast two-hybrid screen. It is also possible that other as yet unidentified protein domains/motifs are involved in flotillin binding.

A disappointing aspect of this screen was that none of the clones identified have been duplicated. In a quality yeast two-hybrid screen where strongly interacting proteins are identified only a small number of clones would be expected and the same clone would normally be detected on numerous occasions. However, this was not the case in this study, for which there may be a number of reasons. In the initial small-scale screen, colonies were picked over a 21-day period, which in hindsight was too long, as the yeast may begin to grow as a result of non-specific interactions. When the

second larger-scale screen was performed, this was rectified with colonies being picked over a 10-day period. Also in the small-scale screen DNA was isolated from colonies which grew on either the triple or the quadruple dropout media. Again this was altered in the large-scale screen with only colonies being investigated which grew on the quadruple dropout media, in which there is presumably a more stringent interaction. In the small-scale screen the majority of the clones were sequenced and analysed. However in the large-scale screen a smaller number were sent for sequencing, with only 12 known or hypothetical proteins being identified. Therefore it is possible if more of the clones from this larger screen were sequenced duplication of clones would be observed. However, as only half of the clones screened initially from the large-scale screen encoded known or hypothetical proteins it was not expected that further screening would produce duplication of interesting proteins. Therefore in the interests of finance and time constraints, further sequencing was not performed.

CHAPTER 6

DISCUSSION

In humans, insulin resistance and hypertension are frequently associated (see section 1.4), however the underlying mechanisms leading to this association have not been identified. In some rodent models, hypertension and insulin resistance are also observed in concert, for example the SHR has been reported to be insulin resistant (Mondon and Reaven, 1988, Reaven et al., 1989). Furthermore, the rodent model of hypertension used in this study, the SHRSP, has also been reported to exhibit peripheral insulin resistance in adipose tissue (Collison et al., 2000). During the course of this study insulin resistance in skeletal muscle of the SHRSP was also demonstrated (James et al., 2001). Hence, the aim of this study was to determine any possible defects in insulin signalling in skeletal muscle of the SHRSP, which may be responsible for the observed insulin resistant phenotype.

eNOS is a protein, which has been suggested to be involved in regulation of glucose transport in skeletal muscle. Nitric oxide (NO) release occurs in response to muscle contraction and the use of NOS inhibitors in skeletal muscle has been reported to decrease contraction-stimulated (but not insulin-stimulated) NO release and glucose transport (Balon and Nadler, 1994, Balon and Nadler, 1997). Furthermore, in endothelial cell cultures both shear stress (Corson et al., 1996, Fisslthaler et al., 2000) and insulin (Montagnani et al., 2001) have been reported to bring about the phosphorylation and activation of eNOS (see section 3.1). Hence it was decided to study eNOS regulation in the SHRSP in response to insulin and AICAR (an activator of AMPK, a kinase thought to function in contraction-stimulated glucose transport, see section 1.3.3.3).

In order to study eNOS regulation by phosphorylation at serine 1177, anti-peptide antibodies were prepared which were raised against peptides corresponding to eNOS protein either phosphorylated or dephosphorylated at this site (described in chapter 3). These antibodies were affinity purified and their specificity characterised (also described in chapter 3). The anti-phospho and -dephospho eNOS antibodies appear to work well when undertaking western blotting, immunoprecipitation and confocal microscopy however, there is some question over the specificity of the antibodies and further experimentation on the SHRSP has not been carried out to date. Using these antibodies in western blotting experiments in the presence and absence of blocking peptides suggested these antibodies were in fact specific to the peptide

against which they had been raised. Antibody binding was blocked only in the presence of the peptide to which the antibody was raised (figure 3.2). Experiments were carried out in which eNOS protein was specifically phosphorylated with AMPK or dephosphorylated using alkaline phosphatase, in order to test the specificity of the antibodies. However, these experiments were inconclusive, as no methodology was available to test the extent of phosphorylation or dephosphorylation of the eNOS protein specifically at serine 1177. Despite this fact, the results described in this thesis suggest the anti-phospho eNOS antibody may be specific however, the anti-dephospho eNOS antibody appears not to discriminate against the phosphorylated or dephosphorylated protein.

The reasons behind the difficulty in determining the specific nature of these antibodies are not clear. Previous studies have reported the generation of phospho-specific eNOS antibodies (Ser-1177) using a method analogous to that used here (Chen et al., 1999), however no reports have been identified describing production of dephospho-specific eNOS antibodies. To further characterise the antibodies an appropriate eNOS phospho Ser-1177 control is required. Using AMPK to phosphorylate eNOS protein, phosphorylation of eNOS at Thr-495 was demonstrated (figure 3.5), under conditions in which AMPK would also have been expected to phosphorylate Ser-1177. In the future it would be important to phosphorylate eNOS protein using another kinase, which has also been reported to phosphorylate eNOS at Ser-1177, for example PKB (Fulton et al., 1999).

Studies of the classical insulin-signalling pathway were also undertaken in skeletal muscle from the SHRSP in order to determine if any defect could be identified. Crude fractionation of unstimulated skeletal muscle showed that various components of the insulin-signalling cascade (GLUT 4, IRS-1, IRS-2 and PI3-kinase p85 subunit) appeared to reside in similar subcellular compartments to that of the normotensive control strain, the WKY. Furthermore, protein expression and activity of PKB was also similar in skeletal muscle from the two strains, thus suggesting that the classical insulin-signalling pathway leading to activation of PKB is intact in the SHRSP. However, it should be noted that one study reported activation of PKB in response to insulin to be normal in skeletal muscle from obese and diabetic patients, despite decreases in insulin-stimulated PI3-kinase activity (Kim et al., 1999). The authors

suggested that only a small activation of PI3-kinase is necessary to promote full activation of PKB. PI3-kinase activity was not examined in this study and future studies could be undertaken to examine IRS-1/IRS-2-asscociated PI3-kinase activity, or recruitment of PI3-kinase to IRS-1/IRS-2 in response to insulin. Expression and tyrosine phosphorylation of the insulin receptor and tyrosine phosphorylation of IRS-1/IRS-2 could also be investigated to ensure the functionality of the insulin-signalling pathway.

Expression of a number of PKC isoforms was studied in skeletal muscle from the SHRSP. Atypical PKCs have been reported to be activated in response to insulin and defects in their activation has been observed in skeletal muscle from type 2 diabetic patients and in various rodent models of insulin resistance (Farese, 2002). However in this study, expression of a number of PKC isoforms was observed to be similar in a variety of skeletal muscles from WKY and SHRSP rats (figure 4.4). In future studies, PKC activity could be examined to check that PKC activity, like PKC expression, is also similar in skeletal muscle from WKY and SHRSP.

The defect in insulin-stimulated glucose transport in skeletal muscle from the SHRSP is therefore not due to defects in expression of IRS-1/IRS-2, PI3-kinase, p85 subunit, PKB or PKC. Neither is it due to a defect in PKB activity.

Therefore, in order to determine if a defect existed in more distal insulin-regulated pathways, regulation of glycogen metabolism was also studied in skeletal muscle of the SHRSP. It is suggested that the primary role of insulin in skeletal muscle is the storage of elevated blood glucose as glycogen and muscle glycogen synthesis has been reported to be decreased by up to 50% in diabetic individuals (Shulman, 2000). Levels of GSK-3α and GSK-3β protein and activity were studied in skeletal muscle from SHRSP and WKY animals (figures 4.5 and 4.6). GSK-3α protein expression was decreased in SHRSP skeletal muscle, compared to WKY, however GSK-3β expression was normal. Furthermore, the levels of both GSK-3α and GSK-3β activity were similar between the two strains, suggesting the GSK-3α protein present has a high specific activity. It is not clear from the current literature, which of the GSK-3 isoforms is most functionally important in regulation of glycogen synthase

activity. However, the data presented in this thesis would suggest that there is some functional redundancy between the two isoforms. It is also possible that GSK-3α is present in skeletal muscle in vast excess, as in the SHRSP where protein levels are greatly reduced, activity of the protein appears to be normal. In addition to GSK-3α expression being reduced in skeletal muscle from SHRSP, the protein present appeared to have a lower molecular weight than the protein present in the WKY muscle. The reason for the decreased molecular weight of the SHRSP protein has not been determined. Studies were carried out to determine if the decreased molecular weight was due to dephosphorylation of the protein, but this does not seem to be the case. Insulin is known to inhibit GSK-3 activity by promoting its phosphorylation via activation of PKB (Cross et al., 1995), it should be noted however that in this study insulin did not inhibit GSK-3 and the reasons for this are unknown. Further studies of glycogen metabolism in these animals showed no differences in the levels of glycogen, glycogen synthesis, or glycogen phosphorylase activity in skeletal muscle from SHRSP compared to that from WKY.

Skeletal muscles consist of a variety of fibres that have specific roles in muscle metabolism and fibre distribution is known to differ in various muscle types and different skeletal muscle fibre types are known to have varying sensitivities to insulin and exercise (see section 1.3.1). Skeletal muscles from WKY and SHRSP were extensively fibre-typed in order to determine if any morphological differences could be observed that might account for the insulin resistant phenotype (figure 4.10). Muscle fibre typing showed the fibre staining patterns to be similar in skeletal muscle from WKY and SHRSP, suggesting there are similar numbers of the various fibre types in each of these strains. Thus it is unlikely that fibre-type differences are the reason behind the observed insulin resistance in the SHRSP.

During the course of this work, studies in skeletal muscle of the SHRSP reported the over expression of the lipid raft associated proteins caveolin and flotillin (James et al., 2001). Lipid rafts and caveolae have been suggested to be important in insulin signal transduction, for example the insulin receptor has been reported to reside in caveolae (Gustavsson et al., 1999, Yamamoto et al., 1998). Furthermore, PI3-kinase is reported to be required, but not sufficient, to promote increased glucose uptake and GLUT 4 translocation in response to insulin (Wiese et al., 1995, Sharma et al., 1997,

Guilherme and Czech, 1998). A PI3-kinase independent pathway required for insulin-stimulated GLUT 4 translocation and glucose uptake has recently been identified (Baumann et al., 2000) and has been suggested to require components of lipid raft domains (see section 1.2.7.3).

To investigate further the role of flotillin in insulin-stimulated glucose uptake a yeast-two hybrid screen was performed, using human flotillin-1 as the bait protein (chapter 5). However, although many interesting proteins were identified in the screen, a number of positive clones have been generated, which have likely resulted from non-specific interactions, the reasons for which are discussed in chapter 5. Due to time constraints and the lack of duplication of positive clones, biochemical studies have not been performed on the more interesting clones identified and therefore it cannot be conclusively stated whether these proteins are indeed flotillin interacting proteins, with possible roles in insulin signal transduction.

In future studies it will be important to investigate the expression and activity of the proteins involved in the CAP-Cbl (PI3-kinase independent pathway) required for GLUT 4 translocation in skeletal muscle, and specifically determine if any defects in this pathway are observed in the SHRSP. For example studies could be undertaken to determine levels of expression of CAP, Cbl and TC10. Furthermore, phosphorylation of Cbl and activation of TC10 in response to insulin could also be determined.

Therefore, the only alterations observed in components of the insulin-signalling pathway in this study have been decreased expression of GSK-3α and increased expression of flotillin. There are a number of possibilities as to why this is the case. It has been suggested in the Zucker rat that the defect in insulin signalling in skeletal muscle is due to decreased GLUT 4 translocation to the plasma membrane as opposed to decreased expression of the protein (Abel et al., 1996). Furthermore, in insulin resistant and diabetic individuals, GLUT 4 translocation to the plasma membrane in response to insulin is also suggested to be defective (Hunter and Garvey, 1998). However, due to the lack of a robust skeletal muscle fractionation procedure, the translocation of GLUT 4 to the plasma membrane/T-tubules in response to insulin was not determined in this study. During the course of this work, increased expression of the SNARE proteins VAMP 2 and syntaxin 4 was reported in

skeletal muscle from the SHRSP (James et al., 2001). These proteins likely have a role in GLUT 4 trafficking in skeletal muscle and their over expression may possibly function to perturb GLUT 4 vesicle trafficking. It is also possible that these SNARE proteins are over expressed in order to compensate for other unknown defects. Over expression of SNARE proteins has previously been reported in the insulin resistant Zucker diabetic fatty rat (Maier et al., 2000), suggesting that upregulation of SNARE proteins may be evident in a range of insulin resistant models.

It is possible that the 'classical' insulin-signalling pathway is indeed intact in skeletal muscle from the SHRSP, but in the realms of the unknown where insulin-signalling meets GLUT 4 vesicle trafficking, there is an as yet unidentified defect preventing GLUT 4 insertion into the surface membrane. This defect may be a defect in vesicle trafficking, in vesicle docking and fusion or in activation of a latent activity present in the transporter.

6.1 Conclusion

In this study, the expression levels and intracellular localisation of a variety of components of the insulin-signalling cascade have been reported to be normal in skeletal muscle from SHRSP, as compared to the normotensive WKY control. Expression and activity of PKB was also observed to be similar in the two strains. Expression and activity of a variety of proteins involved in glycogen metabolism was also observed to be normal in skeletal muscle from SHRSP, with one exception. GSK-3α protein levels are reduced in SHRSP skeletal muscle, however activity of this protein appears normal. Flotillin-1, a component of lipid rafts and a protein involved in a PI3-kinase independent pathway required for GLUT 4 translocation, is over expressed in SHRSP skeletal muscle. However, the significance of the alteration in expression of these proteins is not known.

BIBLIOGRAPHY

Abel,E.D., Peroni,O., Kim,J.K., Kim,Y.B., Boss,O., Hadro,E., Minnemann,T., Shulman,G.I., and Kahn,B.B. (2001). Adipose-selective targeting of the GLUT4 gene impairs insulin action in muscle and liver. Nature *409*, 729-733.

Abel, E. D., Shepherd, P. R., and Kahn, B. B. Glucose Transporters and Pathophysiologic States. (1996). Diabetes Mellitus 530-543. Edited by: LeRoith, D, Taylor, S. I, and Olefsky, J. M.

Accili,D., Drago,J., Lee,E.J., Johnson,M.D., Cool,M.H., Salvatore,P., Asico,L.D., Jose,P.A., Taylor,S.I., and Westphal,H. (1996). Early neonatal death in mice homozygous for a null allele of the insulin receptor gene. Nat. Genet. *12*, 106-109.

Aitman,T.J., Glazier,A.M., Wallace,C.A., Cooper,L.D., Norsworthy,P.J., Wahid,F.N., al Majali,K.M., Trembling,P.M., Mann,C.J., Shoulders,C.C., Graf,D., St Lezin,E., Kurtz,T.W., Kren,V., Pravenec,M., Ibrahimi,A., Abumrad,N.A., Stanton,L.W., and Scott,J. (1999). Identification of Cd36 (Fat) as an insulin-resistance gene causing defective fatty acid and glucose metabolism in hypertensive rats. Nat. Genet. *21*, 76-83.

Aitman,T.J., Gotoda,T., Evans,A.L., Imrie,H., Heath,K.E., Trembling,P.M., Truman,H., Wallace,C.A., Rahman,A., Dore,C., Flint,J., Kren,V., Zidek,V., Kurtz,T.W., Pravenec,M., and Scott,J. (1997). Quantitative trait loci for cellular defects in glucose and fatty acid metabolism in hypertensive rats. Nat. Genet. *16*, 197-201.

Alessi,D.R., Andjelkovic,M., Caudwell,B., Cron,P., Morrice,N., Cohen,P., and Hemmings,B.A. (1996). Mechanism of activation of protein kinase B by insulin and IGF-1. EMBO J. *15*, 6541-6551.

Alessi,D.R. and Cohen,P. (1998). Mechanism of activation and function of protein kinase B. Curr. Opin. Genet. Dev. *8*, 55-62.

Alessi,D.R., James,S.R., Downes,C.P., Holmes,A.B., Gaffney,P.R., Reese,C.B., and Cohen,P. (1997). Characterization of a 3-phosphoinositide-dependent protein kinase which phosphorylates and activates protein kinase B alpha. Curr. Biol. *7*, 261-269.

Altschul,S.F., Gish,W., Miller,W., Myers,E.W., and Lipman,D.J. (1990). Basic local alignment search tool. J. Mol. Biol. *215*, 403-410.

Anderson,R.G. (1998). The caveolae membrane system. Annu. Rev. Biochem. *67*, 199-225.

Araki,E., Lipes,M.A., Patti,M.E., Bruning,J.C., Haag,B., III, Johnson,R.S., and Kahn,C.R. (1994). Alternative pathway of insulin signalling in mice with targeted disruption of the IRS-1 gene. Nature *372*, 186-190.

Armstrong,R.B. and Phelps,R.O. (1984). Muscle fiber type composition of the rat hindlimb. Am. J. Anat. *171*, 259-272.

Auger,K.R., Serunian,L.A., Solttoff,S.P., Libby,P. and Cantley,L.C. (1989). PDGF-dependent tyrosine phosphorylation of novel polyphosphoinositides in intact cells. Cell *57*, 167-175.

Bailyes,E.M., Nave,B.T., Soos,M.A., Orr,S.R., Hayward,A.C., and Siddle,K. (1997). Insulin receptor/IGF-I receptor hybrids are widely distributed in mammalian tissues: quantification of individual receptor species by selective immunoprecipitation and immunoblotting. Biochem. J. *327 (Pt 1)*, 209-215.

Balon,T.W. and Nadler,J.L. (1994). Nitric oxide release is present from incubated skeletal muscle preparations. J. Appl. Physiol *77*, 2519-2521.

Balon,T.W. and Nadler,J.L. (1997). Evidence that nitric oxide increases glucose transport in skeletal muscle. J. Appl. Physiol *82*, 359-363.

Bandyopadhyay,G., Standaert,M.L., Galloway,L., Moscat,J., and Farese,R.V. (1997a). Evidence for involvement of protein kinase C (PKC)-zeta and noninvolvement of diacylglycerol-sensitive PKCs in insulin-stimulated glucose transport in L6 myotubes. Endocrinology *138*, 4721-4731.

Bandyopadhyay,G., Standaert,M.L., Zhao,L., Yu,B., Avignon,A., Galloway,L., Karnam,P., Moscat,J., and Farese,R.V. (1997b). Activation of protein kinase C (alpha, beta, and zeta) by insulin in 3T3/L1 cells. Transfection studies suggest a role for PKC-zeta in glucose transport. J. Biol. Chem. *272*, 2551-2558.

Baumann,C.A., Ribon,V., Kanzaki,M., Thurmond,D.C., Mora,S., Shigematsu,S., Bickel,P.E., Pessin,J.E., and Saltiel,A.R. (2000). CAP defines a second signalling pathway required for insulin-stimulated glucose transport. Nature *407*, 202-207.

Bell,G.I., Burant,C.F., Takeda,J., and Gould,G.W. (1993). Structure and function of mammalian facilitative sugar transporters. J. Biol. Chem. *268*, 19161-19164.

Bellacosa,A., Testa,J.R., Staal,S.P., and Tsichlis,P.N. (1991). A retroviral oncogene, akt, encoding a serine-threonine kinase containing an SH2-like region. Science *254*, 274-277.

Bickel,P.E., Scherer,P.E., Schnitzer,J.E., Oh,P., Lisanti,M.P., and Lodish,H.F. (1997). Flotillin and epidermal surface antigen define a new family of caveolae-associated integral membrane proteins. J. Biol. Chem. *272*, 13793-13802.

Bollen,M., Keppens,S., and Stalmans,W. (1998). Specific features of glycogen metabolism in the liver. Biochem. J. *336 (Pt 1)*, 19-31.

Bonen,A., Luiken,J.J., Arumugam,Y., Glatz,J.F., and Tandon,N.N. (2000). Acute regulation of fatty acid uptake involves the cellular redistribution of fatty acid translocase. J. Biol. Chem. *275*, 14501-14508.

Boo,Y.C., Sorescu,G., Boyd,N., Shiojima,I., Walsh,K., Du,J., and Jo,H. (2002). Shear stress stimulates phosphorylation of endothelial nitric-oxide synthase at Ser1179 by Akt-independent mechanisms: role of protein kinase A. J. Biol. Chem. *277*, 3388-3396.

Bradford,M.M. (1976). A rapid and sensitive method for the quantitation of microgram quantities of protein utilizing the principle of protein-dye binding. Anal. Biochem. *72*, 248-254.

Brant,A.M., McCoid,S., Thomas,H.M., Baldwin,S.A., Davies,A., Parker,J.C., Gibbs,E.M., and Gould,G.W. (1992). Analysis of the glucose transporter content of islet cell lines: implications for glucose-stimulated insulin release. Cell Signal. *4*, 641-650.

Brown,D.A. and London,E. (1997). Structure of detergent-resistant membrane domains: does phase separation occur in biological membranes? Biochem. Biophys. Res. Commun. *240*, 1-7.

Brown,E.J., Beal,P.A., Keith,C.T., Chen,J., Shin,T.B., and Schreiber,S.L. (1995). Control of p70 s6 kinase by kinase activity of FRAP in vivo. Nature *377*, 441-446.

Browner,M.F. and Fletterick,R.J. (1992). Phosphorylase: a biological transducer. Trends Biochem. Sci. *17*, 66-71.

Bruning,J.C., Michael,M.D., Winnay,J.N., Hayashi,T., Horsch,D., Accili,D., Goodyear,L.J., and Kahn,C.R. (1998). A muscle-specific insulin receptor knockout exhibits features of the metabolic syndrome of NIDDM without altering glucose tolerance. Mol. Cell *2*, 559-569.

Butt,E., Bernhardt,M., Smolenski,A., Kotsonis,P., Frohlich,L.G., Sickmann,A., Meyer,H.E., Lohmann,S.M., and Schmidt,H.H. (2000). Endothelial nitric-oxide synthase (type III) is activated and becomes calcium independent upon phosphorylation by cyclic nucleotide-dependent protein kinases. J. Biol. Chem. *275*, 5179-5187.

Cantley,L.C., Auger,K.R., Carpenter,C.L., Duckworth,B., Graziani,A., Kapeller,R., and Stoltoff,S. (1991). Oncogenes and signal transduction. Cell *64*, 281-302

Calera,M.R., Martinez,C., Liu,H., Jack,A.K., Birnbaum,M.J., and Pilch,P.F. (1998). Insulin increases the association of Akt-2 with Glut4-containing vesicles. J. Biol. Chem. *273*, 7201-7204.

Carpernter,C.L., Duckworth,B.C., Auger,K.R., Cohen,B., Schaffhausen,B.S. and Cantley,L.C. (1990). Purification and characterization of phosphoinositide 3-kinase from rat liver. J. Biol. Chem. *265*, 19704-19711.

Chang,L., Adams,R.D., and Saltiel,A.R. (2002). The TC10-interacting protein CIP4/2 is required for insulin-stimulated Glut4 translocation in 3T3L1 adipocytes. Proc. Natl. Acad. Sci. U. S. A *99*, 12835-12840.

Chang,W.J., Ying,Y.S., Rothberg,K.G., Hooper,N.M., Turner,A.J., Gambliel,H.A., De Gunzburg,J., Mumby,S.M., Gilman,A.G., and Anderson,R.G. (1994). Purification and characterization of smooth muscle cell caveolae. J. Cell Biol. *126*, 127-138.

Cheatham,B., Vlahos,C.J., Cheatham,L., Wang,L., Blenis,J., and Kahn,C.R. (1994). Phosphatidylinositol 3-kinase activation is required for insulin stimulation of pp70 S6 kinase, DNA synthesis, and glucose transporter translocation. Mol. Cell Biol. *14*, 4902-4911.

Chen,W.S., Xu,P.Z., Gottlob,K., Chen,M.L., Sokol,K., Shiyanova,T., Roninson,I., Weng,W., Suzuki,R., Tobe,K., Kadowaki,T., and Hay,N. (2001). Growth retardation and increased apoptosis in mice with homozygous disruption of the Akt1 gene. Genes Dev. *15*, 2203-2208.

Chen,Y.A. and Scheller,R.H. (2001). SNARE-mediated membrane fusion. Nat. Rev. Mol. Cell Biol. *2*, 98-106.

Chen,Z.P., Mitchelhill,K.I., Michell,B.J., Stapleton,D., Rodriguez-Crespo,I., Witters,L.A., Power,D.A., Ortiz de Montellano,P.R., and Kemp,B.E. (1999). AMP-activated protein kinase phosphorylation of endothelial NO synthase. FEBS Lett. *443*, 285-289.

Cherry,P.D., Furchgott,R.F., Zawadzki,J.V. and Jothianandan,D. (1982). Role of endothelial cells in relaxation of isolated arteries by bradykinin. Proc. Natl. Acad. Sci. U.S.A *79*, 2106-2110.

Chiang,S.H., Baumann,C.A., Kanzaki,M., Thurmond,D.C., Watson,R.T., Neudauer,C.L., Macara,I.G., Pessin,J.E., and Saltiel,A.R. (2001). Insulin-stimulated GLUT4 translocation requires the CAP-dependent activation of TC10. Nature *410*, 944-948.

Chiang,S.H., Hou,J.C., Hwang,J., Pessin,J.E., and Saltiel,A.R. (2002). Cloning and functional characterization of related TC10 isoforms, a subfamily of Rho proteins involved in insulin-stimulated glucose transport. J. Biol. Chem. *277*, 13067-13073.

Cho,H., Mu,J., Kim,J.K., Thorvaldsen,J.L., Chu,Q., Crenshaw,E.B., III, Kaestner,K.H., Bartolomei,M.S., Shulman,G.I., and Birnbaum,M.J. (2001a). Insulin resistance and a diabetes mellitus-like syndrome in mice lacking the protein kinase Akt2 (PKB beta). Science *292*, 1728-1731.

Cho,H., Thorvaldsen,J.L., Chu,Q., Feng,F., and Birnbaum,M.J. (2001b). Akt1/PKBalpha is required for normal growth but dispensable for maintenance of glucose homeostasis in mice. J. Biol. Chem. *276*, 38349-38352.

Chou,M.M., Hou,W., Johnson,J., Graham,L.K., Lee,M.H., Chen,C.S., Newton,A.C., Schaffhausen,B.S., and Toker,A. (1998). Regulation of protein kinase C zeta by PI 3-kinase and PDK-1. Curr. Biol. *8*, 1069-1077.

Clark,S.F., Martin,S., Carozzi,A.J., Hill,M.M., and James,D.E. (1998). Intracellular localization of phosphatidylinositide 3-kinase and insulin receptor substrate-1 in adipocytes: potential involvement of a membrane skeleton. J. Cell Biol. *140*, 1211-1225.

Clark,S.F., Molero,J.C., and James,D.E. (2000). Release of insulin receptor substrate proteins from an intracellular complex coincides with the development of insulin resistance. J. Biol. Chem. *275*, 3819-3826.

Clement,S., Krause,U., Desmedt,F., Tanti,J.F., Behrends,J., Pesesse,X., Sasaki,T., Penninger,J., Doherty,M., Malaisse,W., Dumont,J.E., Marchand-Brustel,Y., Erneux,C., Hue,L., and Schurmans,S. (2001). The lipid phosphatase SHIP2 controls insulin sensitivity. Nature *409*, 92-97.

Cohen,P. and Frame,S. (2001). The renaissance of GSK3. Nat. Rev. Mol. Cell Biol. *2*, 769-776.

Collison,M., Glazier,A.M., Graham,D., Morton,J.J., Dominiczak,M.H., Aitman,T.J., Connell,J.M., Gould,G.W., and Dominiczak,A.F. (2000). Cd36 and molecular mechanisms of insulin resistance in the stroke-prone spontaneously hypertensive rat. Diabetes *49*, 2222-2226.

Corson,M.A., James,N.L., Latta,S.E., Nerem,R.M., Berk,B.C., and Harrison,D.G. (1996). Phosphorylation of endothelial nitric oxide synthase in response to fluid shear stress. Circ. Res. *79*, 984-991.

Cross,D.A., Alessi,D.R., Vandenheede,J.R., McDowell,H.E., Hundal,H.S., and Cohen,P. (1994). The inhibition of glycogen synthase kinase-3 by insulin or insulin-like growth factor-1 in the rat skeletal muscle cell line L6 is blocked by wortmannin, but not rapamycin: evidence that wortmannin blocks activation of the mitogen-activated protein kinase pathway in L6 cells between Ras and Raf. Biochem. J. *303*, 21-26.

Cross,D.A., Alessi,D.R., Cohen,P., Andjelkovich,M., and Hemmings,B.A. (1995). Inhibition of glycogen synthase kinase-3 by insulin mediated by protein kinase B. Nature *378*, 785-789.

Cross,D.A., Watt,P.W., Shaw,M., van der,K.J., Downes,C.P., Holder,J.C., and Cohen,P. (1997). Insulin activates protein kinase B, inhibits glycogen synthase kinase-3 and activates glycogen synthase by rapamycin-insensitive pathways in skeletal muscle and adipose tissue. FEBS Lett. *406* , 211-215.

Daugaard,J.R. and Richter,E.A. (2001). Relationship between muscle fibre composition, glucose transporter protein 4 and exercise training: possible consequences in non-insulin- dependent diabetes mellitus. Acta Physiol Scand. *171*, 267-276.

Davidson,A.O., Schork,N., Jaques,B.C., Kelman,A.W., Sutcliffe,R.G., Reid,J.L., and Dominiczak,A.F. (1995). Blood pressure in genetically hypertensive rats. Influence of the Y chromosome. Hypertension *26*, 452-459.

Dimmeler,S., Fleming,I., Fisslthaler,B., Hermann,C., Busse,R., and Zeiher,A.M. (1999). Activation of nitric oxide synthase in endothelial cells by Akt-dependent phosphorylation. Nature *399*, 601-605.

Dohm,G.L. and Dudek,R.W. (1998). Role of transverse tubules (T-tubules) in muscle glucose transport. Adv. Exp. Med. Biol. *441*, 27-34.

Dombrowski,L., Roy,D., Marcotte,B., and Marette,A. (1996). A new procedure for the isolation of plasma membranes, T tubules, and internal membranes from skeletal muscle. Am. J. Physiol *270*, E667-E676.

Donnelly,R. and Connell,J.M. (1992). Insulin resistance: possible role in the aetiology and clinical course of hypertension. Clin. Sci. *83*, 265-275.

Donnelly,R., Emslie-Smith,A.M., Gardner,I.D., and Morris,A.D. (2000). ABC of arterial and venous disease: vascular complications of diabetes. BMJ *320*, 1062-1066.

Douen,A.G., Ramlal,T., Rastogi,S., Bilan,P.J., Cartee,G.D., Vranic,M., Holloszy,J.O., and Klip,A. (1990). Exercise induces recruitment of the "insulin-responsive glucose transporter". Evidence for distinct intracellular insulin- and exercise- recruitable transporter pools in skeletal muscle. J. Biol. Chem. *265*, 13427-13430.

Drab,M., Verkade,P., Elger,M., Kasper,M., Lohn,M., Lauterbach,B., Menne,J., Lindschau,C., Mende,F., Luft,F.C., Schedl,A., Haller,H., and Kurzchalia,T.V. (2001). Loss of caveolae, vascular dysfunction, and pulmonary defects in caveolin-1 gene-disrupted mice. Science *293*, 2449-2452.

Edgar,A.J. and Polak,J.M. (2001). Flotillin-1: gene structure: cDNA cloning from human lung and the identification of alternative polyadenylation signals. Int. J. Biochem. Cell Biol. *33*, 53-64.

Embi,N., Rylatt,D.B., and Cohen,P. (1980). Glycogen synthase kinase-3 from rabbit skeletal muscle. Separation from cyclic-AMP-dependent protein kinase and phosphorylase kinase. Eur. J. Biochem. *107*, 519-527.

Fantin,V.R., Wang,Q., Lienhard,G.E., and Keller,S.R. (2000). Mice lacking insulin receptor substrate 4 exhibit mild defects in growth, reproduction, and glucose homeostasis. Am. J. Physiol Endocrinol. Metab *278*, E127-E133.

Farese,R.V. (2002). Function and dysfunction of aPKC isoforms for glucose transport in insulin-sensitive and insulin-resistant states. Am. J. Physiol Endocrinol. Metab *283*, E1-11.

Fields,S. and Song,O. (1989). A novel genetic system to detect protein-protein interactions. Nature *340*, 245-246.

Fisslthaler,B., Dimmeler,S., Hermann,C., Busse,R., and Fleming,I. (2000). Phosphorylation and activation of the endothelial nitric oxide synthase by fluid shear stress. Acta Physiol Scand. *168*, 81-88.

Fleming,I. and Busse,R. (1999). Signal transduction of eNOS activation. Cardiovasc. Res. *43*, 532-541.

Fleming,I., Fisslthaler,B., Dimmeler,S., Kemp,B.E., and Busse,R. (2001). Phosphorylation of Thr(495) regulates Ca(2+)/calmodulin-dependent endothelial nitric oxide synthase activity. Circ. Res. *88*, E68-E75.

Frame,S. and Cohen,P. (2001). GSK3 takes centre stage more than 20 years after its discovery. Biochem. J. *359*, 1-16.

Frame,S., Cohen,P., and Biondi,R.M. (2001). A common phosphate binding site explains the unique substrate specificity of GSK3 and its inactivation by phosphorylation. Mol. Cell *7*, 1321-1327.

Fryer,L.G., Hajduch,E., Rencurel,F., Salt,I.P., Hundal,H.S., Hardie,D.G., and Carling,D. (2000). Activation of glucose transport by AMP-activated protein kinase via stimulation of nitric oxide synthase. Diabetes *49*, 1978-1985.

Fujii,N., Hayashi,T., Hirshman,M.F., Smith,J.T., Habinowski,S.A., Kaijser,L., Mu,J., Ljungqvist,O., Birnbaum,M.J., Witters,L.A., Thorell,A., and Goodyear,L.J. (2000). Exercise induces isoform-specific increase in 5'AMP-activated protein kinase activity in human skeletal muscle. Biochem. Biophys. Res. Commun. *273*, 1150-1155.

Fulton,D., Fontana,J., Sowa,G., Gratton,J.P., Lin,M., Li,K.X., Michell,B., Kemp,B.E., Rodman,D., and Sessa,W.C. (2002). Localization of endothelial nitric-oxide synthase phosphorylated on serine 1179 and nitric oxide in Golgi and plasma membrane defines the existence of two pools of active enzyme. J. Biol. Chem. *277*, 4277-4284.

Fulton,D., Gratton,J.P., McCabe,T.J., Fontana,J., Fujio,Y., Walsh,K., Franke,T.F., Papapetropoulos,A., and Sessa,W.C. (1999). Regulation of endothelium-derived nitric oxide production by the protein kinase Akt. Nature *399*, 597-601.

Galbiati,F., Engelman,J.A., Volonte,D., Zhang,X.L., Minetti,C., Li,M., Hou,H., Jr., Kneitz,B., Edelmann,W., and Lisanti,M.P. (2001). Caveolin-3 null mice show a loss of caveolae, changes in the microdomain distribution of the dystrophin-glycoprotein complex, and t- tubule abnormalities. J. Biol. Chem. *276*, 21425-21433.

Galbiati,F., Volonte,D., Goltz,J.S., Steele,Z., Sen,J., Jurcsak,J., Stein,D., Stevens,L., and Lisanti,M.P. (1998). Identification, sequence and developmental expression of invertebrate flotillins from Drosophila melanogaster. Gene *210*, 229-237.

Gilboe,D.P., Larson,K.L., and Nuttall,F.Q. (1972). Radioactive method for the assay of glycogen phosphorylases. Anal. Biochem. *47*, 20-27.

Goalstone,M.L. and Draznin,B. (1998). What does insulin do to Ras? Cell Signal. *10*, 297-301.

Gould,G.W. and Holman,G.D. (1993). The glucose transporter family: structure, function and tissue-specific expression. Biochem. J. *295 (Pt 2)*, 329-341.

Govers,R. and Rabelink,T.J. (2001). Cellular regulation of endothelial nitric oxide synthase. Am. J. Physiol Renal Physiol *280*, F193-F206.

Guerra,C., Navarro,P., Valverde,A.M., Arribas,M., Bruning,J., Kozak,L.P., Kahn,C.R., and Benito,M. (2001). Brown adipose tissue-specific insulin receptor knockout shows diabetic phenotype without insulin resistance. J. Clin. Invest *108*, 1205-1213.

Guilherme,A. and Czech,M.P. (1998). Stimulation of IRS-1-associated phosphatidylinositol 3-kinase and Akt/protein kinase B but not glucose transport by beta1-integrin signaling in rat adipocytes. J. Biol. Chem. *273*, 33119-33122.

Gustavsson,J., Parpal,S., Karlsson,M., Ramsing,C., Thorn,H., Borg,M., Lindroth,M., Peterson,K.H., Magnusson,K.E., and Stralfors,P. (1999). Localization of the insulin receptor in caveolae of adipocyte plasma membrane. FASEB J. *13*, 1961-1971.

Halse,R., Pearson,S.L., McCormack,J.G., Yeaman,S.J., and Taylor,R. (2001). Effects of tumor necrosis factor-alpha on insulin action in cultured human muscle cells. Diabetes *50*, 1102-1109.

Harris,M.B., Ju,H., Venema,V.J., Liang,H., Zou,R., Michell,B.J., Chen,Z.P., Kemp,B.E., and Venema,R.C. (2001). Reciprocal phosphorylation and regulation of endothelial nitric-oxide synthase in response to bradykinin stimulation. J. Biol. Chem. *276*, 16587-16591.

Hawley,S.A., Davison,M., Woods,A., Davies,S.P., Beri,R.K., Carling,D., and Hardie,D.G. (1996). Characterization of the AMP-activated protein kinase kinase from rat liver and identification of threonine 172 as the major site at which it phosphorylates AMP-activated protein kinase. J. Biol. Chem. *271*, 27879-27887.

Hayashi,T., Hirshman,M.F., Fujii,N., Habinowski,S.A., Witters,L.A., and Goodyear,L.J. (2000). Metabolic stress and altered glucose transport: activation of AMP-activated protein kinase as a unifying coupling mechanism. Diabetes *49*, 527-531.

Hayashi,T., Hirshman,M.F., Kurth,E.J., Winder,W.W., and Goodyear,L.J. (1998). Evidence for 5' AMP-activated protein kinase mediation of the effect of muscle contraction on glucose transport. Diabetes *47*, 1369-1373.

Hayashi,T., Wojtaszewski,J.F., and Goodyear,L.J. (1997). Exercise regulation of glucose transport in skeletal muscle. Am. J. Physiol *273*, E1039-E1051.

Hazarika,P., Dham,N., Patel,P., Cho,M., Weidner,D., Goldsmith,L., and Duvic,M. (1999). Flotillin 2 is distinct from epidermal surface antigen (ESA) and is associated with filopodia formation. J. Cell Biochem. *75*, 147-159.

Hebert,D.N. and Carruthers,A. (1992). Glucose transporter oligomeric structure determines transporter function. Reversible redox-dependent interconversions of tetrameric and dimeric GLUT1. J. Biol. Chem. *267*, 23829-23838.

Henriksen,E.J., Bourey,R.E., Rodnick,K.J., Koranyi,L., Permutt,M.A., and Holloszy,J.O. (1990). Glucose transporter protein content and glucose transport capacity in rat skeletal muscles. Am. J. Physiol *259*, E593-E598.

Higaki,Y., Hirshman,M.F., Fujii,N., and Goodyear,L.J. (2001). Nitric oxide increases glucose uptake through a mechanism that is distinct from the insulin and contraction pathways in rat skeletal muscle. Diabetes *50*, 241-247.

Hunter,S.J. and Garvey,W.T. (1998). Insulin action and insulin resistance: diseases involving defects in insulin receptors, signal transduction, and the glucose transport effector system. Am. J. Med. *105*, 331-345.

Ignarro,L.J., Byrns,R.E., Buga,G.M. and Wood,K.S. (1987). Endothelium-derived relaxing factor from pulmonary artery and vein possesses pharmacologic and chemical properties identical to those of nitric oxide radical. Circ. Res. *61*, 886-879.

Iritani,N., Fukuda,E., Nara,Y., and Yamori,Y. (1977). Lipid metabolism in spontaneously hypertensive rats (SHR). Atherosclerosis *28*, 217-222.

Itoh,T. and Takenawa,T. (2002). Phosphoinositide-binding domains. Functional units for temporal and spatial regulation of intracellular signalling. Cell Signal. *14*, 733-743.

James,D.E., Brown,R., Navarro,J., and Pilch,P.F. (1988). Insulin-regulatable tissues express a unique insulin-sensitive glucose transport protein. Nature *333*, 183-185.

James,D.E., Strube,M., and Mueckler,M. (1989). Molecular cloning and characterization of an insulin-regulatable glucose transporter. Nature *338*, 83-87.

James,D.J., Cairns,F., Salt,I.P., Murphy,G.J., Dominiczak,A.F., Connell,J.M., and Gould,G.W. (2001). Skeletal muscle of stroke-prone spontaneously hypertensive rats exhibits reduced insulin-stimulated glucose transport and elevated levels of caveolin and flotillin. Diabetes *50*, 2148-2156.

James,P., Halladay,J., and Craig,E.A. (1996). Genomic libraries and a host strain designed for highly efficient two- hybrid selection in yeast. Genetics *144*, 1425-1436.

Jefferies,H.B., Fumagalli,S., Dennis,P.B., Reinhard,C., Pearson,R.B., and Thomas,G. (1997). Rapamycin suppresses 5'TOP mRNA translation through inhibition of p70s6k. EMBO J. *16*, 3693-3704.

Jeffs,B., Clark,J.S., Anderson,N.H., Gratton,J., Brosnan,M.J., Gauguier,D., Reid,J.L., Macrae,I.M., and Dominiczak,A.F. (1997). Sensitivity to cerebral ischaemic insult in a rat model of stroke is determined by a single genetic locus. Nat. Genet. *16*, 364-367.

Joost,H.G. and Thorens,B. (2001). The extended GLUT-family of sugar/polyol transport facilitators: nomenclature, sequence characteristics, and potential function of its novel members. Mol. Membr. Biol. *18*, 247-256.

Joshi,R.L., Lamothe,B., Cordonnier,N., Mesbah,K., Monthioux,E., Jami,J., and Bucchini,D. (1996). Targeted disruption of the insulin receptor gene in the mouse results in neonatal lethality. EMBO J. *15*, 1542-1547.

Ju,H., Zou,R., Venema,V.J., and Venema,R.C. (1997). Direct interaction of endothelial nitric-oxide synthase and caveolin-1 inhibits synthase activity. J. Biol. Chem. *272*, 18522-18525.

Katsuki,S., Arnold,W., Mittal,C. and Murad,F. (1977) Stimulation of guanylate cyclase by sodium nitroprusside, nitroglycerin and nitric oxide in various tissue preparations and comparison to the effects of sodium azide and hydroxylamine. J. Cycl. Nucl. Res. *3*, 23-35.

Katz,E.B., Stenbit,A.E., Hatton,K., DePinho,R., and Charron,M.J. (1995). Cardiac and adipose tissue abnormalities but not diabetes in mice deficient in GLUT4. Nature *377*, 151-155.

Kim,J.K., Michael,M.D., Previs,S.F., Peroni,O.D., Mauvais-Jarvis,F., Neschen,S., Kahn,B.B., Kahn,C.R., and Shulman,G.I. (2000). Redistribution of substrates to adipose tissue promotes obesity in mice with selective insulin resistance in muscle. J. Clin. Invest *105*, 1791-1797.

Kim,Y.B., Nikoulina,S.E., Ciaraldi,T.P., Henry,R.R., and Kahn,B.B. (1999). Normal insulin-dependent activation of Akt/protein kinase B, with diminished activation of phosphoinositide 3-kinase, in muscle in type 2 diabetes. J. Clin. Invest *104*, 733-741.

Kimura,A., Baumann,C.A., Chiang,S.H., and Saltiel,A.R. (2001). The sorbin homology domain: a motif for the targeting of proteins to lipid rafts. Proc. Natl. Acad. Sci. U.S.A *98*, 9098-9103.

Kimura,A., Mora,S., Shigematsu, S., Pessin,J.E., and Saltiel,A.R. (2002). The insulin receptor catalyzes the tyrosine phosphorylation of caveolin-1. J. Biol. Chem. *277*, 30153-30158.

Kohn,A.D., Summers,S.A., Birnbaum,M.J., and Roth,R.A. (1996). Expression of a constitutively active Akt Ser/Thr kinase in 3T3-L1 adipocytes stimulates glucose uptake and glucose transporter 4 translocation. J. Biol. Chem. *271*, 31372-31378.

Kulkarni,R.N., Bruning,J.C., Winnay,J.N., Postic,C., Magnuson,M.A., and Kahn,C.R. (1999). Tissue-specific knockout of the insulin receptor in pancreatic beta cells creates an insulin secretory defect similar to that in type 2 diabetes. Cell *96*, 329-339.

Kurth-Kraczek,E.J., Hirshman,M.F., Goodyear,L.J., and Winder,W.W. (1999). 5' AMP-activated protein kinase activation causes GLUT4 translocation in skeletal muscle. Diabetes *48*, 1667-1671.

Kurtz,T.W., Montano,M., Chan,L., and Kabra,P. (1989). Molecular evidence of genetic heterogeneity in Wistar-Kyoto rats: implications for research with the spontaneously hypertensive rat. Hypertension *13*, 188-192.

Kurtz,T.W. and Morris,R.C., Jr. (1987). Biological variability in Wistar-Kyoto rats. Implications for research with the spontaneously hypertensive rat. Hypertension *10*, 127-131.

Kyriakis,J.M., App,H., Zhang,X.F., Banerjee,P., Brautigan,D.L., Rapp,U.R., and Avruch,J. (1992). Raf-1 activates MAP kinase-kinase. Nature *358*, 417-421.

Lawrence,J.C., Jr. and Roach,P.J. (1997). New insights into the role and mechanism of glycogen synthase activation by insulin. Diabetes *46*, 541-547.

Le Good,J.A., Ziegler,W.H., Parekh,D.B., Alessi,D.R., Cohen,P., and Parker,P.J. (1998). Protein kinase C isotypes controlled by phosphoinositide 3-kinase through the protein kinase PDK1. Science *281*, 2042-2045.

Leslie,N.R. and Downes,C.P. (2002). PTEN: The down side of PI 3-kinase signalling. Cell Signal. *14*, 285-295.

Letiges,M., Plomann,M., Standaert,M.L., Bandyopadhyay,G., Sajan,M.P., Kanoh,Y., and Farese,R.V. (2002). Knockout of PKC alpha enhances insulin signaling through PI3K. Mol. Endocrinol. *16*, 847-858.

Li,S., Couet,J., and Lisanti,M.P. (1996). Src tyrosine kinases, Galpha subunits, and H-Ras share a common membrane-anchored scaffolding protein, caveolin. Caveolin binding negatively regulates the auto-activation of Src tyrosine kinases. J. Biol. Chem. *271*, 29182-29190.

Li,S., Okamoto,T., Chun,M., Sargiacomo,M., Casanova,J.E., Hansen,S.H., Nishimoto,I., and Lisanti,M.P. (1995). Evidence for a regulated interaction between heterotrimeric G proteins and caveolin. J. Biol. Chem. *270*, 15693-15701.

Lin,R.C. and Scheller,R.H. (2000). Mechanisms of synaptic vesicle exocytosis. Annu. Rev. Cell Dev. Biol. *16*, 19-49.

Lisanti,M.P., Scherer,P.E., Vidugiriene,J., Tang,Z., Hermanowski-Vosatka,A., Tu,Y., Cook,R.F., and Sargiacomo,M. (1994). Characterization of caveolin-rich membrane domains isolated from an endothelial-rich source: implications for human disease. J. Cell. Biol. *126*, 111-126

Liu,J., Kimura,A., Baumann,C.A., and Saltiel,A.R. (2002). APS facilitates c-Cbl tyrosine phosphorylation and GLUT4 translocation in response to insulin in 3T3-L1 adipocytes. Mol. Cell Biol. *22*, 3599-3609.

Liu,S.C., Wang,Q., Lienhard,G.E., and Keller,S.R. (1999). Insulin receptor substrate 3 is not essential for growth or glucose homeostasis. J. Biol. Chem. *274*, 18093-18099.

Livingstone,C., James,D.E., Rice,J.E., Hanpeter,D., and Gould,G.W. (1996). Compartment ablation analysis of the insulin-responsive glucose transporter (GLUT4) in 3T3-L1 adipocytes. Biochem. J. *315 (Pt 2)*, 487-495.

Maier,V.H., Melvin,D.R., Lister,C.A., Chapman,H., Gould,G.W., and Murphy,G.J. (2000). v- and t-SNARE protein expression in models of insulin resistance: normalization of glycemia by rosiglitazone treatment corrects overexpression of cellubrevin, vesicle-associated membrane protein-2, and syntaxin 4 in skeletal muscle of Zucker diabetic fatty rats. Diabetes *49*, 618-625.

Markuns,J.F., Wojtaszewski,J.F., and Goodyear,L.J. (1999). Insulin and exercise decrease glycogen synthase kinase-3 activity by different mechanisms in rat skeletal muscle. J. Biol. Chem. *274*, 24896-24900.

Martin,T.P., Bodine-Fowler,S., Roy,R.R., Eldred,E., and Edgerton,V.R. (1988). Metabolic and fiber size properties of cat tibialis anterior motor units. Am. J. Physiol *255*, C43-C50.

Mastick,C.C., Brady,M.J., and Saltiel,A.R. (1995). Insulin stimulates the tyrosine phosphorylation of caveolin. J. Cell Biol. *129*, 1523-1531.

Matsumoto,K., Yamada,T., Natori,T., Ikeda,K., Yamada,J., and Yamori,Y. (1991). *Genetic variability in* SHR (SHRSR), SHRSP and WKY strains. Clin. Exp. Hypertens. A *13*, 925-938.

Mayer,B. and Hemmens,B. (1997). Biosynthesis and action of nitric oxide in mammalian cells. Trends Biochem. Sci. *22*, 477-481.

Mellor,H. and Parker,P.J. (1998). The extended protein kinase C superfamily. Biochem. J. *332 (Pt 2)*, 281-292.

Merrill,G.F., Kurth,E.J., Hardie,D.G., and Winder,W.W. (1997). AICA riboside increases AMP-activated protein kinase, fatty acid oxidation, and glucose uptake in rat muscle. Am. J. Physiol *273*, E1107-E1112.

Michael,M.D., Kulkarni,R.N., Postic,C., Previs,S.F., Shulman,G.I., Magnuson,M.A., and Kahn,C.R. (2000). Loss of insulin signaling in hepatocytes leads to severe insulin resistance and progressive hepatic dysfunction. Mol. Cell *6*, 87-97.

Michell,B.J., Chen,Z., Tiganis,T., Stapleton,D., Katsis,F., Power,D.A., Sim,A.T., and Kemp,B.E. (2001). Coordinated control of endothelial nitric-oxide synthase phosphorylation by protein kinase C and the cAMP-dependent protein kinase. J. Biol. Chem. *276*, 17625-17628.

Michell,B.J., Griffiths,J.E., Mitchelhill,K.I., Rodriguez-Crespo,I., Tiganis,T., Bozinovski,S., de Montellano,P.R., Kemp,B.E., and Pearson,R.B. (1999). The Akt kinase signals directly to endothelial nitric oxide synthase. Curr. Biol. *9*, 845-848.

Misura,K.M., Scheller,R.H., and Weis,W.I. (2000). Three-dimensional structure of the neuronal-Sec1-syntaxin 1a complex. Nature *404*, 355-362.

Mondon,C.E. and Reaven,G.M. (1988). Evidence of abnormalities of insulin metabolism in rats with spontaneous hypertension. Metabolism *37*, 303-305.

Montagnani,M., Chen,H., Barr,V.A., and Quon,M.J. (2001). Insulin-stimulated activation of eNOS is independent of Ca2+ but requires phosphorylation by Akt at Ser(1179). J. Biol. Chem. *276*, 30392-30398.

Mu,J., Brozinick,J.T., Jr., Valladares,O., Bucan,M., and Birnbaum,M.J. (2001). A role for AMP-activated protein kinase in contraction- and hypoxia- regulated glucose transport in skeletal muscle. Mol. Cell *7*, 1085-1094.

Mueckler,M., Caruso,C., Baldwin,S.A., Panico,M., Blench,I., Morris,H.R., Allard,W.J., Lienhard,G.E., and Lodish,H.F. (1985). Sequence and structure of a human glucose transporter. Science *229*, 941-945.

Munoz,P., Rosemblatt,M., Testar,X., Palacin,M., Thoidis,G., Pilch,P.F., and Zorzano,A. (1995). The T-tubule is a cell-surface target for insulin-regulated recycling of membrane proteins in skeletal muscle. Biochem. J. *312 (Pt 2)*, 393-400.

Nave,B.T., Ouwens,M., Withers,D.J., Alessi,D.R., and Shepherd,P.R. (1999). Mammalian target of rapamycin is a direct target for protein kinase B: identification of a convergence point for opposing effects of insulin and amino-acid deficiency on protein translation. Biochem. J. *344 (Pt 2)*, 427-431.

Newgard,C.B., Brady,M.J., O'Doherty,R.M., and Saltiel,A.R. (2000). Organizing glucose disposal: emerging roles of the glycogen targeting subunits of protein phosphatase-1. *Diabetes 49, 1967-1977.*

Okada,T., Kawano,Y., Sakakibara,T., Hazeki,O., and Ui,M. *(1994). Essential role of* phosphatidylinositol 3-kinase in insulin-induced glucose transport and antilipolysis in rat adipocytes. Studies with a selective inhibitor wortmannin. J. Biol. Chem. *269*, 3568-3573.

Okamoto K, Yamori Y Nagaoka A. Establishment of the Stroke-prone Spontaneously Hypertensive Rat (SHR). (1974). Circulation research, supplement I, 143-153.

Okamoto,T., Schlegel,A., Scherer,P.E., and Lisanti,M.P. (1998). Caveolins, a family of scaffolding proteins for organizing "preassembled signaling complexes" at the plasma membrane. J. Biol. Chem. *273*, 5419-5422.

Ottinger,E.A., Botfield,M.C., and Shoelson,S.E. (1998). Tandem SH2 domains confer high specificity in tyrosine kinase signaling. J. Biol. Chem. *273*, 729-735.

Palmer,R.M.J., Ferrige,A.G. and Moncada,S. (1987). Nitric oxide release accounts for the biological activity of endothelium derived relaxing factor. Nature *327*, 524-526.

Parker,P.J., Caudwell,F.B., and Cohen,P. (1983). Glycogen synthase from rabbit skeletal muscle; effect of insulin on the state of phosphorylation of the seven phosphoserine residues in vivo. Eur. J. Biochem. *130*, 227-234.

Patti,M.E. and Kahn,C.R. (1998). The insulin receptor--a critical link in glucose homeostasis and insulin action. J. Basic Clin. Physiol Pharmacol. *9*, 89-109.

Pessin,J.E. and Saltiel,A.R. (2000). Signaling pathways in insulin action: molecular targets of insulin resistance. J. Clin. Invest *106*, 165-169.

Pessin,J.E., Thurmond,D.C., Elmendorf,J.S., Coker,K.J., and Okada,S. (1999). Molecular basis of insulin-stimulated GLUT4 vesicle trafficking. Location! Location! Location! J. Biol. Chem. *274*, 2593-2596.

Pette,D. and Staron,R.S. (1990). Cellular and molecular diversities of mammalian skeletal muscle fibers. Rev. Physiol Biochem. Pharmacol. *116*, 1-76.

Ploug,T., Galbo,H., Vinten,J., Jorgensen,M., and Richter,E.A. (1987). Kinetics of glucose transport in rat muscle: effects of insulin and contractions. Am. J. Physiol *253*, E12-E20.

Proud,C.G., Wang,X., Patel,J.V., Campbell,L.E., Kleijn,M., Li,W., and Browne,G.J. (2001). Interplay between insulin and nutrients in the regulation of translation factors. Biochem. Soc. Trans. *29*, 541-547.

Pulverer,B.J., Kyriakis,J.M., Avruch,J., Nikolakaki,E., and Woodgett,J.R. (1991). Phosphorylation of c-jun mediated by MAP kinases. Nature *353*, 670-674.

Raught,B., Gingras,A.C., and Sonenberg,N. (2001). The target of rapamycin (TOR) proteins. Proc. Natl. Acad. Sci. U.S.A *98*, 7037-7044.

Ravichandran,L.V., Esposito,D.L., Chen,J., and Quon,M.J. (2001). Protein kinase C-zeta phosphorylates insulin receptor substrate-1 and impairs its ability to activate phosphatidylinositol 3-kinase in response to insulin. J. Biol. Chem. *276*, 3543-3549.

Razani,B., Combs,T.P., Wang,X.B., Frank,P.G., Park,D.S., Russell,R.G., Li,M., Tang,B., Jelicks,L.A., Scherer,P.E., and Lisanti,M.P. (2002a). Caveolin-1-deficient mice are lean, resistant to diet-induced obesity, and show hypertriglyceridemia with adipocyte abnormalities. J. Biol. Chem. *277*, 8635-8647.

Razani,B., Engelman,J.A., Wang,X.B., Schubert,W., Zhang,X.L., Marks,C.B., Macaluso,F., Russell,R.G., Li,M., Pestell,R.G., Di Vizio,D., Hou,H., Jr., Kneitz,B., Lagaud,G., Christ,G.J., Edelmann,W., and Lisanti,M.P. (2001). Caveolin-1 null mice are viable but show evidence of hyperproliferative and vascular abnormalities. J. Biol. Chem. *276*, 38121-38138.

Razani,B., Wang,X.B., Engelman,J.A., Battista,M., Lagaud,G., Zhang,X.L., Kneitz,B., Hou,H., Jr., Christ,G.J., Edelmann,W., and Lisanti,M.P. (2002b). Caveolin-2-deficient mice show evidence of severe pulmonary dysfunction without disruption of caveolae. Mol. Cell Biol. *22*, 2329-2344.

Reaven,G.M., Chang,H., Hoffman,B.B., and Azhar,S. (1989). Resistance to insulin-stimulated glucose uptake in adipocytes isolated from spontaneously hypertensive rats. Diabetes *38*, 1155-1160.

Redpath,N.T., Foulstone,E.J., and Proud,C.G. (1996). Regulation of translation elongation factor-2 by insulin via a rapamycin-sensitive signalling pathway. EMBO J. *15*, 2291-2297.

Reid,M.B. (1998). Role of nitric oxide in skeletal muscle: synthesis, distribution and functional importance. Acta Physiol Scand. *162*, 401-409.

Roberts,C.K., Barnard,R.J., Jasman,A., and Balon,T.W. (1999). Acute exercise increases nitric oxide synthase activity in skeletal muscle. Am. J. Physiol *277*, E390-E394.

Ross,S.A., Scott,H.M., Morris,N.J., Leung,W.Y., Mao,F., Lienhard,G.E., and Keller,S.R. (1996). Characterization of the insulin-regulated membrane aminopeptidase in 3T3-L1 adipocytes. J. Biol. Chem. *271*, 3328-3332.

Round,J.M., Matthews,Y., and Jones,D.A. (1980). A quick, simple and reliable histochemical method for ATPase in human muscle preparations. Histochem. J. *12*, 707-710.

Roy,D. and Marette,A. (1996). Exercise induces the translocation of GLUT4 to transverse tubules from an intracellular pool in rat skeletal muscle. Biochem. Biophys. Res. Commun. *223*, 147-152.

Rylatt,D.B., Aitken,A., Bilham,T., Condon,G.D., Embi,N., and Cohen,P. (1980). Glycogen synthase from rabbit skeletal muscle. Amino acid sequence at the sites phosphorylated by glycogen synthase kinase-3, and extension of the N-terminal sequence containing the site phosphorylated by phosphorylase kinase. Eur. J. Biochem. *107*, 529-537.

Sakamoto,K. and Goodyear,L.J. (2002). Invited Review: Intracellular signaling in contracting skeletal muscle. J. Appl. Physiol *93*, 369-383.

Sakamoto,K., Hirshman,M.F., Aschenbach,W.G., and Goodyear,L.J. (2002). Contraction regulation of Akt in rat skeletal muscle. J. Biol. Chem. *277*, 11910-11917.

Saltiel,A.R. (2000). Series introduction: the molecular and physiological basis of insulin resistance: emerging implications for metabolic and cardiovascular diseases. J. Clin. Invest *106*, 163-164.

Samani,N.J., Swales,J.D., Jeffreys,A.J., Morton,D.B., Naftilan,A.J., Lindpaintner,K., Ganten,D., and Brammar,W.J. (1989). DNA fingerprinting of spontaneously hypertensive and Wistar-Kyoto rats: implications for hypertension research. J. Hypertens. *7*, 809-816.

Satoh,S., Nishimura,H., Clark,A.E., Kozka,I.J., Vannucci,S.J., Simpson,I.A., Quon,M.J., Cushman,S.W., and Holman,G.D. (1993). Use of bismannose photolabel to elucidate insulin-regulated GLUT4 subcellular trafficking kinetics in rat adipose cells. Evidence that exocytosis is a critical site of hormone action. J. Biol. Chem. *268*, 17820-17829.

Schmidt,H.H., Lohmann,S.M., and Walter,U. (1993). The nitric oxide and cGMP signal transduction system: regulation and mechanism of action. Biochim. Biophys. Acta *1178*, 153-175.

Schulte,T., Paschke,K.A., Laessing,U., Lottspeich,F., and Stuermer,C.A. (1997). Reggie-1 and reggie-2, two cell surface proteins expressed by retinal ganglion cells during axon regeneration. Development *124*, 577-587.

Scott,P.H., Brunn,G.H., Kohn,A.D., Roth,R.A. and Lawrence,J.C., Jr. (1998). Evidence of insulin-stimultaed phosphoryaltaion and activation of the mammalian target of rapamycin mediated by a protein kinase B signaling pathway. Proc. Natl. Acad. Sci. U.S.A *95*, 7772-7777.

Sharma,P.M., Egawa,K., Gustafson,T.A., Martin,J.L., and Olefsky,J.M. (1997). Adenovirus-mediated overexpression of IRS-1 interacting domains abolishes insulin-stimulated mitogenesis without affecting glucose transport in 3T3-L1 adipocytes. Mol. Cell Biol. *17*, 7386-7397.

Sharma,P.M., Egawa,K., Huang,Y., Martin,J.L., Huvar,I., Boss,G.R., and Olefsky,J.M. (1998). Inhibition of phosphatidylinositol 3-kinase activity by adenovirus-mediated gene transfer and its effect on insulin action. J. Biol. Chem. *273*, 18528-18537.

Shepherd,P.R., Withers,D.J., and Siddle,K. (1998). Phosphoinositide 3-kinase: the key switch mechanism in insulin signalling. Biochem. J. *333 (Pt 3)*, 471-490.

Shulman,G.I. (2000). Cellular mechanisms of insulin resistance. J. Clin. Invest *106*, 171-176.

Simons,K. and Toomre,D. (2000). Lipid rafts and signal transduction. Nat. Rev. Mol. Cell Biol. *1*, 31-39.

Skolnik,E.Y., Batzer,A., Li,N., Lee,C.H., Lowenstein,E., Mohammadi,M., Margolis,B., and Schlessinger,J. (1993). The function of GRB2 in linking the insulin receptor to Ras signaling pathways. Science *260*, 1953-1955.

Smart,E.J., Graf,G.A., McNiven,M.A., Sessa,W.C., Engelman,J.A., Scherer,P.E., Okamoto,T., and Lisanti,M.P. (1999). Caveolins, liquid-ordered domains, and signal transduction. Mol. Cell Biol. *19*, 7289-7304.

Sonenberg,N. and Gingras,A.C. (1998). The mRNA 5' cap-binding protein eIF4E and control of cell growth. Curr. Opin. Cell Biol. *10*, 268-275.

Soos,M.A., Field,C.E., and Siddle,K. (1993). Purified hybrid insulin/insulin-like growth factor-I receptors bind insulin-like growth factor-I, but not insulin, with high affinity. Biochem. J. *290 (Pt 2)*, 419-426.

Soos,M.A. and Siddle,K. (1989). Immunological relationships between receptors for insulin and insulin-like growth factor I. Evidence for structural heterogeneity of insulin-like growth factor I receptors involving hybrids with insulin receptors. Biochem. J. *263*, 553-563.

Sowers,J.R., Epstein,M., and Frohlich,E.D. (2001). Diabetes, hypertension, and cardiovascular disease: an update. Hypertension *37*, 1053-1059.

Stambolic,V., Suzuki,A., de la Pompa,J.L., Brothers,G.M., Mirtsos,C., Sasaki,T., Ruland,J., Penninger,J.M., Siderovski,D.P., and Mak,T.W. (1998). Negative regulation of PKB/Akt-dependent cell survival by the tumor suppressor PTEN. Cell *95*, 29-39.

Standaert,M.L., Galloway,L., Karnam,P., Bandyopadhyay,G., Moscat,J., and Farese,R.V. (1997). Protein kinase C-zeta as a downstream effector of phosphatidylinositol 3-kinase during insulin stimulation in rat adipocytes. Potential role in glucose transport. J. Biol. Chem. *272*, 30075-30082.

Stenbit,A.E., Tsao,T.S., Li,J., Burcelin,R., Geenen,D.L., Factor,S.M., Houseknecht,K., Katz,E.B., and Charron,M.J. (1997). GLUT4 heterozygous knockout mice develop muscle insulin resistance and diabetes. Nat. Med. *3*, 1096-1101.

Stephens,L.R., Hughes,K.T., and Irvine,R.F. (1991). Pathway of phosphatidylinositol(3,4,5)-trisphosphate synthesis in activated neutrophils. Nature *351*, 33-39.

Stokoe,D., Stephens,L.R., Copeland,T., Gaffney,P.R., Reese,C.B., Painter,G.F., Holmes,A.B., McCormick,F., and Hawkins,P.T. (1997). Dual role of phosphatidylinositol-3,4,5-trisphosphate in the activation of protein kinase B. Science *277*, 567-570.

Sturgill,T.W. and Wu,J. (1991). Recent progress in characterization of protein kinase cascades for phosphorylation of ribosomal protein S6. Biochim. Biophys. Acta *1092*, 350-357.

Sun,X.J., Crimmins,D.L., Myers,M.G., Jr., Miralpeix,M., and White,M.F. (1993). Pleiotropic insulin signals are engaged by multisite phosphorylation of IRS-1. Mol. Cell Biol. *13*, 7418-7428.

Sutton,R.B., Fasshauer,D., Jahn,R., and Brunger,A.T. (1998). Crystal structure of a SNARE complex involved in synaptic exocytosis at 2.4 A resolution. Nature *395*, 347-353.

Suzuki,K. and Kono,T. (1980). Evidence that insulin causes translocation of glucose transport activity to the plasma membrane from an intracellular storage site. Proc. Natl. Acad. Sci. U.S.A *77*, 2542-2545.

Tamemoto,H., Kadowaki,T., Tobe,K., Yagi,T., Sakura,H., Hayakawa,T., Terauchi,Y., Ueki,K., Kaburagi,Y., Satoh,S., and . (1994). Insulin resistance and growth retardation in mice lacking insulin receptor substrate-1. Nature *372*, 182-186.

Tanti,J.F., Gremeaux,T., Grillo,S., Calleja,V., Klippel,A., Williams,L.T., Van Obberghen,E., and Marchand-Brustel,Y. (1996). Overexpression of a constitutively active form of phosphatidylinositol 3-kinase is sufficient to promote Glut 4 translocation in adipocytes. J. Biol. Chem. *271* , 25227-25232.

Thomas,S.R., Chen,K., and Keaney,J.F., Jr. (2002). Hydrogen peroxide activates endothelial nitric-oxide synthase through coordinated phosphorylation and dephosphorylation via a phosphoinositide 3-kinase-dependent signaling pathway. J. Biol. Chem. *277*, 6017-6024.

Tsuruzoe,K., Emkey,R., Kriauciunas,K.M., Ueki,K., and Kahn,C.R. (2001). Insulin receptor substrate 3 (IRS-3) and IRS-4 impair IRS-1- and IRS-2- mediated signaling. Mol. Cell Biol. *21*, 26-38.

van der Kaay.J., Batty,I.H., Cross,D.A., Watt,P.W., and Downes,C.P. (1997). A novel, rapid, and highly sensitive mass assay for phosphatidylinositol 3,4,5-trisphosphate (PtdIns(3,4,5)P3) and its application to measure insulin-stimulated PtdIns(3,4,5)P3 production in rat skeletal muscle in vivo. J. Biol. Chem. *272*, 5477-5481.

Vanhaesebroeck,B., Leevers,S.J., Panayotou,G., and Waterfield,M.D. (1997). Phosphoinositide 3-kinases: a conserved family of signal transducers. Trends Biochem. Sci. *22*, 267-272.

Voet,D and Voet,J.G. Biochmeistry. (1995). Published by John Wiley and Sons. ISBN:0-471-58651-X

Vojtek,A.B., Hollenberg,S.M., and Cooper,J.A. (1993). Mammalian Ras interacts directly with the serine/threonine kinase Raf. Cell *74*, 205-214.

Volonte,D., Galbiati,F., Li,S., Nishiyama,K., Okamoto,T., and Lisanti,M.P. (1999). Flotillins/cavatellins are differentially expressed in cells and tissues and form a hetero-oligomeric complex with caveolins in vivo. Characterization and epitope-mapping of a novel flotillin-1 monoclonal antibody probe. J. Biol. Chem. *274*, 12702-12709.

Wallberg-Henriksson,H., Constable,S.H., Young,D.A., and Holloszy,J.O. (1988). Glucose transport into rat skeletal muscle: interaction between exercise and insulin. J. Appl. Physiol *65*, 909-913.

Welsh,G.I., Miller,C.M., Loughlin,A.J., Price,N.T., and Proud,C.G. (1998). Regulation of eukaryotic initiation factor eIF2B: glycogen synthase kinase-3 phosphorylates a conserved serine which undergoes dephosphorylation in response to insulin. FEBS Lett. *421*, 125-130.

White,M.F. and Kahn,C.R. (1994). The insulin signaling system. J. Biol. Chem. *269*, 1-4.

White,M.F., Livingston,J.N., Backer,J.M., Lauris,V., Dull,T.J., Ullrich,A., and Kahn,C.R. (1988). Mutation of the insulin receptor at tyrosine 960 inhibits signal transmission but does not affect its tyrosine kinase activity. Cell *54*, 641-649.

Whitman,M.,Downes,P.C., Keeler,M., Keller,T. and Cantley,L. (1989) Type I phosphatidylinositol kinase makes a novel inositol phospholipid, phosphatidylinositol-3-phosphate. Nature *332*, 644-646.

Wiese,R.J., Mastick,C.C., Lazar,D.F., and Saltiel,A.R. (1995). Activation of mitogen-activated protein kinase and phosphatidylinositol 3'-kinase is not sufficient for the hormonal stimulation of glucose uptake, lipogenesis, or glycogen synthesis in 3T3-L1 adipocytes. J. Biol. Chem. *270*, 3442-3446.

Winder,W.W. (2001). Energy-sensing and signaling by AMP-activated protein kinase in skeletal muscle. J. Appl. Physiol *91*, 1017-1028.

Withers,D.J., Gutierrez,J.S., Towery,H., Burks,D.J., Ren,J.M., Previs,S., Zhang,Y., Bernal,D., Pons,S., Shulman,G.I., Bonner-Weir,S., and White,M.F. (1998). Disruption of IRS-2 causes type 2 diabetes in mice. Nature *391*, 900-904.

Wojtaszewski,J.F., Nielsen,J.N., and Richter,E.A. (2002). Invited Review: Effect of acute exercise on insulin signaling and action in humans. J. Appl. Physiol *93*, 384-392.

Wojtaszewski,J.F., Nielsen,P., Hansen,B.F., Richter,E.A., and Kiens,B. (2000). Isoform-specific and exercise intensity-dependent activation of 5'-AMP- activated protein kinase in human skeletal muscle. J. Physiol *528*, 221-226.

Wojtaszewski,J.F. and Richter,E.A. (1998). Glucose utilization during exercise: influence of endurance training. Acta Physiol Scand. *162*, 351-358.

Yamamoto,M., Toya,Y., Schwencke,C., Lisanti,M.P., Myers,M.G., Jr., and Ishikawa,Y. (1998). Caveolin is an activator of insulin receptor signaling. J. Biol. Chem. *273*, 26962-26968.

Yeh,J.I., Gulve,E.A., Rameh,L., and Birnbaum,M.J. (1995). The effects of wortmannin on rat skeletal muscle. Dissociation of signaling pathways for insulin- and contraction-activated hexose transport. J. Biol. Chem. *270*, 2107-2111.

Zierath,J.R., Krook,A., and Wallberg-Henriksson,H. (2000). Insulin action and insulin resistance in human skeletal muscle. Diabetologia *43*, 821-835.

Zimmet,P., Alberti,K.G., and Shaw,J. (2001). Global and societal implications of the diabetes epidemic. Nature *414*, 782-787.

Zisman,A., Peroni,O.D., Abel,E.D., Michael,M.D., Mauvais-Jarvis,F., Lowell,B.B., Wojtaszewski,J.F., Hirshman,M.F., Virkamaki,A., Goodyear,L.J., Kahn,C.R., and Kahn,B.B. (2000). Targeted disruption of the glucose transporter 4 selectively in muscle causes insulin resistance and glucose intolerance. Nat. Med. *6*, 924-928.

Zuniga,F.A., Shi,G., Haller,J.F., Rubashkin,A., Flynn,D.R., Iserovich,P., and Fischbarg,J. (2001). A three-dimensional model of the human facilitative glucose transporter Glut1. J. Biol. Chem. *276*, 44970-44975.

APPENDIX

Bait vector

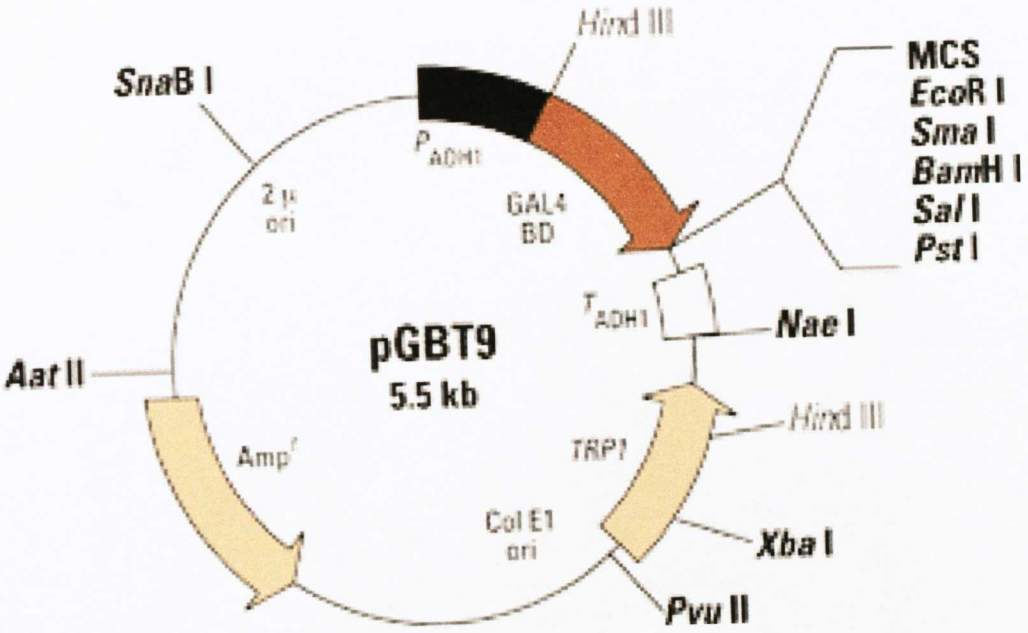

Library Vector